**US Army Corps
of Engineers®**
Engineer Research and
Development Center

Chemical Reductive Transformations of Synthetic Organic Compounds

Probe Compound Studies and Mechanistic Modeling

Gary R. Peyton, Mary H. LeFaivre,
and Stephen W. Maloney

December 2001

20020103 163

Construction Engineering
Research Laboratory

**US Army Corps
of Engineers**®
Engineer Research and
Development Center

Chemical Reductive Transformations of Synthetic Organic Compounds

Probe Compound Studies and Mechanistic Modeling

Gary R. Peyton, Mary H. LeFaivre,
and Stephen W. Maloney

December 2001

Foreword

Contents

List of Figures and Tables

Tables

1 Introduction

Background

Reduction of munitions-related compounds has been under study using a variety of methods. At the Construction Engineering Research Laboratory (CERL) and many other locations, investigations have been undertaken using biological methods (anaerobic transformation), electrochemical methods (using a Nafion membrane-based reactor), and zero valent iron. A fourth method of chemical reduction using reducing radicals, described here, is the outgrowth of work originally targeting chemical oxidation. A study of chemical oxidation of propellant wastewater found an alternative and much faster route to chemical reduction. The propellant wastewater normally contains 100 to 300 mg/L of ethanol, and the presence or absence of oxygen was found to greatly affect the disappearance of dinitrotoluene (DNT), which is the target compound for removal in propellant wastewater.

Further study indicated that the principal oxidant in the study, the hydroxyl radical, was reacting with ethanol to produce a reducing compound, the 1-hydroxyethyl (HE) radical. The HE radical reacted with DNT as much as 100 times faster than the oxidizing radical. It also reacted very rapidly with dissolved oxygen (DO), and the extent of treatment would depend very strongly on DO concentration. An attempt to model the rate and extent of reaction versus oxygen concentration yielded conflicting results. The rate constants predicted steady-state concentrations in a flow through system at the extremes of oxygen concentration, from a low of approximately 0.3 mg/L to a high of 25 mg/L. The intermediate values were not well predicted, and seemed to jump from high to low steady-state removal, with overlapping values depending on whether the reaction was being observed as the oxygen level increased, versus when the oxygen level in the flow through system started high and was reduced. This result suggests that the intermediate region has two stable reaction pathways, and that an underlying mechanism is responsible for the jump from one system to the other. This type of system is generally referred to as bistable. The study reported here used mechanistic modeling to examine these potential underlying reactions to determine if they could be controlled so as to promote the chemical reduction of substituted aromatic compounds. This study used DNT as the probe compound, but the process would also be applicable to other substituted aromatic

and aliphatic compounds such as chlorinated alkanes and chlorinated aromatic compounds.

Objective

The general objectives of this project were to investigate the reductive pathway by which contaminants may be removed; develop a kinetic model, based on new data, that explains the anomalous results obtained in previous flow experiments; and to investigate the possibility of bistable/oscillating behavior to determine whether this behavior may be responsible for the previous results. A specific objective of this study was to develop a mechanism that describes the overall reaction of 1-hydroxyethyl radical (and intermediates formed when producing the HE radical from reaction of ethanol and hydroxyl radical) with DNT. The resulting mechanism would be a model of the pathways of reaction, and rate constants for those pathways including all important intermediates, expressed graphically for the overall model, and in individual chemical reaction equations for the intermediates and end-products.

Approach

This study used the mechanistic modeling approach, which involves postulating reactions between compounds, assessing the potential for these reactions to occur and the rate at which they occur, and determining whether the postulated reactions could be fast enough to be significant in the reaction pathway. These reactions were then isolated by using excess concentrations of compounds, or radical scavengers, so that the postulated reaction could be studied directly. In the basic reaction of HE with DNT, for example, an excess of ethanol is added to the system. This excess ensures that all of the hydroxyl radicals react with ethanol and form HE, rather than react directly with DNT. This procedure allows the rate constant to be measured within close approximation because the loss of hydroxyl radical to the reaction with DNT becomes negligible. This report includes a number of reactions that have not been described in previous studies, and documents the rate constants measured as well as the by-products formed.

The general steps in this method are:

1. Review existing literature to identify all possible candidate reactions that might participate in the pathway

2. Construct a mechanistic model that includes all the candidate reactions

3. Eliminate unimportant reactions on the basis of experimental evidence or calculations that show a particular pathway to be unimportant

4. Derive the differential rate equations from the reduced mechanism

5. Solve these kinetic equations either analytically or numerically to further eliminate unimportant terms

6. Identify existing rate constants and verify them in this system

7. Measure new rate constants if necessary, or estimate their values from literature values for similar rate constants to use in the rate equations

8. Use inestimable rate constants as adjustable parameters in fitting the predictions of the kinetic equations to existing and newly acquired experimental data.

Mode of Technology Transfer

The results of this study will be presented at scientific meetings and will form the basis of articles in professional publications. It is anticipated that the results of this study will be used to develop a portable bench-scale reactor that can be tested on Army wastewaters.

This report will be made accessible through the World Wide Web (WWW) at: http://www.cecer.army.mil

2 Background

Prior Mechanistic Knowledge

Previous studies in this laboratory (Peyton et al. 1995) have demonstrated that, in the presence of suitable precursors (e.g., ethanol), nitroaromatic compounds such as DNT could be destroyed by reducing radicals. In the same study, this reaction was also shown to be effective for the destruction of highly halogenated compounds, making it a candidate reaction for treatment of polychlorinated biphenyls. This reductive reaction removed DNT from solution even in highly oxidizing environments, as in the presence of ozone, hydrogen peroxide, and hydroxyl radicals, which might be expected to consume the reducing radicals. Destruction of DNT and other nitroaromatics by this pathway was found to be faster than destruction by the oxidizing radicals, when high concentrations of OH-radical scavengers were present. A mechanistic model (Maloney, Boddu, and Peyton 1997) was developed for the DNT/ethanol/H_2O_2/UV system, which successfully described DNT removal as a function of oxygen concentration in solution, since oxygen competes for reducing radical. This mechanism is shown in Figure 1. As further proof of the fundamental appropriateness of the model, it also proved successful in predicting DNT removal results from other oxidation systems such as ozone/UV (Maloney, Boddu, and Peyton 1997).

When the model was extended from batch experiments to flow systems, it was found that the theoretical model predicted a gradual transition from nearly complete DNT removal at low DO concentration (below 10^{-6} M) to almost no DNT removal at higher oxygen concentration (above 10^{-3} M). The experimental results obtained from flow experiments, however, showed what appeared to be a much sharper transition from extensive DNT removal to little DNT removal, with the appearance of a step function, rather than the sigmoid appearance of the model prediction (Figure 2). The exact shape of the curve at the transition point could not be determined, possibly because it occurred very close to the detection limit of the DO meter being used, where precision and accuracy are less than optimum. It appeared, however, that the transition region was from 1×10^{-5} to 3×10^{-6} M DO. Adjusting parameters such as rate constants in the existing model did not yield a satisfactory fit to the flow data. It was noted that the sharp transition was similar in appearance to behavior observed in some bistable reaction systems (Gray and Scott 1990, p 4), and that the proposed reaction mechanism

contained some features common to bistability, such as feedback loops in chain reactions. Furthermore, bistability in the transition region could have the effect of complicating the appearance of the curve in the transition region.
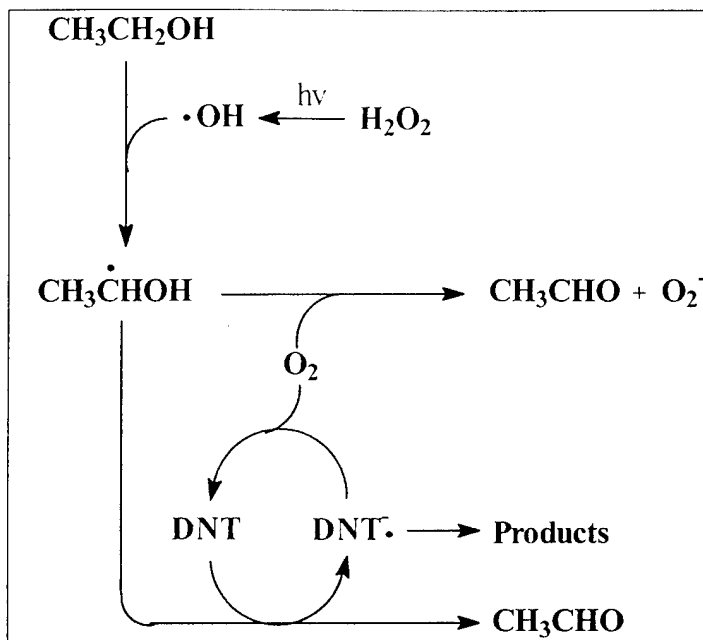
Figure 1. Proposed mechanism of DNT removal by reductive species in aqueous ethanol solution (Peyton et al. 1995).
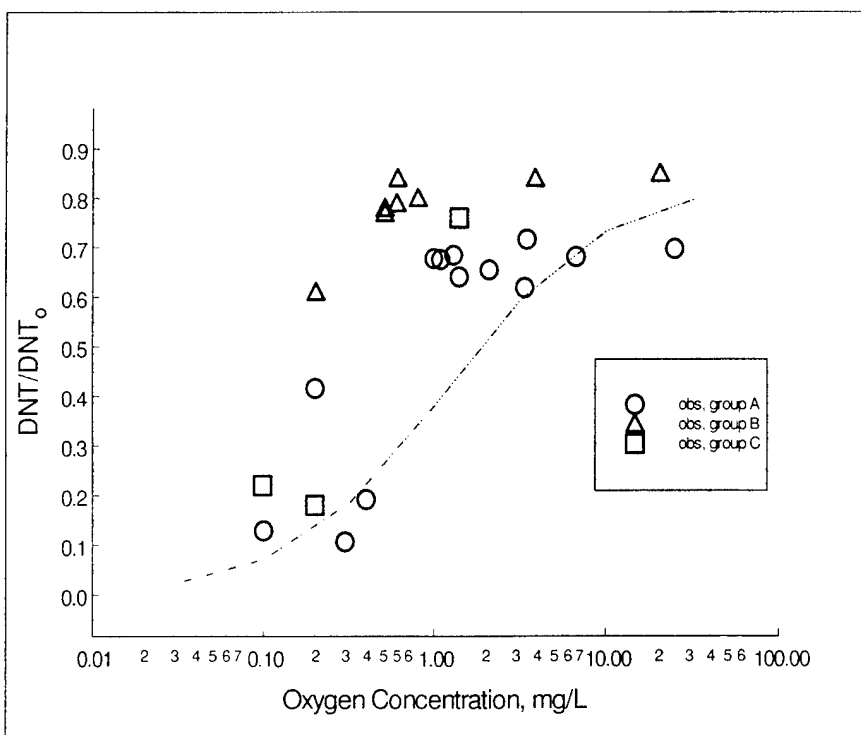
Figure 2. Comparison of observed DNT removal (obs) during flow experiments with that predicted by the mechanistic/kinetic model developed from batch data (Maloney, Boddu, and Peyton 1997). Dashed line indicates kinetic model prediction.

Since bistability in a chemical reaction system can lead to drastic changes in system behavior (concentration changes of products and reactants) in response to small input changes, the operational robustness of wastewater treatment processes utilizing bistable chemical reaction systems could be greatly affected and unpredictable treatment results obtained. If the bistability of the system was unrecognized, the treatment process might not perform as designed, at times suddenly appearing to quit working, and likely prompting a fruitless search for possible equipment failure. It is therefore important to understand the mechanistic reason for the behavior shown in Figure 2, and to determine whether bistability can typically occur in this type of advanced oxidation/reduction treatment system.

Oscillating and Bistable Systems

Description

Bistability in chemical reaction systems means that a system has two stable states available to it. This situation is the exception in chemical reaction systems, in which, typically reactants are mixed and react until they "run down," (i.e., until they reach the composition of lowest energy). Figure 3 shows a simplified diagrammatic representation of a bistable system (adapted from Gray and Scott 1990), with the control variable (concentration, flow, temperature, etc.) plotted on the horizontal axis and the response (i.e., the observable property, such as contaminant concentration remaining) on the vertical axis. The response is a complex function of composition and conditions, but only the response to the control variable is plotted here. The system has two states (i.e., values of the response variable) available to it in region A-B. If initially the value of the control variable starts on the right hand side of the diagram, then moves to the left, the response variable will increase as the point representing the system moves along the bottom line. If point B is reached and the driving variable continues to decrease, the only stable value of the observed property that is available to the system lies on the upper branch, so a transition to that state occurs. This transition can cause a rapid change in the observed property (y-axis). If the value of the control variable approached from the left to the same point in the middle, the value of the response (observed property) would be different, following the upper line. Thus, the system can operate at two different response values for the same value of the control variable. An upset in the system composition could change conditions such that the temporary (unstable) state of the system lies closer to the other branch, causing a transition to the other stable branch.

observed
response

B A
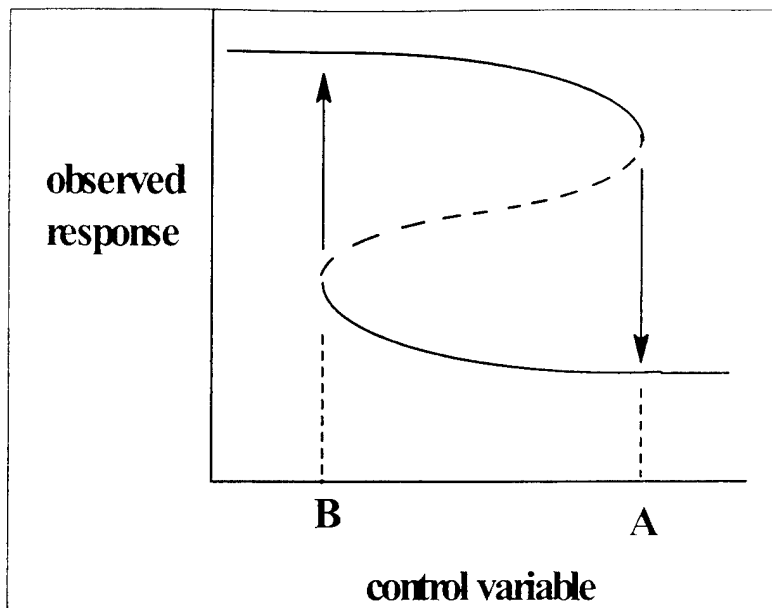
control variable

Figure 3. Diagrammatic representation of reaction system that has two stable states (i.e., allowed values of the response) in the region where the control variable is in the range of A to B. Dashed portion of curve is an unstable state.

Oscillations can occur when the system contains a driving force that tends to "push" the operating point across the bottom line to the left and across the top line to the right. When the point arrives at the right-hand side of the upper curve, it reaches a region where it has only one value of the response variable available to it (i.e., on the bottom curve at a considerably different value of the response variable). The response variable changes to the new value (i.e., the system chemistry changes) and the point now lies in a region where the control variable is pushed to the left along the bottom line. When the control variable reaches the left-hand side of the bottom line, it makes a similar transition to the upper curve. The net result is that the response variable exhibits periodic behavior (i.e., oscillates). Systems that exhibit this behavior tend to be "normal" under most conditions, but bistable in some small region of conditions and oscillatory in another region. This system is represented diagrammatically in Figure 4 as an example from the chemical literature (Boissonade and De Kepper 1980).

In wastewater treatment, reaching the end of one branch could mean a sudden unexpected shift in effluent concentration of a contaminant. A temporary change in feed stream composition could force the operating point closer to the other branch of the bistable system, so that when the feed stream composition returned to its previous value, it could recover to the other branch. Even oscillatory behavior could occur undetected if the effluent composition was not monitored frequently enough for the pattern to become obvious, which would typically be the case.
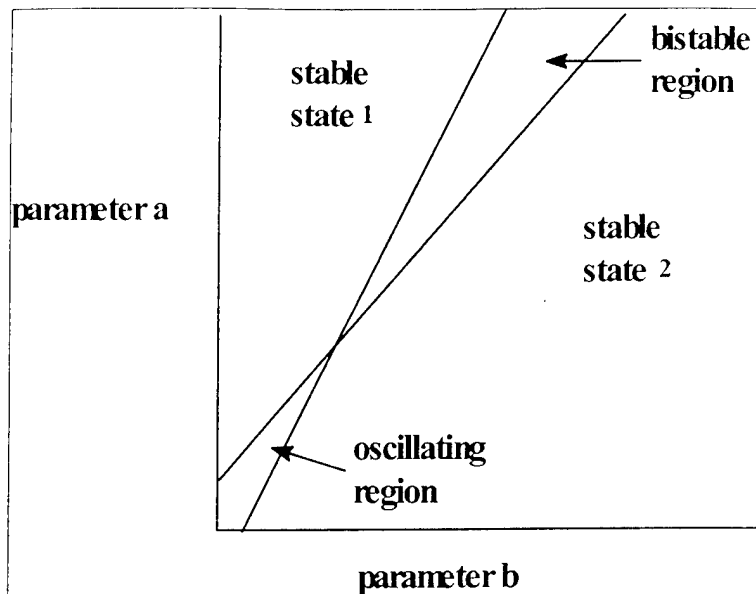
Figure 4. Two-parameter system for which most of parameter
space is occupied by stable states 1 and 2. A small region of
bistability and a smaller region of oscillatory behavior are present
(adapted from Gray and Scott 1990).

Requirements and Characteristics of Bistability

A primary requirement for bistability is the existence of a feedback loop with
amplification (Gray and Scott 1990, p 5), so that an intermediate or product can
influence the rate of earlier steps. This feedback can be chemical or physical
(e.g., thermal). A simple example of chemical feedback resulting in autocatalysis
is the core mechanism by which oxygen and hydrogen react during combustion:

$$H + O_2 \rightarrow OH + O$$

$$OH + H_2 \rightarrow H_2O + H$$

$$O + H_2 \rightarrow OH + H$$
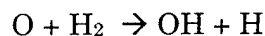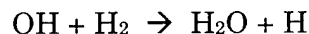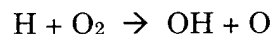
For which the stoichiometric reaction is:

$$H + 3H_2 + O_2 \rightarrow 3H + 2H_2O$$
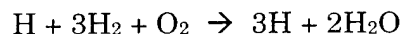
For each H atom reacting with dioxygen, three more H atoms are produced.
Thus, the rate of the reaction is amplified, and the reaction may "run away," re-
sulting in explosion.

Bistability is easier to create in a continuously fed stirred tank reactor (CSTR) than in a closed (batch) system, in which the reaction can simply "run down" when reactants are not replenished. Even the following simple autocatalytic process can exhibit bistable behavior:

$$A + 2B \rightarrow 3B \qquad rate = k_1 AB^2$$

The steady-state condition for this reaction in a reactor with retention time $t_R = V_R/Q$ (V_R=reactor volume and Q=liquid flow rate) and feed concentrations A_o and B_o is:

$$(A_0\text{-}A)/t_R - k_1 A(A_o + B_o\text{-}A)^2 = 0 \qquad \text{[Eq 1]}$$

where the relationship $A_o + B_o = A + B$ from the reaction stoichiometry has been used to eliminate B. The first term in equation 1 represents the flow (F), i.e., reactor feed and washout, while the second represents chemical reaction (R). For steady-state operation, the net inflow must equal the rate of chemical reaction, so if R and F are plotted versus the extent of reaction ($\xi = 1\text{-}A/A_o$), the "flow diagrams" shown in Figure 5 result (adapted from Gray and Scott 1990, p 21). The flow term (F in the figure) is linear in ξ since it differs only by the constant A_o/t_R. The reaction term (R in the figure) is small at low and high conversion, with a maximum at an intermediate value. Since both terms must be equal for steady-state operation, the points at which the curves cross represent solutions to the steady-state equation. Thus, only one solution exists toward the lower-left corner in (a), two solutions are seen in (b) at the lower-left and at the tangent point, three solutions exist in (c), and so forth, until in (e) only one solution exists because the flow line has dropped below the reaction curve in the lower-left corner of the plot. When the extent of reaction for all of the solutions is plotted versus flow rate, the characteristic shape of a cubic autocatalysis curve (such as shown in Figure 3) results (see bottom, Figure 5).

One characteristic of multistable systems is hysteresis effects.[*] Behavior resembling hysteresis effects were observed in previous laboratory experiments (Maloney, Boddu, and Peyton 1997) in which steady state appeared to be reached for the DO concentration, which then abruptly changed to a new, quite different value even though no experimental conditions were changed. These effects were

---

[*] E. Atlee Jackson, mathematical physicist, expert and author in nonlinear dynamics, and Professor Emeritus, Department of Physics, University of Illinois, personal communication.

observed several times during the course of earlier work, referred to above. It
was also observed that, even though the ratio of oxygen to nitrogen in the sparge
gas was continuously variable, it was very difficult to get the DO concentration
to stabilize in the range of the transition point described earlier. These observa-
tions are consistent with bistable behavior.
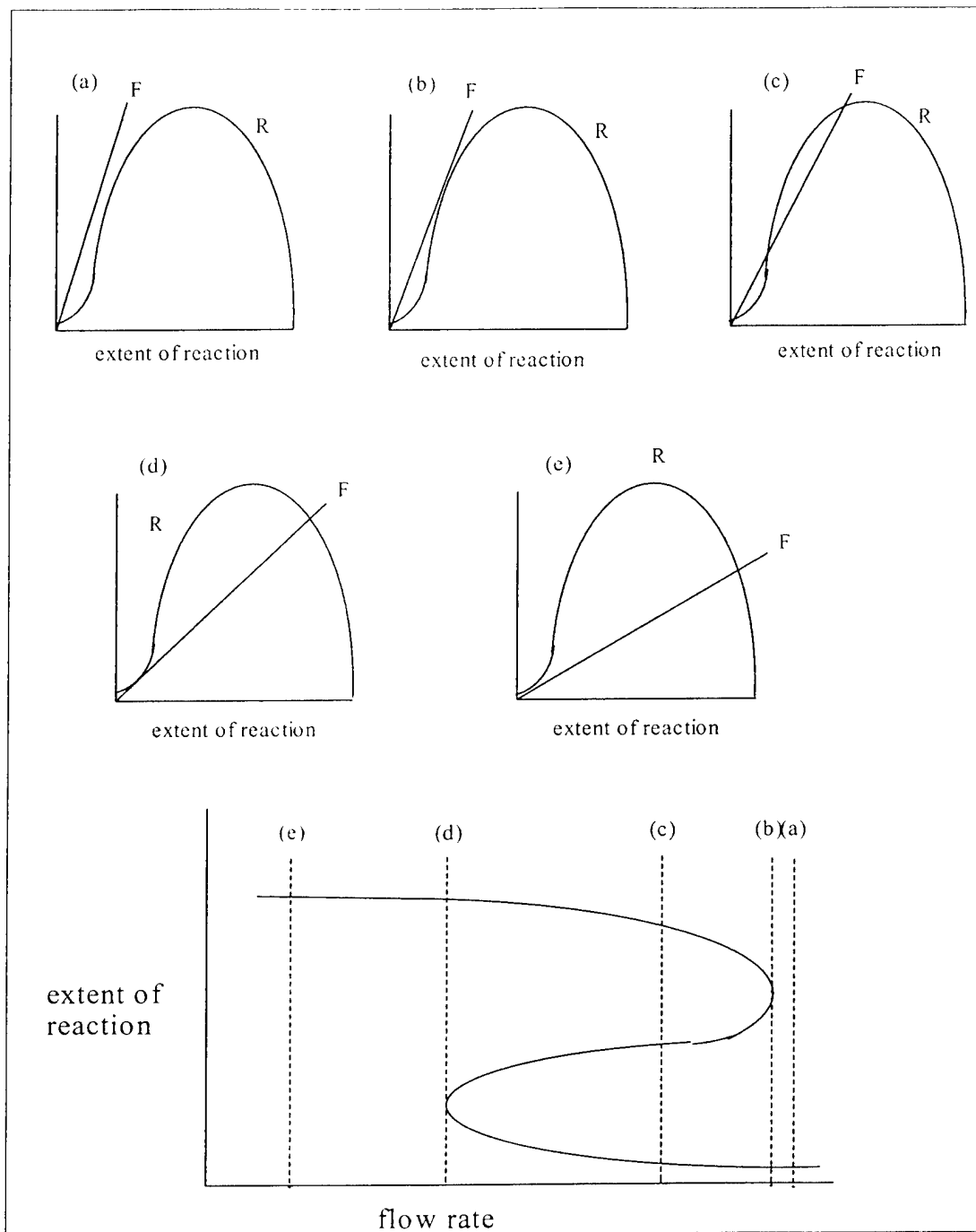
**Figure 5. Relationship between flow diagram and multiple stable states. State diagram at
bottom is the locus of intersections between flow (F) and reaction (R) curves in flow diagrams
(above) for all possible flow rates. Vertical slices a-e on state diagram correspond to individual
flow diagrams a-e above.**

There are two ways to find multistability: by experiment and by mathematical analysis of the system of rate equations. Both methods require a certain amount of searching, since even in a system that can exhibit multistable behavior, it usually occurs only under a narrow range of conditions. Because of the complexities in mathematical analysis of large systems of rate equations, it was desirable to start with the simplest mechanism that would describe the essential features of the chemical reaction system. In the present study, this mechanism is referred to as the core system.

The Core System

Sensitivity analyses on the DNT flow data (Maloney, Boddu, and Peyton 1997) referred to earlier, indicated that the best correlation was between DNT removal and acetaldehyde concentration in the effluent. The correlation between these two variables was even slightly better than the inverse correlation between DNT removal and oxygen concentration, prompting an investigation into the hydroxyl radical chemistry of acetaldehyde to determine whether some unique pathways could be present, which would cause unusual behavior. Conversion of ethanol to acetaldehyde to acetic acid occurs readily in nature, and is often represented by the following reaction sequence:

$$CH_3CH_2OH \xrightarrow{[O]} CH_3CHO \xrightarrow{[O]} CH_3COOH$$
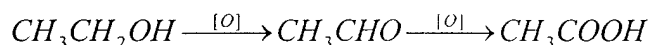
where the symbol [O] represents oxidation. This equation is, however, misleading in its simplicity, and the system of free radical reactions that perform this conversion was found to be especially complicated. It was found from the literature during the previous study (Maloney, Boddu, and Peyton 1997) that ethanol reacts with hydroxyl radical to give 1-hydroxyethyl radical, which is a strongly reducing species that was responsible for the removal of DNT from solution by reduction (Peyton et al. 1995). The acetaldehyde/hydroxyl radical system was found to be even more complicated. The acetyl radical $CH_3C(O)\bullet$, formed by the reaction of OH radical with acetaldehyde

$$CH_3C(O)H + HO\bullet \rightarrow CH_3C(O)\bullet + H_2O$$
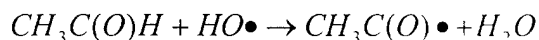
is an oxidizing radical; however, it also adds water on the sub-ms time scale to form the hydrate, $CH_3C(OH)_2\bullet$ (shown below), which is a strong reducing radical (Schuchmann and von Sonntag 1988).

$$CH_3C(O)\bullet + H_2O \Leftrightarrow CH_3C(OH)_2\bullet$$
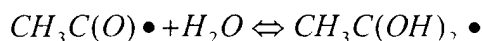
This hydrate, the 1,1-dihydroxyethyl radical, has since been shown in this laboratory to reduce DNT in the same manner as the ethanol radical (1-hydroxyethyl radical), which is shown schematically in Figure 6, where hydrate radical R reacts with DNT (products not shown). The acetyl radical (B), produced by the reaction of OH radical with acetaldehyde (A) (reaction represented simply by the first-order rate constant k_1) and the 1,1-dihydroxyethyl radical (R) both rapidly add oxygen to form the acetylperoxyl radical (Y) and the 1,1-dihydroxyperoxyl radical (not shown), respectively. The acetylperoxyl radical is the most strongly oxidizing peroxyl radical known (Schuchmann and von Sonntag 1988), and therefore should be capable of hydrogen abstraction from organic compounds, forming peroxyacetic acid $CH_3C(O)O_2H$ and a carbon-centered radical. Hydrogen atom abstraction from acetaldehyde would regenerate acetyl radical (B), establishing a chain process. The peroxyl radical RO_2 (the product of R+X, not shown) formed by reaction of the reducing radical R with oxygen should rapidly eliminate superoxide (von Sonntag 1987), leaving acetic acid as a byproduct. Reaction of R with oxygen to form RO_2 occurs in competition with reductive reaction of R with DNT (Figure 6). The reaction is shown, but the product RO_2 is not, since it does not further affect the reaction system. Also not shown is the fact that acetaldehyde reacts with water to form a hydrate (H), which can also form the reducing radical R directly by reaction with hydroxyl radical (shown with complete reaction later on Figure 13).
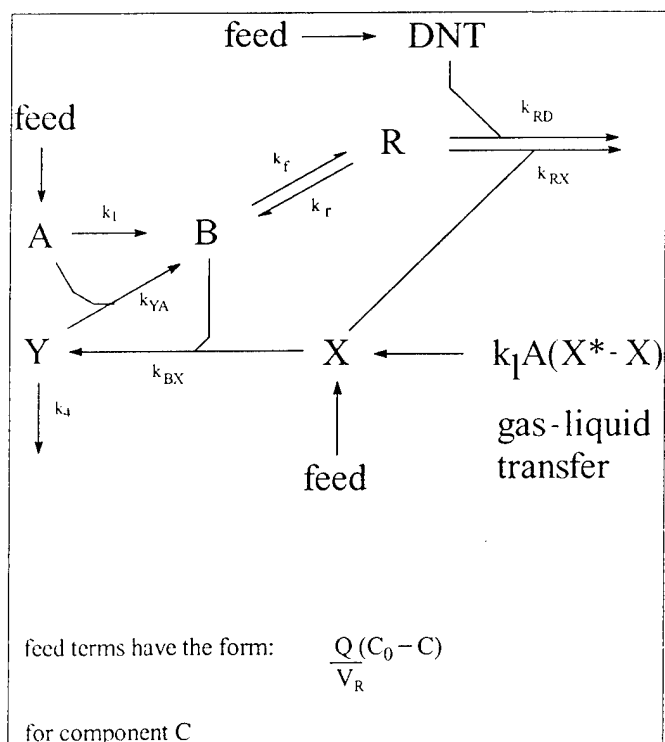
Figure 6. Proposed reaction pathway for the core system.
A=acetaldehyde, B=acetyl radical, DNT=2,4-dinitrotoluene,
R=acetyl hydrate radical, X=oxygen, Y=peroxyacetyl radical.

Although the discussion in later sections will show that the complete mechanism for the acetaldehyde/hydroxyl radical system is considerably more complicated, the "Core System" shown in Figure 6 contains the essential features that make this reaction system unique and provide the possibility of bistable or oscillatory behavior. An oxidative and a reductive radical are both formed from the same parent compound, and exist in rapid equilibrium. Both are capable of very fast reaction with oxygen forming peroxyl radicals, in competition with other reactions such as reduction of DNT by R or reaction of Y with acetaldehyde. Thus, when oxygen is present, peroxyl radical formation would typically be the predominant fate of R and B. The chain reaction of Y with acetaldehyde, however, serves to amplify the production of radicals provided by the initiation step (hydroxyl radical formation), and, to the extent allowed by various rate constants in the system, could "run away." If the rate of oxygen consumption exceeds the rate of oxygen regeneration (from superoxide disproportionation – not shown) plus the rate of any oxygen transfer into solution, depletion of the oxygen content could rapidly occur to the point that the chain reaction is shut off due to lack of oxygen. At this point, the reductive reaction would dominate until enough oxygen accumulates in the system to allow reestablishment of the chain reaction. If no other rapid pathways are available to the acetyl radical, it could be pulled across the equilibrium to react as reducing radical R.

It can be seen, therefore, that the core system has the potential for strange behavior and a mechanism that could conceivably lend itself to producing a bistable or even an oscillatory system. Whether this system can actually behave in that manner depends on the values of the rate constants of the component reactions. As an example, it is assumed that the diagram in Figure 3 applies to the present system (there may well be more than one controlling variable), that the y-axis represents oxygen concentration or transfer rate, and that the x-axis represents a different (currently unidentified) variable. For a single value of the variable x, multiple values of the oxygen concentration may exist, in turn controlling the DNT concentration (D) at different values for each allowed oxygen state. An even simpler example would be if x was a cubic function of D, which can be visualized by imagining Figure 3 to be a plot of D versus the reciprocal of oxygen concentration, then rotating that plot by 90 degrees. It is also possible that the system is not bistable at all, but that the plot of D/D_o versus $\log[O_2]$ (Figure 2) simply has a sigmoid curve shape with a much sharper transition than that represented by the calculated curve in Figure 2, which was obtained from the mechanism using the ethanol radical but none of the free-radical chemistry from the acetaldehyde system discussed earlier. This curve shape could be produced by higher-order oxygen terms in the equation representing D as a function of oxygen concentration, or other functions that generate forms approaching step functions. This latter case would be mathematically simpler than multistability, but could still cause practical difficulties in treatment plants.

3 Experimental Methods

Reactor

Kinetic experiments were carried out in a 0.25-L reactor constructed from a European-style 3-necked flask (Ace Glass, Vineland, NJ) carrying a central 24/40 joint and two 19/32 standard-taper ground glass joints on opposite sides of the flask. To this flask was added a second 24/40 joint on the front and a threaded thermometer port on the back of the flask. Figure 7 shows a diagram of the apparatus (the neck detail is not exact). The central 24/40 joint held a quartz lamp well that extended almost to the bottom of the flask, leaving room for a magnetic stir bar. A small ultraviolet (UV) "pen lamp" emitting almost exclusively at 254 nm (lamp envelope selected to eliminate the 185 nm mercury [Hg] line) was used in the lamp well, and the photon flux reaching the reactor charge was determined by chemical actinometry using hydrogen peroxide (Peyton, Smith, and Peyton 1987). The other 24/40 joint held a DO probe with an electronic unit that read to the nearest 0.1 mg/L (lowest nonzero reading 0.1 mg/L). The two 19/32 joints and the thermometer port were adapted as water and gas inlets and outlets, using standard "Ace-thread" adapters from Ace Glass to hold and seal polytetrafluoroethylene (PTFE) tubing for gas introduction.

Reactor feed entered through 1/8-in. PTFE tubing routed to the side and bottom of the reactor. Reactor effluent was pumped through 1/16-in. PTFE tubing drawing from the surface of the liquid. The effluent pump was run slightly faster than the feed pump to ensure constant volume in the reactor. Sparge gas entered through PTFE tubing that extended to the bottom of the reactor. Most of the gas exited through a sidearm on one of the adapters, but a small amount was pulled through the liquid effluent tube along with the liquid. In some experiments, the reactor was operated in the "gas blanket" mode, in which a slow gentle gas stream flowed across the surface of the water, instead of bubbling through it, in order to avoid the sparging of volatile compounds such as acetaldehyde. This effect was accomplished by withdrawing the gas inlet tube until it was just above the surface of the water in the reactor, which was operated in both flow and batch modes, with liquid charge volumes of 0.207 and 0.250 L, respectively. Liquid flow rate through the reactor was measured by diverting the effluent flow through a graduated buret and timing the liquid meniscus travel with a stopwatch. The diameter of the buret was large enough to allow

gas/liquid separation, so that the few gas bubbles pulled over by the liquid effluent did not interfere with flow measurement.

In flow experiments, DO was measured in the reactor feed by passing influent through a PTFE cell containing a second DO probe. A sampling point was located in the feed line and samples were also taken from the reactor effluent. A valve was located just downstream of the in-line sampling point to avoid any possibility of back flow from the reactor during sampling. At specified sampling times, effluent was sampled before influent, to avoid sampling during the slight upset in steady-state operation following inlet sampling.
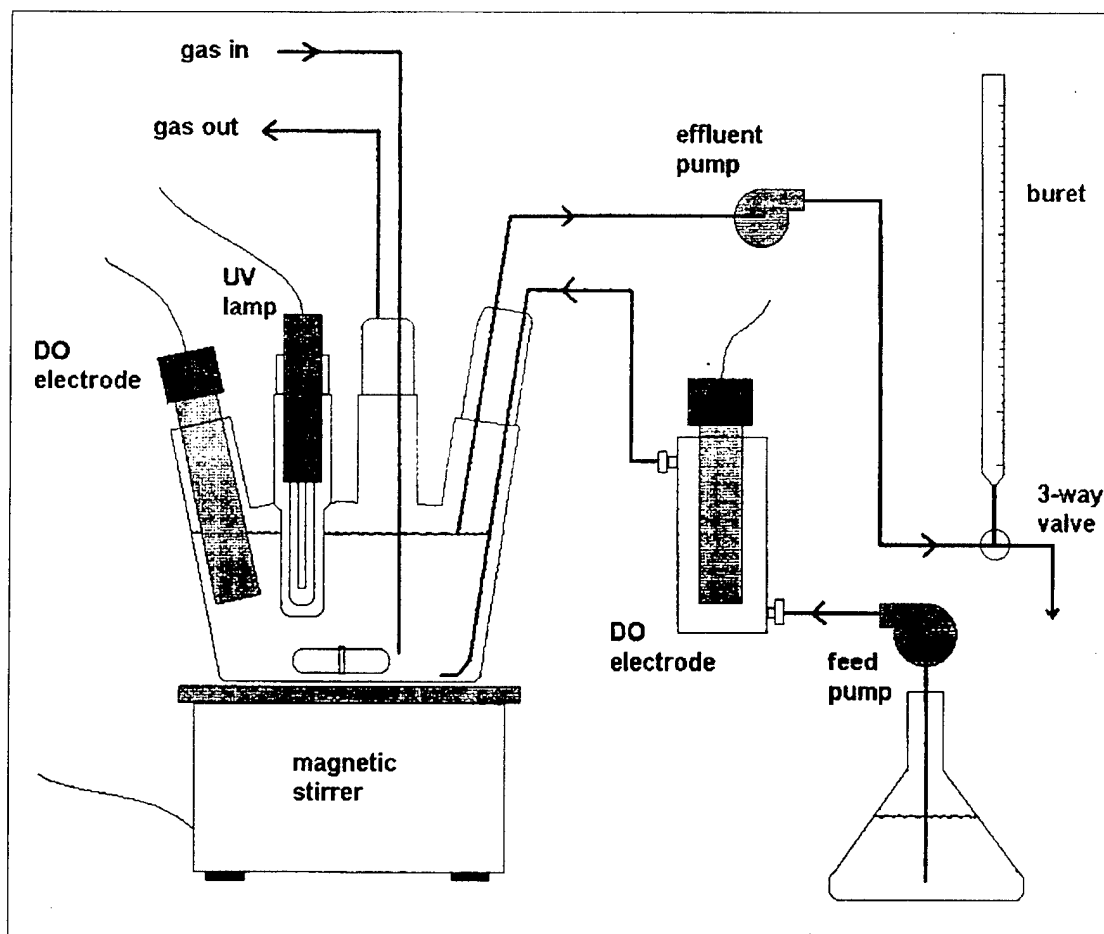
Figure 7. Diagram of reactor and experimental apparatus. Components are not drawn to scale and the three-dimensional reactor is rendered in two dimensions. Effluent pump was operated slightly faster than feed pump to maintain liquid level. UV lamp is enclosed in a quartz lamp well.

Oxygen/nitrogen gas mixtures were sparged into the reactor through the porous fritted glass tube while the reactor contents were magnetically stirred. Stir rate was set and checked using a phototachometer. Gas flow rate was measured and controlled using mass flow controllers (Unit Instruments, Inc., Orange, CA) that have upset recovery times of 1-2 seconds. Multiple units were used when gas mixing was required. The lower flow rates required in some experiments later necessitated the use of calibrated tube-and-ball rotameters (Cole-Parmer Instrument Co., Vernon Hills, IL), the inlet pressure of which was held constant by a downstream pressure regulator located upstream of the rotameter.

Analytical Methods

Acetaldehyde (A) concentration was measured by high-performance liquid chromatography (HPLC) using a C_{18} column with UV detection. Acetic acid (AA) and formic acid concentrations were determined by ion exclusion liquid chromatography. Formaldehyde was identified and quantified as the dinitrophenylhydrazine (DNPH) derivative after reaction with 2,4-DNPH under nitrogen-deaerated conditions. Peroxyacetic acid (PAA) was determined by the kinetic method of Davies and Deary (1988), which distinguishes between hydrogen peroxide (P) and PAA by the difference in the catalyzed rate of reaction with iodide. This method was claimed to allow quantitation of PAA in the presence of a thousand-fold excess of hydrogen peroxide, but was found under the conditions of the present study to be slightly less robust (see next chapter on **Results and Discussion**). Hydrogen peroxide was determined colorimetrically as the Ti(IV) complex, using a modification of the method given by Parker (1928), which was demonstrated to quantitatively recover hydrogen peroxide from the H_2O_2-acetaldehyde adduct 1-hydroxy-ethylhydroperoxide (see next chapter for discussion).

Computational Methods

Systems of differential rate equations were numerically integrated using the Stiff Differential Equation Integrator capability of the commercial software package SCIENTIST for Windows (MicroMath Scientific Software, Salt Lake City, UT). Although this software included routines for curve fitting by variation of parameters using least squares or other criteria, the equation systems under study proved to be too complex to allow utilization of these capabilities, and optimization studies (variation of rate constants to fit experimental data) were performed manually. Typically, whenever possible, equation sets were partially solved and simplified analytically prior to use of the software, but in most cases in the present study, the possibility of oscillating reaction systems and

unsatisfied equilibria made simplifications such as assuming satisfied equilibria and steady-state conditions inadvisable. It was usually possible to analytically solve rate equation sets for smaller systems, particularly under the steady-state assumption. Specific details of various calculations are supplied in the next chapter.

4 Results and Discussion

Reactor Characterization

Modeling of chemical processes inside the reactor requires accurate knowledge of transfer rates into and out of the reactor for photons and chemical species. For most chemical species, it is sufficient to determine the liquid flow rate and influent and effluent concentrations. For oxygen gas, however, the mass transfer coefficient must be known for the conditions used in the experiments, implying good measurement and control of gas flow and stirring rates, as described in the experimental section. It was expected that the critical threshold oxygen transfer rate would be at the point that oxygen transfer into the reactor just balances oxygen consumption. For the present project, the mass transfer coefficients of the reactor and photon transfer rates into the reactor were determined experimentally.

Radiative Transfer

The photon transfer characteristics are important, since the rate of a photochemical reaction can be described by $rate = \phi_e F I_o$, where ϕ_e is the quantum efficiency of the reaction, F is the fraction of photons captured, and I_o is the rate of photon input (einsteins/L-s). The fraction of photons captured depends on the effective path length, and the rate of photon input is measured by actinometry experiments, measuring the rate of hydrogen peroxide disappearance (see Chapter 3). The photon input rate was measured for the mini-reactor under batch conditions, where the reactor liquid volume (V_R) was 0.250 L, and in flow mode, where the reactor operates with a liquid volume of 0.207 L. At a flow rate (Q) of 30 mL/min, the Q/V_R value is 0.145 min^{-1} and the residence time is 6.9 min. The smaller volume in flow mode reflects a different liquid level, which is maintained by the effluent pump. The different liquid level, in turn, covers a slightly different fraction of the quartz lamp well, which might be expected to result in the capture of a different fraction of the photons and perhaps a different effective pathlength as well.

The results of several sets of experiments gave photon input rates of 0.164±0.023 mE/L-min (three batch experiments, V_R=0.250L), 0.188±0.004 (four flow experiments, V_R=0.207 L), and 0.187±0.030 (three batch experiments, V_R=0.207 L).

For these experiments, flow actinometry was performed using flow rates of 5 to 10 mL/min. Multiplication of 0.188 mE/L-s by the ratio of reactor volumes in the second to the first set (i.e., 207/250 as a dilution ratio) gives 0.156 mE/L-s, indicating that the larger liquid volume does indeed capture more photons. The capture was not proportionately greater, however, since in that case the input rates would have been equal without a dilution correction.

Oxygen Mass Transfer

Oxygen is transferred into the reactor by both gas absorption and influx of oxygen in the feed liquid. Preliminary experiments in the mini (0.25L) reactor without gas sparging demonstrated rapid oxygen depletion and resultant DNT removal. Gas sparging was necessary to maintain oxygen levels for experiments.

Two methods of measurement of the mass transfer coefficient for the mini-reactor were tried. The mass transfer equation

$$\frac{dX}{dt} = k_l a (X^* - X) + \frac{Q}{V_R}(X_o - X) \qquad \text{[Eq 2]}$$

where X = oxygen concentration, X^* = liquid-phase oxygen concentration in equilibrium with the sparge gas, and X_o = the oxygen concentration in the influent stream, gives, at steady state:

$$k_l a = -\frac{Q}{V_R}\frac{(X_o - X)}{(X^* - X)} \qquad \text{[Eq 3]}$$

The mass transfer coefficient $k_l a$ was calculated from the steady-state oxygen concentrations.

The other ("dynamic") method used the integrated version of equation 2:

$$X = \frac{\phi}{\theta}(1 - e^{-\theta t}) + X_i e^{-\theta t} \qquad \text{[Eq 4]}$$

where

$$\phi = k_l a X^* + \frac{Q}{V_R}X_o \qquad \text{[Eq 5]}$$

and

$$\theta = k_l a + \frac{Q}{V_R}$$
[Eq 6]

In this method, the influent to the reactor was nitrogen-sparged water, and the reactor was sparged with oxygen. Gas flow to the reactor was measured and controlled with mass flow controllers, DO into and out of the reactor was measured with DO electrodes, and the stir rate was set at 400 rpm using a photo-tachometer. The integrated equation was fit to the observed oxygen accumulation curve using $k_l a$ as a fitting parameter. The dynamic method gave more consistent results, and more closely simulates the actual experiments, because of the higher transfer rates. The $k_l a$ values were measured for three relatively low flow rates, chosen to avoid acetaldehyde sparging in the anticipated DNT experiments. Gas flow rates (Q_g) of 40, 60, and 80 mL/min were used, resulting in determinations of $k_l a$ values shown below for 30 mL/min liquid flow and 400 rpm stir rate.

Q_g = 40 mL/min $k_l A$ = 0.102 ± 0.020 min^{-1} (3 experiments)

Q_g = 60 mL/min $k_l A$ = 0.153 ± 0.001 min^{-1} (2 experiments)

Q_g = 80 mL/min $k_l A$ = 0.191 ± 0.014 min^{-1} (5 experiments)

Acetaldehyde/Hydrogen Peroxide/Ultraviolet Radiation (APU) System

Mathematical Analysis To Identify Oscillating/Bistable Systems

No experimental methods have been found to search for multistability. Virtually all of the multistable systems have been found by accident during experiments, by extension from known systems, or by mathematical analysis of reaction system rate equations. The impetus for investigating the possibility in the present system was the similarity of several experimental observations to behavior often encountered in multistable systems. Aside from a few unsuccessful attempts to simulate prior conditions and behavior, the main thrust of the present multistability investigation was through a mathematical approach.

The set of equations used to represent the system of reactions can be represented by a surface in the hyperspace that has the variables as its axes. This surface cannot be visualized since it has more than three dimensions, but if it could, it would look different for each set of parameters (rate constants, etc.) selected from parameter space. For example, if the system had only two dependent variables, it could be represented for one set of parameters by a two-dimensional.

plot. Changing the value of one parameter by discrete amounts could be represented by a stack of two-dimensional plots arranged along an axis representing the value of the parameter, or as a surface using the parameter as the third dimension. Extension to higher dimensionality and a greater number of parameters cannot easily be represented graphically.

Methods were sought to try to determine whether the reaction system of interest has regions of bistable or oscillating behavior. In principle, these methods might be divided into two classifications. The first and more elegant of those would be methods that treat the entire set of surfaces representing the set of equations in parameter space, seeking to analytically determine values of the parameters for which the system would be bistable or oscillatory. Despite a large volume of research on this topic, there are apparently no theorems that generate general methods that can be applied to this approach to analytically locate regions of multistability, and "one simply has to search for interesting behavior"* (i.e., multistable behavior, through individual calculations).

The second and considerably more labor-intensive approach (searching) is to select values of the parameters (rate constants), plug them into the set of equations, and test the resulting equation set for instability, multiple stationary states, etc. Three different methods were used for testing the resulting equations for multistability: Local Stability Analysis, Steady-State Solutions, and Flow Diagrams. These methods are described in more detail below. The labor-intensive nature of searching for multistability can be illustrated by an example. If an equation system had 4 unknown rate constants and only 5 values for each were investigated, that would require testing 625 equation sets. However, testing only 5 values of a rate constant (e.g., 10^5, $10^{5.5}$, 10^6, $10^{6.5}$, 10^7) does not do a thorough job of examining the entire set of surfaces corresponding to the evaluation of the equation set for all values of the parameters, since multistable regions are frequently only a small portion of the parameter space (e.g., Figure 4). It is therefore of utmost importance to limit, to the greatest extent possible, the number and range of rate constant values tested. For this reason, the "Core System" discussed in Chapter 2 was selected as a simpler system containing the essence of the larger system and most likely to exhibit interesting behavior, since it contains the feedback and "flip-flop" mechanisms. The following tests were then applied to the core system.

---

* E. Atlee Jackson, mathematical physicist, expert and author in nonlinear dynamics, and Professor Emeritus, Department of Physics, University of Illinois, personal communication.

Core System Rate Equations – The following rate equations for the core system were derived from the diagram in Figure 6.

$$dB/dt = k_1A + k_{YA}YA + k_rR - k_fB - k_{BX}BX \qquad \text{[Eq 7]}$$

$$dR/dt = k_fB - k_{RD}RD - k_{RX}RX - k_rR \qquad \text{[Eq 8]}$$

$$dY/dt = k_{BX}BX - k_{YA}YA - k_4Y \qquad \text{[Eq 9]}$$

$$dX/dt = k_1a(X^*-X) + (X_o-X) Q/V_R - k_{XB}BX - k_{RX}RX \qquad \text{[Eq 10]}$$

$$dD/dt = (D_o-D) Q/V_R - k_{RD}RD \qquad \text{[Eq 11]}$$

The various species are represented by A=acetaldehyde, B=acetyl radical, Y=acetylperoxyl radical, R=acetylperoxyl hydrate radical, X=oxygen, and D=DNT. This system of equations is considerably simplified compared with the set from the complete mechanism. Wherever possible, subscripts from the complete mechanism are used, while numbered subscripts are unique to the core system in Figure 6. This system was assumed for the work described in the next two sections.

Local stability analysis

In an attempt to identify regions where bistable/oscillating behavior might occur, the core system, assumed to operate in batch mode, was subjected to local stability analysis (Gray and Scott 1990, p 63) in which the system of rate equations were subjected to tests to determine whether a small perturbation from equilibrium concentration will continue to grow (system unstable) or decay back to the equilibrium value (system stable). This analysis is carried out numerically, which means that values must be selected for the rate constants, for substitution into the rate equations. In many cases, these rate constants are not available from the literature; therefore, a range of values over several orders of magnitude must be tried. To completely span the region of parameter space most likely to represent reality, all possible combinations of the values shown in Table 1 were tried. These calculations did not identify any points that demonstrated instability. This result was not unexpected, since instability is more often found in open (i.e., flow) systems in which reactant replenishment is possible. However, oscillations can occur in batch systems (e.g., the popularized demonstrations carried out in flasks and petri dishes), and failure to locate regions of bistability does not necessarily mean that there are none.

Table 1. Values of rate constants and initial concentrations used in local stability analysis.

$k_1 = 6.2 \times 10^{-6}\ s^{-1}$
$k_{RD} = 2.0 \times 10^{7}\ M^{-1}s^{-1}$
$k_{AX} = k_{BX} = 2.0 \times 10^{9}\ M^{-1}s^{-1}$
$k_{YA} = 1 \times 10^{5},\ 10^{6},\ 10^{7},\ 10^{8}\ M^{-1}s^{-1}$
$k_4 = 1 \times 10^{2},\ 10^{3},\ 10^{4}\ s^{-1}$
$X^* = 1 \times 10^{-3},\ 10^{-4}\ M$
$X_o = 1 \times 10^{-3},\ 10^{-6}\ M$
$A_o = 10^{-4},\ 5 \times 10^{-3}\ M$

Similar calculations were carried out for the core system in flow mode. Again, no instabilities were detected for the values of the rate constants used. Again, this result does not prove that none exist, since it is possible that one or more small regions were simply missed, since the different values of the rate constants tried were a half order of magnitude apart. These calculations are extremely tedious, occupying the entire summer work of one graduate student in mathematics, and result in only one number for each test, the sign of which has to be correct to indicate instability. In other words, the test for a particular point gives no indication of whether a region of instability might be "right next door." This approach was therefore abandoned for other approaches that might give more insight.

Steady-state solutions

The second method used to try to locate regions of multistability was the evaluation of steady-state solutions to the rate equations, represented graphically. Although steady-state solutions cannot describe the behavior of the experimental system as a function of time, they can be useful to determine whether multiple states can exist. The rate equations shown above for the core system were partially solved within the steady-state approximation to eliminate all equations except those for DNT and for oxygen, which was solved (rearranged) for D, giving, respectively:

$$D^2 [k_{RD}w_1] + D [w_1w_2 - k_{RD}w_1D_o - k_fk_r + \delta] - D_o [w_1w_2 - k_fk_r] = 0 \qquad \text{[Eq 12]}$$

and

$$D = \{w_1{}^2w_2X\theta - w_1{}^2w_2\phi + w_1w_2Xk_1k_{BX}A - w_1X\theta k_fk_r + w_1Xk_{RX}k_fk_1A + w_1\phi k_fk_r - Xk_1Ak_fk_r(k_{BX}-1)\} / \Gamma \qquad \text{[Eq 13]}$$

where

$$\Gamma = k_D(w_1{}^2\phi - w_1{}^2X\theta - w_1Xk_1k_{BX}A),$$

$$w_1 = \gamma X + k_f,$$

$$w_2 = k_r + k_{RX}X,$$

$$\gamma = k_{BX}(1 - f_{YA}),$$

$$\delta = k_{RD}k_fk_1AV_R/Q,$$

$$\theta = k_1a + Q/V_R, \text{ and}$$

$$\phi = k_1aX^* + X_oQ/V_R.$$

From the definitions of w_1 and w_2 it can be seen that the quadratic equation in D (Equation 12) is also quadratic in oxygen (X) while the D equation (13) is cubic in X in the numerator and quadratic in the denominator. In view of the previous discussion of the role of cubic equations in multistability, this approach appeared promising for finding multistable behavior.

The D values calculated from both the quadratic and first-order D equations (12 and 13) were plotted as a function of oxygen concentration for a given set of rate constants. Since both equations must be satisfied, the points at which the curves intersect are solutions. One such plot is shown in Figure 8 for the values of rate constants and other parameters shown in Table 2, which are values that were determined in the optimization described next. Several other values, including several from Table 1, were also tried, with the same general outcome. For convenience, the calculational program specifies $f_{YA} = (1 + k_4/k_{YA}A)^{-1}$ rather than both k_{YA} and k_4, since only the ratio is important at this level of detail. It can be seen that multiple solutions exist, as shown by two crossings of the curves. However, only one crossing, that of the quartic curve with quadratic root 1, lies in physically meaningful space (i.e., $[O_2] \geq 0$, $[DNT] \geq 0$). The vertical line at about $[O_2] = 0.003$ mM is a vertical asymptote that is approached from either side by the branches of the quartic equation. The crossing of the quartic with quadratic root 2 lies left of the y-axis and actually below the x-axis as well. Other values of the rate constants gave up to four crossings, but in all cases tested by extensive variation of the rate constants, it was not possible to obtain more than one physically meaningful (i.e., >0) solution (i.e., no multiplicity of physically meaningful states was detected). As before, it was not possible to test all possible combinations of all rate constants. In addition, if the core system was shown to have no multistability, it still would not prove that the full system had none. On the other hand if multistability was detected in the core system, it would probably occur in the full system as well.
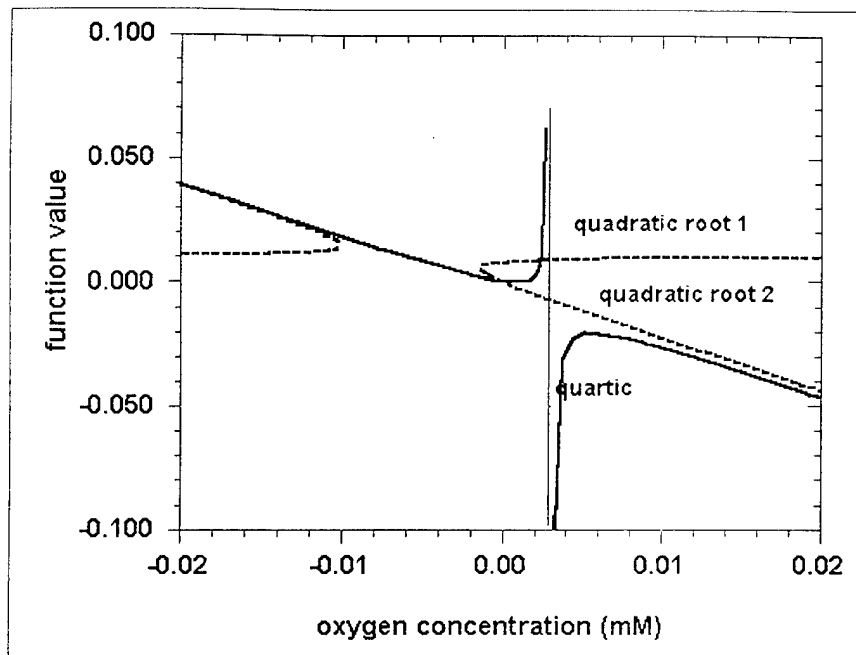
Figure 8. Graphical solution to steady-state simulation of the core system.
The vertical line at x=0.0032 is a vertical asymptote for the two curve
branches (solid lines - quartic) that approach it from either side.

Table 2. Values of rate constants and concentrations used in steady-state simulation of core system.

Rate Constant	Value	Description
k_{BX}	2×10^7 L/mol-s	$B+X \rightarrow Y$
f_{YA}	0.8	Fraction of Y reacting with A
k_f	2×10^4 s^{-1}	$B \rightarrow R$
k_{RX}	5×10^8 L/mol-s	$R+X \rightarrow AA+HO_2$
k_R	3×10^4 s^{-1}	$R \rightarrow B$
V_R	0.265 L	Volume of reactor
Q_R	0.013 L/min	Liquid flow rate
k_D	2.4×10^8 L/mol-s	$R+DNT \rightarrow AA+DNT+H^+$
k_1	1×10^{-4} s^{-1}	Conversion of A to Y by reaction with hydroxyl radical
A_R	1×10^{-3} M	Steady-state A concentration in the reactor
D_o	5×10^{-6} M	Influent DNT concentration
$k_l a$	0.006 s^{-1}	Oxygen mass transfer coefficient in reactor
X^*	3.15×10^{-6} M	Liquid-phase oxygen conc. in equilibrium with sparge gas
X_o	3.15×10^{-6} M	Influent oxygen concentration

Flow diagrams

The third method (Gray and Scott 1990, p 20), discussed in Chapter 2, has some
similarities to the steady-state solution method described above. The steady
state for a continuous stirred tank reactor (CSTR) operated in the flow mode is
reached when concentration accumulation or depletion of reactants is zero; that
is, when replacement of a reactant equals reaction and production of a product

equals washout. A graphical solution can, therefore, be obtained by individually plotting both the chemical reaction portion (R) and the feed/washout portion (F) of the rate equation, versus the extent of reaction ($1-C/C_o$). The points at which the two curves intersect are solutions, and diagrams that give more than one solution indicate multistability. It can be seen from Figure 5 that a special recurve feature must be present in the reaction curve to permit multiple crossings. Flow diagrams for a variety of values of rate constants were calculated and plotted. All lacked the recurve feature and all gave a single solution.

Discussion of negative multistability testing results

No regions of multistability were identified by any of the three methods of stability testing used for the core system in either the batch or flow mode. This does not prove that multistability does not exist in this system – only that it was not found. In addition, failure to find multistability in the core system does not mean that it does not exist in the full reaction system for the values of the rate constants tested. Other evidence discussed in Chapter 2 still seems to support the possibility of multistability. One argument is the occurrence of an obvious feedback step in the reaction mechanism, analogous to that shown in Chapter 2. The sequence

$$OH + A \rightarrow B$$

$$B + X \rightarrow Y$$

$$Y + A \rightarrow B + W$$

$$B + X \rightarrow Y$$

$$Y + A \rightarrow B + W$$

has the sum stoichiometric reaction

$$OH + 3A + 2X + 2B \rightarrow 3B + 2W$$
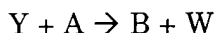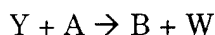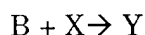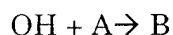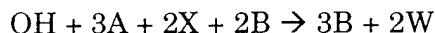
which represents an amplification of B. Furthermore, the entire chain reaction was initiated by only one OH, is supplied with reactants as long as oxygen and acetaldehyde are present, and appears to be limited only by competition for B by other species.

This amplification in B is analogous to the well-known iodate/arsenite chemical "clock" (Gray and Scott 1990, p 13), which has an amplification in I^-:

$$IO_3^- + 5\ I^- + 6H^+ \rightarrow 3\ I_2 + 3H_2O$$

$$AsO_3^{3-} + H_2O + I_2 \rightarrow AsO_4^{3-} + 2H^+ + 2I^-$$
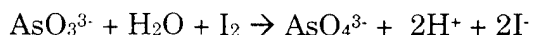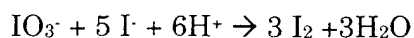
which, when added together, has the sum stoichiometric reaction

$$IO_3^- + 5I^- + 3AsO_3^{3-} \rightarrow 3AsO_4^{3-} + 6I^-$$
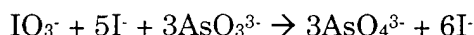
It thus appears that, despite the fact that it has not been found, multistability behavior seems very likely to occur somewhere in this system, and further multistability testing of the more complicated system is desirable.

Determination of Unknown Rate Constants

During the course of mechanism development, several reactions were included for which precedent could be found for the reaction or similar reactions, but no measurement of the rate constants had been reported. In a few cases such as k_{SW} (S=superoxide, W=peroxyacetic acid), new reactions were postulated during this investigation, and it was desirable to provide evidence for the reaction, in addition to measurement of the rate constant. In another case, the reaction of PAA with acetaldehyde, values of k_{AW} had been reported under considerably different conditions, but the rate constant was measured again, to ensure that under the conditions of the present study, this reaction was not occurring at a significant rate in samples awaiting analysis. In many cases, estimation of values for particular rate constants within an order of magnitude with reasonable certainty is possible when values are available for similar compounds. Two examples of this situation are (1) postulating the reaction of the reducing 1,1-dihydroxyethyl radical with hydrogen peroxide by analogy with the reaction with 1-hydroxyethyl radical (Seddon and Allen 1967), and (2) the reaction of dioxygen with carbon-centered radicals to form peroxyl radicals, which occurs at a near diffusion-controlled rate for most carbon-centered radicals (von Sonntag 1987, p 65).

As will be seen later, values for several rate constants were determined by various means during the course of model development. It was known early in the project, however, that values of the following rate constants would be important to the final modeling effort, and individual series of experiments were designed for their measurement. An added complication results from the known formation of adducts between carbonyl compounds and hydrogen peroxide, in the same

manner as aldehydes form hydrates. For this reason, the equilibrium constant for this reaction was investigated and implications of this reaction were explored. Abbreviations and subscript letters are listed in Table 3 for the various species of interest in this study.

Table 3. Abbreviations and subscripts for chemical species.

Species Type	Species Chemical Formula (1)	Species Name	Abbrev. in text (2)	Subscript in equations (2)
inorganic	HO·	hydroxyl radical	OH	O
	HOH or H_2O	water	n/u	n/u
	O_2	oxygen or dioxygen	X	X
	O_2·¯	superoxide	S	S
	HO_2·	hydroperoxyl radical	n/u	n/u
	H_2O_2	hydrogen peroxide	P	P
	CO_2	carbon dioxide	n/u	n/u
organic compounds	HCHO or CH_2O	formaldehyde	F	F
	HCO_2H	formic acid	n/u	n/u
	CH_3CHO	acetaldehyde	A	A
	$CH_3C(OH)_2H$	1,1-dihydroxyethane or acetaldehyde hydrate	H	H
	CH_3CH_2OH	ethanol or ethyl alcohol	E	E
	$CH_3CH(OH)O_2H$	1-hydroxyethylhydroperoxide	M	M
	$CH_3C(O)OH$	acetic acid	AA	n/u
	$CH_3C(O)O_2H$	peroxyacetic acid or peracetic acid	PAA	W
	$2,4-(NO_2)_2\phi CH_3$	2,4-dinitrotoluene	DNT	D
organic radicals	CH_3·	methyl radical	n/u	n/u
	$CH_3C(O)$·	acetyl radical	B or Ac (in compounds)	B
	$CH_3C(O)O$·	acetate radical or acetoxyl radical	n/u	n/u
	$CH_3C(O)O_2$·	peroxyacetyl radical	Y	Y
	$CH_3CH(OH)$·	1-hydroxyethyl radical	G	G
	$CH_3C(OH)_2$·	1,1-dihydroxyethyl radical	R	R
	$CH_3CH(OH)(O·)$	1-hydroxyethoxyl radical	n/u	n/u
	$CH_3C(OH)(O_2H)$·	1-hydroxy-1-hydroperoxyethyl radical	n/u	n/u

Notes:

(1) Two conventions from organic chemistry have been used for writing formulas in line: (a) a functional group enclosed in parentheses is attached to the preceding carbon atom, and (b) the symbol ϕ is used to denote an aromatic ring.

(2) n/u = not used. No symbol/subscript was required.

Determination of k_{SW}

Experiments were designed in which hydroxyl radical was generated by UV photolysis of hydrogen peroxide, while superoxide was generated by reaction of hydroxyl radical with hydrogen peroxide (nominal concentration 0.01 to 0.1 M) in the solution. Peroxyacetic acid (PAA, represented as W when a subscript) was included at low concentration (30–400 μM) to prevent it from scavenging a significant portion of either the hydroxyl radicals formed or the UV photons passing into the solution, simplifying the kinetic calculations (described in equations 14 to 25). Since the rate of reaction of superoxide with hydrogen peroxide is slow (Bielski et al. 1985 compiled literature values ranging from k_{SP}=0.5 to 3.0 L/mol-s), only 1 to 2 percent of the superoxide was scavenged by hydrogen peroxide, about the same fraction as reacted with PAA. While this extent of scavenging had little effect on the rest of the reaction system, it provided PAA disappearance sufficiently fast for the reaction rate to be measured.

The mechanistic model used is shown in Figure 9. This model leads to the following equation set, where the meaning of the subscripts is O=hydroxyl radical, P=H_2O_2, S=O_2^- (superoxide), W=PAA= peroxyacetic acid). R_p^i is the photolysis rate of compound i, and k_d is the disproportion rate constant for superoxide, which is a function of pH (Bielski et al. 1985, p 1045).
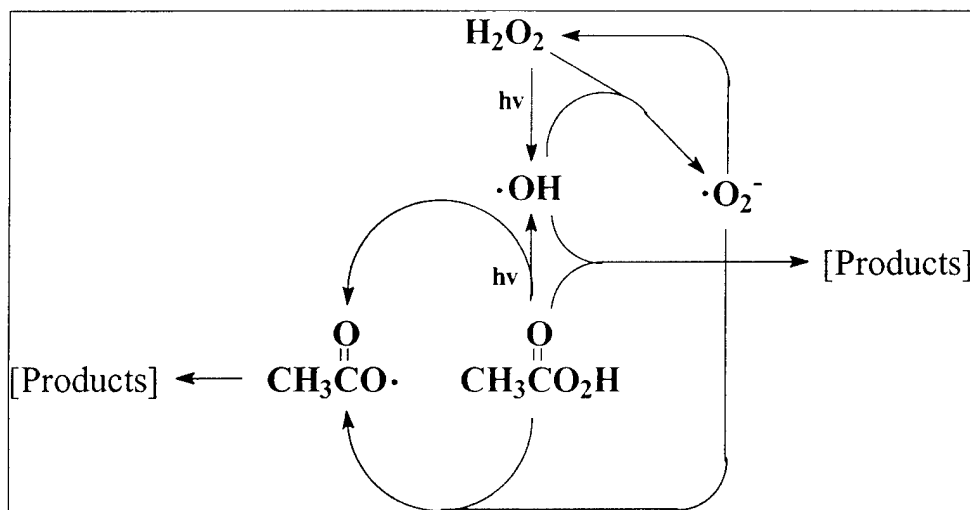
Figure 9. Mechanistic model used to design experiments to measure k_{SW}. H_2O_2 is hydrogen peroxide, •OH is hydroxyl radical, •O_2^- is superoxide, $CH_3C(O)O_2H$ is peracetic acid, and $CH_3C(O)O•$ is acetate radical.

$$dW / dt = -R_p^{W} - k_{OW} OW - k_{SW} SW \qquad \text{[Eq 14]}$$

$$dO / dt = 2R_p^{P} + R_p^{W} - k_{OP}OP - k_{OW} OW \qquad \text{[Eq 15]}$$

$$dP / dt = k_d S^2 - k_{OP} OP - R_p^{\ P}$$ [Eq 16]

$$dS / dt = k_{OP} OP - 2k_d S^2 - k_{SW} SW$$ [Eq 17]

The general form of the photolysis term for species i is

$$R_p^{\ '} = \phi_i F_i I_o$$ [Eq 18]

where ϕ_i is the quantum yield, F_i is the fraction of UV photons absorbed by species i, and I_o is the photon dose rate in einsteins/L-s. The fraction of photons absorbed by species i is given by

$$F_i = f_i (1 - 10^{-A}) \equiv f_i F_T$$ [Eq 19]

where A is the total solution absorbance, F_T is the total fraction of photons absorbed, and f_i is the fraction of absorbed photons that is absorbed by species I having decadic extinction coefficient ε_i:

$$f_i = \varepsilon_i C_i / \Sigma_j \varepsilon_j C_j$$ [Eq 20]

where the sum runs over all UV light absorbers.

The algebraic solution to the quadratic superoxide equation contains a function of the form $\{[1+x]^{1/2}-1\}$, which can be replaced by $x^{1/2}$ when $x^{1/2}>>1$. Reasonable experimental conditions can be chosen ([PAA]<3×10^{-3} M for k_{SW}<1×10^4 L/mol-s) to satisfy this requirement, simplifying the superoxide expression to

$$S = \sqrt{\frac{f_{OP}(f_P + f_W / 2)F_T I_o}{2k_d}} \equiv \beta$$ [Eq 21]

where the symbol β is used in later equations to indicate that the value of the quantity is determined by experimental conditions. The fraction of hydroxyl radical f_{OP} that reacts with hydrogen peroxide is given by

$$f_{OP} = \frac{k_{OP} P}{\Sigma_i k_{Oi} C_i}$$ [Eq 22]

where the sum runs over all species with which OH radical (subscript O) reacts. Substitution of these expressions and the steady-state expression for hydroxyl radical into the peroxyacetic acid and hydrogen peroxide equations gives

$$\frac{\dot{W}}{F_r I_o} = -\tfrac{1}{2} f_W - f_{OW} (f_P + \tfrac{1}{2} f_W) - \beta k_{SW} W \qquad \text{[Eq 23]}$$

and

$$\frac{\dot{P}}{F_r I_o} = -\tfrac{1}{2} [f_{OP} (f_P + \tfrac{1}{2} f_W) + f_P] \cong -1 \qquad \text{[Eq 24]}$$

where experimental conditions can be chosen so that f_{OP} and f_P approach 1, giving the result across the "approximately equal" sign in the above equation, which shows that the hydrogen peroxide disappearance rate is approximately equal to the photon absorption rate. Similarly, choosing a PAA concentration sufficiently low, relative to the hydrogen peroxide concentration, can drive f_W and f_{OW} down to a smaller value than the last term ($\beta k_{SW} W$) in equation 23, allowing an approximate determination of k_{SW} as

$$k_{SW} = \frac{-1}{\beta W} \frac{\dot{W}}{F_r I_o} = \frac{-1}{\beta W} \frac{\dot{W}}{\dot{P}} \qquad \text{[Eq 25]}$$

where the second form is convenient because it automatically incorporates measurement of the UV intensity during the experiment. The error introduced by neglecting the first two terms in the right-hand side of equation 23 can be estimated by assuming that the extinction coefficient and the OH radical rate constant of PAA at 254 nm are approximately the same as those of hydrogen peroxide, 19.6 $M^{-1}cm^{-1}$ (Peyton, Smith, and Peyton 1987) and 2.7×10^7 L/mol-s (Buxton et al. 1988), respectively. This is probably conservative since the OH rate constant for acetic acid is 1.7×10^7 L/mol-s (Buxton et al. 1988). Recent preliminary measurements in this laboratory have given the value $\epsilon^{254}_{PAA} = 19.2$ $M^{-1}cm^{-1}$ for the extinction coefficient of PAA at 254 nm.

A series of ten experiments were carried out, of which, data for three of the first four experiments were unusable, due to the fact that the PAA analytical results were unsatisfactory because hydrogen peroxide was present in a 10^3 excess over PAA. Despite the authors' claims (Davies and Deary 1988), this ratio appears to be just outside the useable range for the kinetic method used for PAA determination under the conditions of this experiment. Another three experiments gave $\beta k_{SW} W$ values that were less than the estimated values of ½ ($f_W + f_{OW}$) as calculated using the assumptions for equation 23, so that the uncertain (i.e., estimated) part of the equation was larger than the quantity being calculated. These values were therefore not considered. Using the above assumptions and data from the four remaining experiments, a range of $500 \le k_{SW} \le 1500$ was determined from three such experiments. The upper bound was determined using

equation 23, assuming the ½ (fw+fow) terms negligibly small, and the lower bound obtained by including the terms, evaluated using the assumptions described above. The upper bound thus obtained is in fair agreement with the preliminary value of 3×10^3 identified by model calibration to the experimental data (see section on **Flow Reactor Studies**). These values are approximately midway between the literature values (Bielski et al. 1985) of $k_{SP}=0.5$ to 3 and $k_{S,AP}=10^6$ for the reaction of superoxide with hydrogen peroxide and acetyl peroxide (AP), respectively. Acetyl peroxide is the third member of the series of peroxides P=HOOH, PAA=AcOOH, and AP=AcOOAc (where Ac = $CH_3C(O)O.$ = acetyl), so it is expected that these two values should bracket the values for PAA.

Determination of k_{AW}

Peracetic acid is known (Schuchmann and von Sonntag 1988) to react with acetaldehyde to yield two molecules of acetic acid.

$$CH_3C(O)O_2H + CH_3C(O)H \rightarrow 2CH_3C(O)OH$$
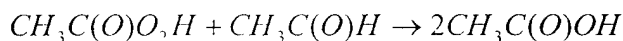
where the convention from organic chemistry is used, that a group shown in parentheses is separately attached to the previous carbon atom. If the reaction was sufficiently fast, the proportion of acetaldehyde, peracetic acid, and acetic acid could change in the samples between the time of sampling and analysis. Although literature values of the rate constant indicated that the amount of conversion would be insignificant as long as the samples were analyzed within a few hours after sampling, measurement of the rate constant under the conditions of the experiments for this study was deemed advisable.

This rate constant was measured by mixing 5 mM acetaldehyde (A) with 5 mM peroxyacetic acid (W) and monitoring the disappearance rate of each compound. The disappearance rates of A and W are given by

$$\frac{dA}{dt} = -k_{AW} AW \qquad \text{[Eq 26]}$$

and

$$\frac{dW}{dt} = -k_{AW} AW \qquad \text{[Eq 27]}$$

so that the disappearance rate of either compound, divided by the product of the concentrations of A and W, gives the value of the rate constant. The value of k_{AW} calculated from the A disappearance rates from three experiments was found to

be k_{AW}=0.018$\pm$0.004 L/mol-s, compared to published values of 0.015 (Schuchmann and von Sonntag 1988) and 0.012 (Allan 1964). Since the maximum acetaldehyde concentrations found in flow experiments were typically 2 mM or less (see discussion below), the pseudo-first order rate constant for W disappearance would be k'_W=k_{AW}A=0.018(2x10^{-3}) s^{-1}=3.6x10^{-5} s^{-1}, or a half-life of 5.3 hours. Since holding times in the HPLC sample tray could easily exceed this period, samples were instead analyzed for PAA immediately by the kinetic method, rather than by HPLC. Half-lives for acetaldehyde would be longer, because of the higher concentration (but same disappearance rate), with calculated values of k'_A=k_{AW}W = 1.25x10^{-6} s^{-1} and a half-life of 154 hours. This is, in fact, a considerably conservative estimate, since the W concentration would be decreasing at the same time, lowering the reaction rate. Thus, after each W half life of 5.3 hours, the A disappearance rate would have dropped by another factor of 2. The 24-hour holding times sometimes experienced by samples for acetaldehyde in the sampling tray are therefore acceptable.

Equations 26 and 27 indicate that peracetic acid and acetaldehyde should disappear at the same rate. It was observed, however, that W always disappeared faster than A, indicating that another reaction was occurring and consuming W on approximately the same time scale. Other reactions such as that of superoxide with peroxyacetic acid, discussed above, are candidate reactions, but no mechanism can be suggested at this time.

Formation of a hydrogen peroxide-acetaldehyde adduct

Acetaldehyde and hydrogen peroxide are expected to form an adduct analogous to the hydrate formation. It is important to know the equilibrium constant for the formation of this adduct, in order to predict whether its formation will impact the chemistry of the acetaldehyde/hydrogen peroxide/UV (APU) system. Kooijman and Ghijsen (1947) reported such a measurement, but the technique used was to measure the total concentration of all solute species by freezing point depression. While ingenious, this technique is not particularly accurate, and depends heavily on correct and complete mechanistic assumptions.

The system assumed by Kooijman and Ghijsen included addition of a second acetaldehyde molecule to the hydroxyhydroperoxide to form a second adduct, but no higher addition products, as have been suggested for more concentrated nonaqueous systems (Swern 1970, p 25).

$$\underset{(A)}{\overset{\overset{\textstyle O}{\overset{\textstyle \|}{}}}{CH_3CH}} + \underset{(P)}{HOOH} \longrightarrow \underset{(M)}{\overset{\overset{\textstyle OH}{\overset{\textstyle |}{}}}{\underset{\underset{\textstyle |}{\underset{\textstyle OOH}{}}}{CH_3CH}}}$$
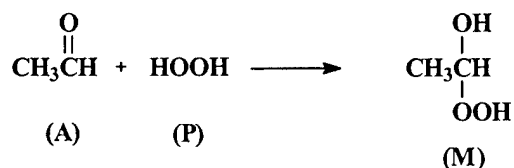
The dissociation constants for the mono- and di-adduct are given by

$$
\underset{\text{(A)}}{\overset{\overset{\text{O}}{\overset{\|}{}}}{CH_3CH}} \quad + \quad \underset{\text{(M)}}{\overset{\overset{\text{OH}}{\overset{|}{}}}{\underset{\overset{|}{OOH}}{CH_3CH}}} \quad \longrightarrow \quad \underset{\text{(D)}}{\overset{\overset{\text{OH} \quad \text{OH}}{\overset{| \quad\quad |}{}}}{CH_3CH \quad HCCH_3}}
$$
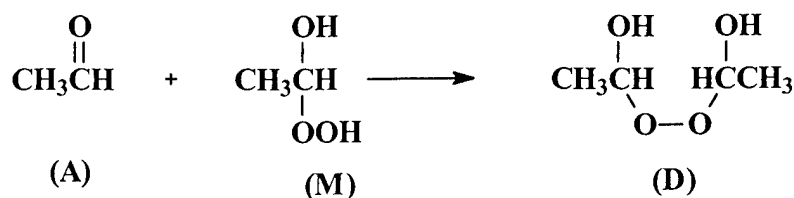
$$K_1 = \frac{[A][P]}{[M]} \quad \text{and} \quad K_2 = \frac{[M][A]}{[D]}$$

for which Kooijman and Ghijsen reported a value of $K_1 = 0.0208$, and the value of $K_2 = 0.0981$ can be calculated from their results, in which the second constant was expressed as PA^2/D rather than MA/D.

In view of the uncertainty of the freezing point depression technique, it was deemed advisable to perform a separate measurement of these equilibrium constants. Formation of the hydroperoxide was found in this study to complicate the chromatographic determination of acetaldehyde in the presence of hydrogen peroxide, due to dissociation of the adduct to A and P on the timescale of the chromatographic process (reaction half-life of about 19 min with 20 mM H_2O_2) once the sample was injected, thereby interfering with quantitation. The analytical method was therefore modified by adding a buffer to the mobile phase to catalyze M breakdown when quantitation of A was desired, and by acidifying the mobile phase and placing the HPLC mobile phase and column in a refrigerator or cold room to retard dissociation of the adduct(s) when their quantitation was required. In this manner, an approximate measurement of the equilibrium constants was made by assuming that the extinction coefficient of the adducts was similar to that of hydrogen peroxide, since the adducts were also peroxides and the organic component was an even worse chromophore than is the peroxide group -OO-. The validity of this assumption was verified by measurement of the UV spectra of acetaldehyde-hydrogen peroxide mixtures.

The resulting chromatograms revealed five peaks instead of the four that would be consistent with the mechanism assumed by Kooijman and Ghijsen. Higher adducts are known to form in neat systems (Swern 1970, p 25). However, the two smallest peaks were observed to always form exactly in parallel (kinetically) and in the same proportion, consistent with their being geometric isomers of Di. If so, then their concentrations could be lumped together, and Kooijman and Ghijsen's mechanism would be correct. Under these assumptions, the data in this study yielded values of $K_1 = 0.0260 \pm 0.0221$ and $K_2 = 0.206 \pm 0.101$, in fair

agreement with the values of Kooijman and Ghijsen. Because of the fewer number of experiments, the spread in experimental values, and the assumption about the extinction coefficients in this study, the K_1 value of Kooijman and Ghijsen was used in further calculations. The value of K_2 was not needed, since the contribution of the diadduct was only a few percent and would not be kinetically significant in the system reported here.

Implications of acetaldehyde-hydrogen peroxide adduct formation

It will be shown in a later section that adduct formation was insignificant under some conditions and quite significant under others. Therefore, the possible effects of photolysis, redox reactions, and hydroxyl radical chemistry must be considered. As will be seen, the inclusion of the reactions of M complicates the modeling of the acetaldehyde/OH radical reaction system considerably, introducing many additional unknown rate constants. It is therefore essential to understand this subsystem in order to identify which reactions may be disregarded in the final mechanistic model.

Photolysis of 1-hydroxyethylhydroperoxide (M) should proceed as with any peroxide, breaking the O-O bond to form a hydroxyl radical and an organic oxy-radical (Figure 10), for which three fates are most likely: (1) rearrangement to acetyl hydrate radical, (2) loss of water to form acetyl radical, and (3) reaction of the OH and hydrate radicals in the solvent cage to form acetic acid. Since the organic radical products of steps 1 and 2 are in rapid equilibrium, this sequence is equivalent to photolysis of P followed by reaction with A or H (acetaldehyde hydrate, or 1,1-dihydroxyethane), and thus does not change the outcome much from the rest of the mechanism. Since the third reaction forms acetic acid, it can be shown to be the equivalent of photolyzing P to 2 OH radicals, letting one OH react with A or H and the other react with P. Simulations show that the effect is minimal, representing only about 5 percent of the reaction rate of A and H, and contributing to essentially the same reaction channel as would other pathways. The contribution of M photolysis to OH production is also small compared to that from H_2O_2 photolysis, so that as a first approximation, photolysis of M may be disregarded in the mechanism.

The possible effects of M+OH radical are potentially more significant. OH-radical attack is expected to occur at the lone H-atom on the O-bound carbon atom (Figure 11), producing 1-hydroxy-1-hydroperoxyethyl radical, for which four reaction channels can be postulated. Channel a is the typical reaction with oxygen, followed by elimination of hydroperoxyl radical (HO_2). Channel b is a direct elimination of HO_2 through an intramolecular H-atom transfer, which should be relatively fast, channel c is a O-O bond scission, which seems energetically

unfavorable since it produces OH radical, and channel d is a different intramolecular H-atom transfer which looks reasonable and leads to a lower energy radical. However, channel d was discarded on the basis of mass balance considerations, because the methyl radical is known to further react to produce either formaldehyde or products that would not be identified and would therefore show up as a mass balance defect in the products. Mass balance was typically achieved between A and AA in anoxic experiments and A, AA, and F in oxic experiments, with a low yield of F relative to AA. A higher yield of F would be expected if channel d was an important pathway. Finally, channel a, though reasonable, was discarded because of the low observed PAA yields. Therefore, channel b was assumed in the mechanism used to generate the kinetic model.
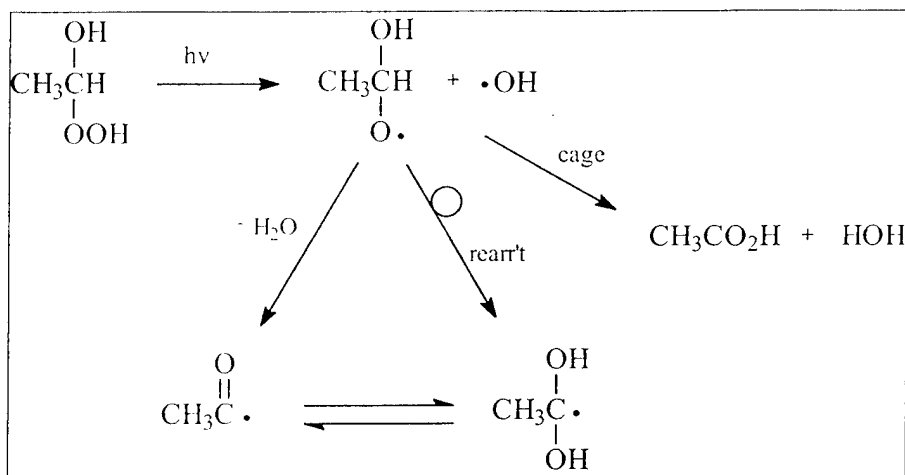
Figure 10. Proposed photolysis pathways for 1-hydroxyethylhydroperoxide $CH_3CH(OH)OOH$. $CH_3CH(OH)O\bullet$ is 1-hydroxyethoxy radical, $\bullet OH$ is hydroxyl radical, CH_3CO_2H is acetic acid, HOH is water, $CH_3C(O)\bullet$ is acetyl radical, and $CH_3C(OH)_2\bullet$ is 1,1-dihydroxyethyl radical.

A third class of reactions must be considered — those in which M reacts as a peroxide with a reducing radical. This class of reactions includes the Haber-Weiss reaction (S+P) since S is the conjugate base of the hydroperoxyl radical. The typical reaction is the same as Fenton's reaction, with a donor giving an electron to the peroxide, which splits the O-O bond with one fragment carrying the donated electron. The rate constant for the reaction between 1-hydroxyethyl (G) and hydrogen peroxide

$$CH_3CH(OH)\bullet + HOOH \rightarrow CH_3CHO + H^+ + HO^- + \bullet OH$$
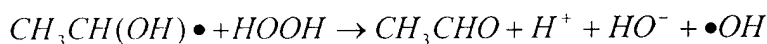
has been reported (Seddon and Allen 1967) to be $k_{GP}=1.5 \times 10^5$ $M^{-1}s^{-1}$. Other examples of this reaction type are known (Ross and Neta 1982) as well. With a hydrogen peroxide concentration of 0.05 M, the pseudo-first-order rate constant for reaction of G with H_2O_2 is $k_{GP}P=1.5 \times 10^5 (0.05)=7.5 \times 10^3$, compared with

$k_{GX}X=4.6 \times 10^9 (3 \times 10^{-6})=1.4 \times 10^4$ at the experimental oxygen detection limit (0.1 mg/L) in some nitrogen-equilibrated experiments. This means that the reactions of the reducing radicals S (superoxide), R (1,1-dihydroxyethyl radical), and G (1-hydroxyethyl radical) with peroxides P (hydrogen peroxide), M (1-hydroxyethyl-hydroperoxide), and PAA (acetylhydroperoxide) must all be considered. Figure 12 shows these reactions, represented by type.
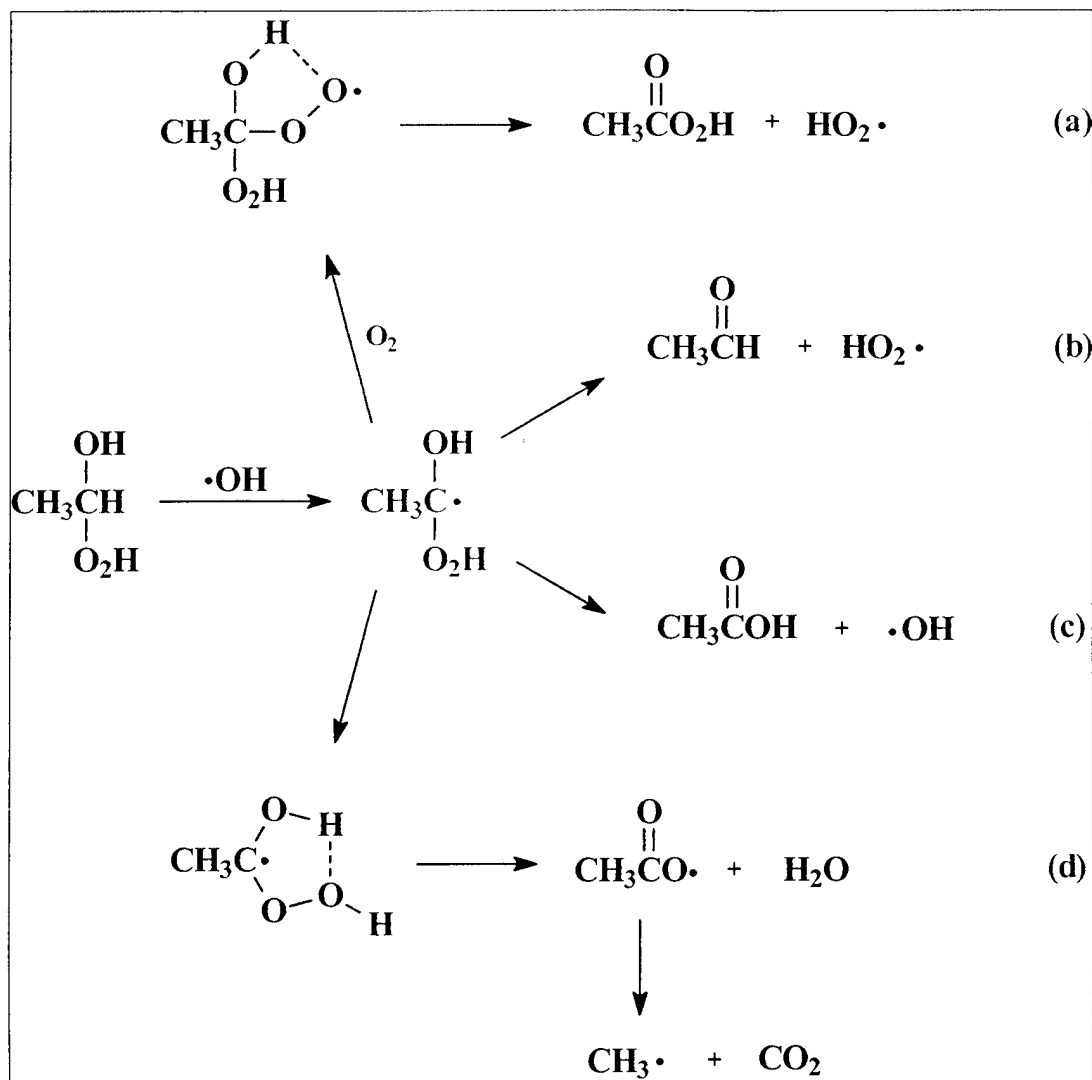
Figure 11. Proposed reaction pathways for 1-hydroxyethylhydroperoxide [$CH_3CH(OH)OOH$] with hydroxyl radical. $CH_3C(OH)(OOH)\bullet$ is 1-hydroperoxy-1-hydroxyethyl radical, $CH_3C(OH)(OOH)O_2\bullet$ is 1-hydroperoxy-1-hydroxyethylperoxyl radical, $\bullet OH$ is hydroxyl radical, O_2 is oxygen, $CH_3C(O)OOH$ is peracetic acid, $HO_2\bullet$ is hydroperoxyl radical, $CH_3C(O)H$ is acetaldehyde, $CH_3C(O)OH$ is acetic acid, $CH_3C(O)O\bullet$ is acetate radical, H_2O is water, $CH_3\bullet$ is methyl radical, and CO_2 is carbon dioxide.
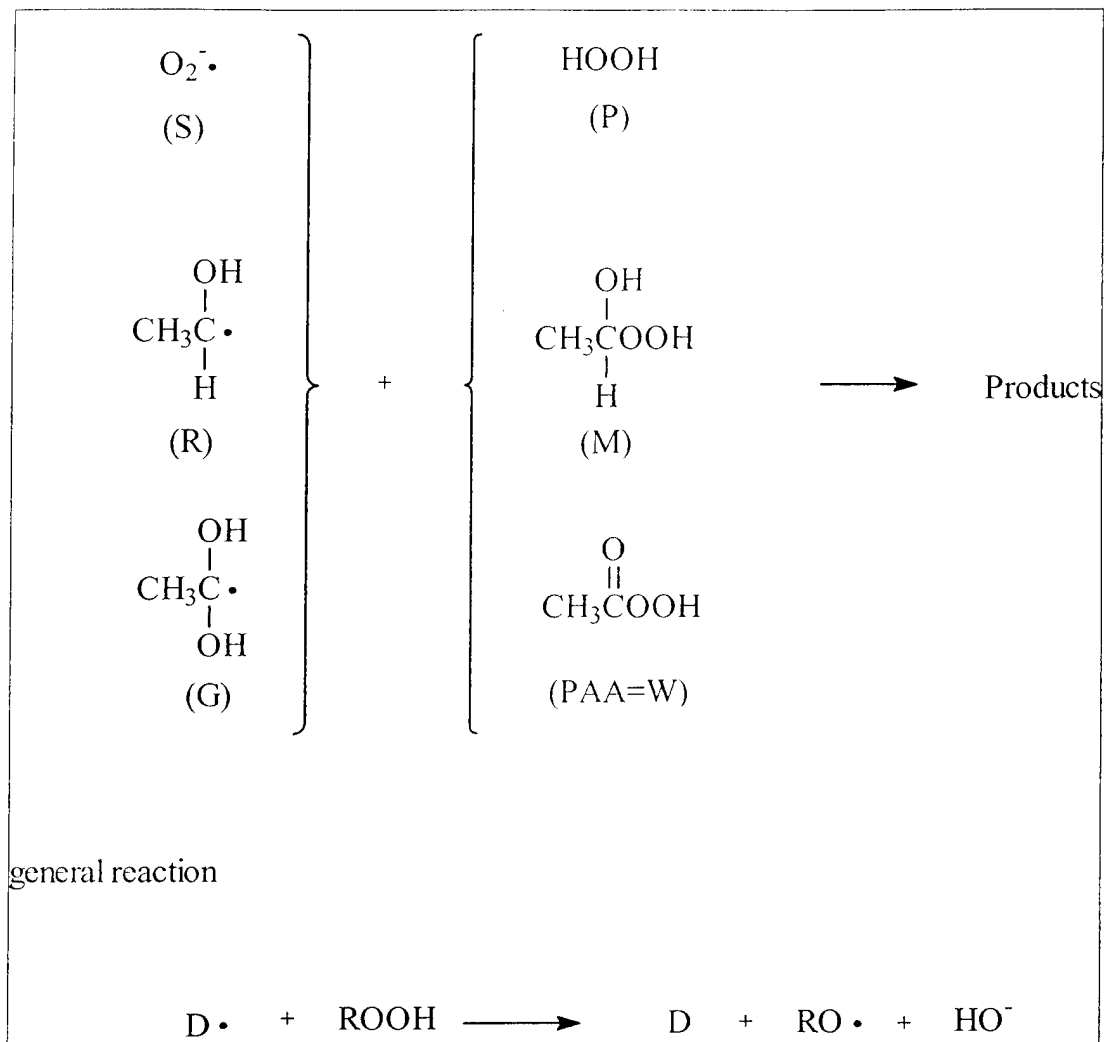
Figure 12. Potential reactions of reducing radicals with hydroperoxides, by analogy with the known reaction of 1-hydroxyethyl radical [CH₃CH(OH)•] with hydrogen peroxide [HOOH]. •O₂⁻ is superoxide, CH₃CH(OH)OOH is 1-hydroxyethyl hydroperoxide, CH₃C(OH)₂• is 1,1-dihydroxyethyl radical, and CH₃C(O)OOH is peracetic acid.

In the reaction of G with P, shown above, hydrogen peroxide was cleaved into two equal pieces, one of which inherited the odd electron. In the case of asymmetric peroxides such as M or PAA, two sets of products are possible, with the lowest-energy pair the more likely. It was assumed in this study that the pair containing hydroxide ion and an organic radical was favored over the pair consisting of a hydroxyl radical and organic oxyanion. This assumption was not tested.

It remains to estimate rate constants for these reactions, since only two of the nine reactions are specifically known. The following basis, a semiquantitative structure-activity relationship (SAR) approach, was used to guide estimates for the assumed rate constant values. In the reaction of a number of known reducing radicals with hydrogen peroxide, more or stronger electron-donating con-

stituents on the radical carbon gave higher rate constants (Ross and Neta 1982). In addition, by comparison of the above reaction with the Haber-Weiss (S+P→X+HO+⁻OH) reaction, it can be seen that organic reducing radicals react faster than superoxide, giving the reactivity order R>G>S. Likewise, the reactivity order of S with the series HOOH<AcOOH<AcOOAc, as discussed earlier, demonstrates the intuitive postulate that electron withdrawing groups increase the rate of acceptance of an electron by a peroxide. This postulation leads to the assumed starting values for these rate constants as shown in Table 4, where known values or values measured during this project are shown in square brackets.

Table 4. Assumed starting values for rate constants.

	M=$CH_3CH(OH)OOH$	P=H_2O_2	PAA=$CH_3C(O)O_2H$
S=$O_2^-\bullet$	negligible	[0.46]	[1.5-3.0x10³]
G=$CH_3CH(OH)\bullet$	1x10⁵	[1.5x10⁵]	3x10⁶
R=$CH_3C(OH)_2\bullet$	1x10⁵	3.0x10⁵	5x10⁶

The values for k_{GM} and k_{RM} were chosen conservatively high, so that any possible impact on the reaction system could be detected immediately by kinetic simulations and values subsequently optimized or determined experimentally. Rate constants for reduction of PAA were held conservatively low, to avoid forcing an impact, but allowing variation of the rate concentration upward to assess its importance. An important difference between superoxide reactions and organic radical reactions is that superoxide was found in preliminary calculations to exist typically at concentrations greater than 10^{-7} M in these systems, while the organic radicals are held to much lower concentrations (10^{-9} to 10^{-13} M) by rapid reaction with oxygen, even in the nitrogen-sparged systems. This point is discussed in more detail in the next section.

Complete mechanism for the APU system

Because of the additional complications discussed above, it is convenient for the discussion that follows to show the complete mechanism as a composite of two figures. The first (Figure 13) represents the APU system without formation of the hydroperoxide $CH_3CH(OH)OOH$ (i.e., M), as is essentially the case at low (2-5 mM) acetaldehyde and H_2O_2 concentrations. The second diagram (Figure 14) represents $CH_3CH(OH)OOH$ (=M) formation and other reactions that result from the presence of that hydroperoxide. DNT has been included in Figure 13 to give an idea of how it fits into the overall reaction scheme. Chemical names, formulas, and abbreviations are listed in Table 3.

Figure 13. Proposed mechanism for the H₂O₂/UV treatment of acetaldehyde [CH₃C(O)H] at low (3-7 mM) concentrations. At H₂O₂ concentrations above 15 mM, the scheme shown in Figure 14 must be included as well. The chemical formulas [subscript symbol] correspond to (left to right, top to bottom) H₂O₂ is hydrogen peroxide [P], HO₂• is hydroperoxyl radical, O₂⁻ is superoxide [S], •OH is hydroxyl radical [O], DNT is 2,4-dinitrotoluene [D], CH₃C(O)OH is acetic acid [AA], CH₃C(OH)₂• is acetyl hydrate radical (or 1,1-dihydroxy-ethyl radical) [R], CH₃C(OH)₂H is acetaldehyde hydrate [H], H₂O is water, CH₃C(O)H is acetaldehyde [A], CH₃CO• is acetyl radical [B], R is acetyl hydrate radical, CH₃C(O)O2• is peroxyacetyl radical [Y], O₂ is dioxygen (oxygen) [X], CH₃C(O)O₂H is peroxyacetic acid =PAA[W], CH₃C(O)O• is acetate radical, CH₃• is methyl radical, CO₂ is carbon dioxide, and CH₂O is formaldehyde [F]. Species with no subscript symbol are products that are not considered important as reactants or do not appear explicitly in the rate equations.

Figure 14. Proposed reaction scheme for formation and reaction of 1-hydroxyethyl hydroperoxide, based on similar reactions reported in the literature. $CH_3CH(OH)OOH$ is 1-hydroxyethyl hydroperoxide, $CH_3CH(OH)O\bullet$ is 1-hydroxyethoxyl radical, $HOOH$ is hydrogen peroxide [P], $HO_2\bullet$ is hydroperoxyl radical, $\bullet O_2^-$ is superoxide [S], $\bullet OH$ is hydroxyl radical [O], $CH_3C(O)OH$ is acetic acid [AA], $CH_3C(OH)_2\bullet$ is acetyl hydrate radical (or 1,1-dihydroxyethyl radical) [R], $CH_3C(OH)(OOH)\bullet$ is 1-peroxy-1-hydroxyethyl radical, H_2O is water, $CH_3C(O)H$ is acetaldehyde [A], $CH_3CO\bullet$ is acetyl radical [B], $CH_3C(OH)_2\bullet$ is acetyl hydrate radical, $CH_3C(OH)(OOH)O_2\bullet$ is 1-peroxy-1-hydroxyethylperoxyl radical, $CH_3C(O)O\bullet$ is acetate radical, O_2 is dioxygen (oxygen) [X], $CH_3C(O)O_2H$ is peroxyacetic acid =PAA[W], $CH_3\bullet$ is methyl radical, and CO_2 is carbon dioxide.

In Figure 13, hydroxyl radical is formed by UV photolysis of hydrogen peroxide, and subsequently reacts with acetaldehyde [CH_3CHO] and its hydrate [$CH_3CH(OH)_2$], formed by the reversible reaction of acetaldehyde with water:

$$CH_3CHO + HOH \Leftrightarrow CH_3CH(OH)_2$$
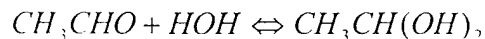
K=H/A=1.2 (Schuchmann and von Sonntag 1988)

Reaction of OH radical with acetaldehyde yields the acetyl radical [$CH_3CO•$] while reaction of OH with hydrate yields 1,1-dihydroxyethyl radical [$CH_3C(OH)_2•$]. Acetyl radical [$CH_3C(O)•$] is an oxidizing radical and is assumed to react with hydrogen peroxide [H_2O_2] at an unknown rate, as well as reacting rapidly with oxygen, as is characteristic of carbon-centered radicals (von Sonntag 1987). Acetyl radical is also in rapid equilibrium with the hydrated acetyl radical [$CH_3C(OH)_2•$], with equilibration times measured in tens of microseconds. The radical $CH_3C(OH)_2•$ is a strong reducing radical, capable of reducing hydrogen peroxide, DNT, oxygen, and many other species. The superoxide [$O_2^-•$] formed by the reduction of oxygen, primarily disproportionates to regenerate hydrogen peroxide and oxygen, but may also react as a reducing radical.

Upon reaction of the acetyl radical [$CH_3C(O)•$] with oxygen [O_2], peroxyacetyl radical [$CH_3C(O)O_2•$] is formed, which is a strong oxidizing radical and should therefore be able to oxidize acetaldehyde to acetyl radical, creating a radical chain reaction. It should also be able to react with acetaldehyde hydrate [1,1-dihydroxyethane] as well. Acetylperoxyl radical [$CH_3C(O)O_2•$] is known to react rapidly with superoxide (k_{YS}~$1x10^9$ M^{-1}s^{-1}, Schuchmann and von Sonntag 1987), and is presumed to react with hydrogen peroxide at an unknown rate. All reactions of acetylperoxy radical with another species are oxidations, forming peroxyacetic acid [$CH_3C(O)O_2H$] as one product. The bimolecular reaction of peroxyacetyl radical [$CH_3C(O)O_2•$] to give acetate radical [$CH_3C(O)O•$] and oxygen, was shown by calculation not to be important, because it is a reaction between two radicals, both of which are present at very low concentrations. Acetyl radical [$CH_3C(O)•$] is in rapid equilibrium with reducing radical $CH_3C(OH)_2•$, as stated above.

Peroxyacetic acid reacts with superoxide with rate constant k_{SW}=500-1500 M^{-1}s^{-1}, determined experimentally in this study. As discussed above and shown in the bottom right of Figure 13, the products are expected to be acetate radical [$CH_3C(O)O•$] and oxygen. From the literature, acetate radical is expected to lose carbon dioxide and yield methyl radical, which reacts with oxygen to produce formaldehyde in a multistep process. Formaldehyde reacts with hydroxyl radical

to produce formic acid, which reacts with hydroxyl radical to give carbon monoxide, but the products of this last reaction are not included in the reaction scheme, as it will be seen that even formaldehyde is far enough down in the reaction scheme that it is seldom present at appreciable concentrations.

Figure 14 shows the subsystem resulting from the formation of the hydroxyhydroperoxide $CH_3C(OH)OOH$ (=M) from the addition of hydrogen peroxide to acetaldehyde across the carbonyl double bond. The adduct M undergoes the photolysis, redox, and hydroxyl radical reactions discussed previously, which are shown as a group in Figure 14. The direct photolysis reactions were determined to be relatively insignificant because of their similarity in outcome to parallel reactions.

Flow Reactor Studies

The acetaldehyde/OH radical system was investigated by performing H_2O_2/UV experiments on aqueous acetaldehyde solutions (APU experiments) while sparging with nitrogen, oxygen, or air. It was verified that acetaldehyde did not photolyze at an appreciable rate under the conditions in this study, compared to the reactions discussed earlier. The APU experiments were performed at low acetaldehyde and hydrogen peroxide concentrations (3 mM nominal) to avoid appreciable formation of the hydroperoxide adduct (M) of acetaldehyde and hydrogen peroxide, eliminating the reactions shown in Figure 14 from consideration. As discussed above, the adduct M has its own hydroxyl radical and photolysis chemistry, which would interfere with rate constant determination in the APU system. Calculated concentrations of the hydroperoxide resulting from mixture of 2.5 mM A and P accounted for only 2 percent of the total speciation of A (i.e., A+H+M), assuming no further reaction to form $A_2P=D$ (shown by calculation to be a good assumption).

Flow reactor studies were conducted in which acetaldehyde, acetic acid, peracetic acid, hydrogen peroxide, formaldehyde, and formic acid were measured, each requiring a different analytical method, in addition to DO, pH, UV absorbance, etc. Each one of these experiments required 4 to 5 days for set up, operation, sample analysis, data analysis, and preliminary data assessment. Before conducting these studies, considerable effort was made to ensure that the analytical methods performed well under the rather unusual matrix conditions present in samples from the reactor during an experiment, so that carbon mass balance could be achieved among the organic reactants and products. Samples were analyzed in triplicate to determine analytical precision.

The results of three experiments are shown in Figures 15, 16, and 17 for experiments using feedstock that was sparged with oxygen, nitrogen, or air, respectively. The discrete data points represent the experimentally determined concentration values of acetaldehyde, acetic acid, hydrogen peroxide, peracetic acid, and formaldehyde, while the lines are the result of model calibration, discussed in the next section on modeling of APU systems. The reactor contents were not sparged, but had a blanket of nitrogen gas passing gently through the reactor headspace, since acetaldehyde was found to outgas from solution rather easily upon direct sparging. Loss of acetaldehyde due to sparging would further complicate the modeling and introduce additional uncertainty. It was later found necessary to correct for acetaldehyde outgassing even without direct sparging. Formic acid concentrations were found to be very low and within the experimental error of concentrations determined in the blank. For this reason, formic acid measurements were later discontinued.
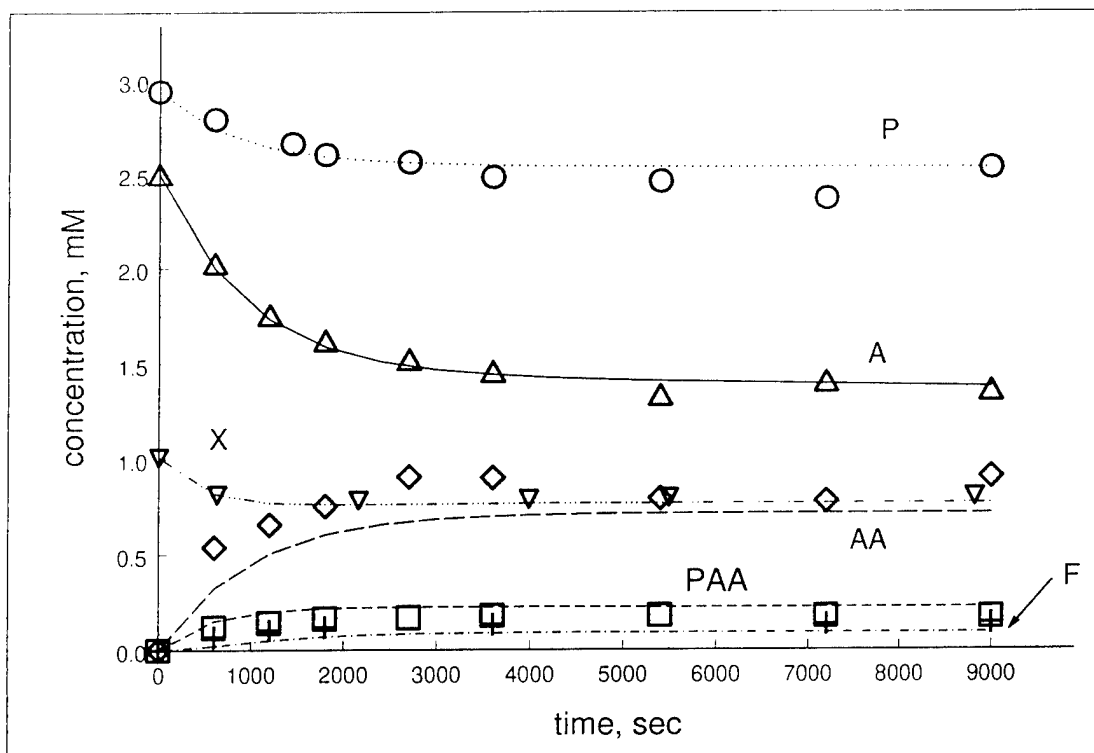
Figure 15. Concentration evolution curves for low-concentration H_2O_2/UV/acetaldehyde flow experiment with oxygen as the equilibration gas. Circles are hydrogen peroxide, triangles are acetaldehyde, inverted triangles are oxygen, diamonds are acetic acid, squares are peracetic acid, and crosses are formaldehyde. Individual symbols indicate experimental values (averaged) and lines represent predictions from kinetic model.
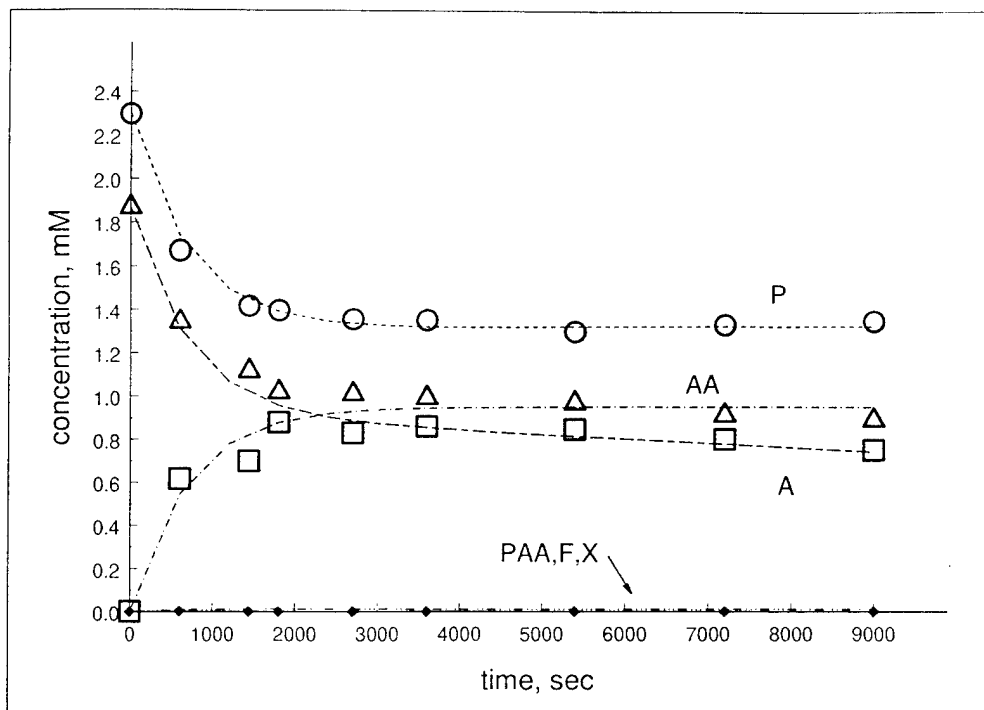
Figure 16. Concentration evolution curves for low-concentration H_2O_2/UV/acetaldehyde flow experiment with nitrogen as the equilibration gas. Circles are hydrogen peroxide, triangles are acetaldehyde, squares are acetic acid, and peracetic acid, formaldehyde, and oxygen concentrations are too low to be resolved on this plot. Individual symbols indicate experimental values (averaged) and lines represent predictions from the kinetic model.
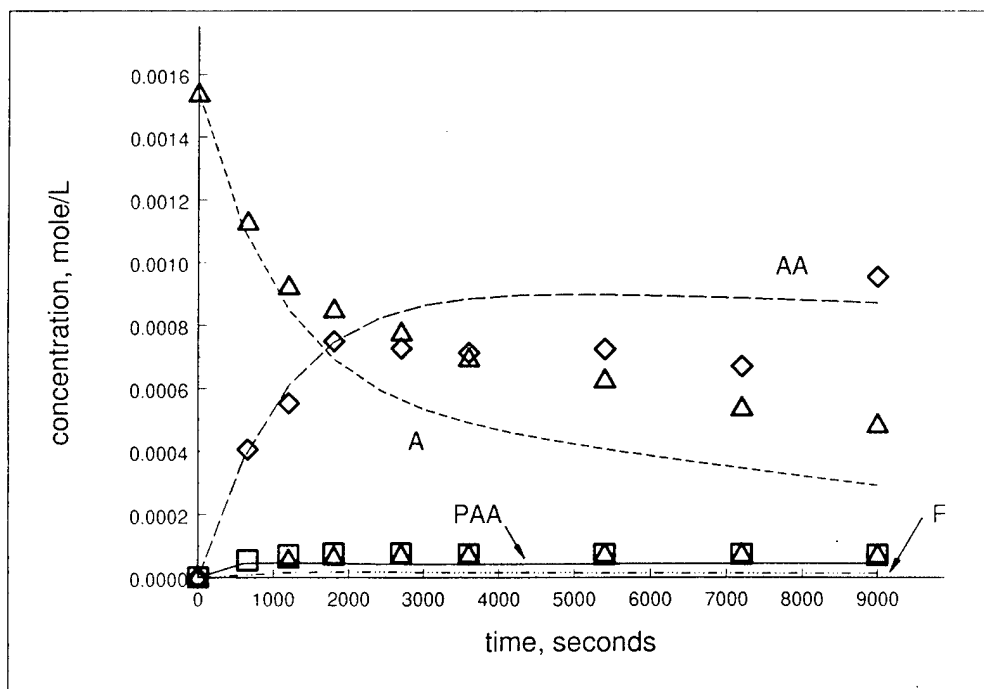
Figure 17. Concentration evolution curves for low-concentration H_2O_2/UV/acetaldehyde flow experiment with air as the equilibration gas. Upper triangles are acetaldehyde, diamonds are acetic acid, squares are peracetic acid, and lower triangles are formaldehyde. Individual symbols indicate experimental values (averaged) and lines represent predictions from the kinetic model.

Table 5. Reactant and product concentrations in flow experiments.

Analyte	Position	Analyte concentrations, mM		
		N_2-sparged	Air-sparged	O_2-sparged
Acetaldehyde	In	1.7	1.3	2.5
	Out	0.9	0.6	1.4
	Difference	0.8	0.7	1.1
Acetic acid	Out	0.80	0.70	0.85
Formic acid	Out	0	0	0 +/- 0.2
Formaldehyde	Out	0.008	0.070	0.135
Peracetic acid	Out	0.00	0.075	0.175
Dissolved oxygen	In	<0.04	0.23	1.01
	Out	<<0.01	0.10	0.80
	Difference	?	0.13	0.21
Hydrogen peroxide	In	2.6	2.3	2.9
	Out	1.3	1.7	2.5
	Difference	1.2	0.6	0.5
Organic mass balance defect	Difference, out - in	0.0	0.1	0.0

It is seen from the data in Figures 15 through 17 and Table 5 that peracetic acid is produced in the oxygenated system and is still detectable at low levels in the air-equilibrated system, while it is below the detection limit in the nitrogen-sparged system. Acetaldehyde destruction is matched by acetic acid production in the nitrogen-sparged system, but is higher in the oxygenated system, while only a slight increase in acetic acid production was observed. Formaldehyde appears in the oxygenated experiment, but only a very little is observed in the nitrogen-sparged experiment. Of particular interest is the significantly larger consumption of hydrogen peroxide in the nitrogen-sparged experiment.

These observations are completely consistent with the proposed limited mechanism for dilute solution (i.e., in the absence of hydroperoxide [M] formation), shown in Figure 13. More acetaldehyde is removed in the presence of oxygen, due to the formation of acetylperoxyl radical, which subsequently attacks acetaldehyde supporting the chain reaction and amplifying the effect of hydroxyl radical formation. Peroxyacetic acid formation is observed in the presence of oxygen, which is required for the formation of peroxyacetyl radical. Formaldehyde is formed from methyl radical, as discussed above, although some could also conceivably be formed by abstraction of a methyl hydrogen in acetaldehyde by hydroxyl radical. However, no intermediate products supporting that abstraction (such as glyoxal or glyoxylic acid) were found (e.g., by DNPH derivatization or anion exclusion chromatography). In addition, the mass balance supports the completeness of the mechanism shown; whereas stable intermediates preceding formaldehyde would be expected to be present in higher concentrations than

formaldehyde, thus causing a mass balance deficit. Both possible reaction pathways for formaldehyde formation require oxygen. Much higher hydrogen peroxide consumption occurs in the absence of oxygen, due to the increased reaction of reducing radicals with hydrogen peroxide resulting from decreased competition from oxygen for the reducing radical. When present, oxygen competes very successfully with hydrogen peroxide for the reducing radicals. The acetic acid contribution is barely changed since it is produced by reaction of either oxygen or hydrogen peroxide with the reducing radical.

Mathematical Modeling of APU System

The objectives of understanding the previous flow data and the search for regions of multistability both require a model that accurately describes the chemical reaction system. The first step in the development of such a model is to model the simplest independent components of the system, which in the present case (after actinometry and mass transfer) is the APU system. After development of such a model, DNT was added into the system and rate constants refined, whereupon the resulting model can be used for exploration of parameter space. The data obtained for the APU system were of sufficient quality that mathematical modeling could be carried out with some confidence that variation of rate constants as parameters could distinguish between pathways and help evaluate rate constants. Contrary to what might be expected by a system with so many rate constants available as variation parameters, it was difficult to find values of the rate constants that fit the model to the experimental data, indicating that it might be possible to determine the rate constants with some accuracy (i.e., that the values were unique). Experimental conditions using the nitrogen- and oxygen-sparged feedstock are sufficiently extreme that it was expected that the chain reaction would dominate the fate of the acetyl radical and all of the PAA-related chemistry in oxygenated solution, while that entire side of the mechanism would more or less "shut off" in the absence of oxygen. In the presence of oxygen, the oxygen so successfully competes for reducing radical that the reaction of reducing radical with anything else (such as hydrogen peroxide) is drastically reduced. This fortunate simplification of the system provides an excellent opportunity to evaluate unknown rate constants, as well as fitting well with the picture of this system as a "flip-flop" or "on-off" mechanism that would be consistent with previous results (Maloney, Boddu, and Peyton 1997).

The oxygenated system was modeled first, varying the unknown rate constants, starting from the estimated or literature values shown in column 2 of Table 6. Values in column 2 that are not marked as a "literature value" (l) or determined in this laboratory (d) were considered to be unknown. Although the software (MicroMath SCIENTIST for Windows) used for integration of the differential

equations includes parameter optimization capabilities, the equation systems under study proved to be too complex to allow utilization of this capability. Therefore, optimization studies were performed manually and were aimed at

Table 6. Values of rate constants in simulations.

Rate Constants	Literature Value or Estimate (1)	Values after APU calibration (2,3)	Values after APUD calibration (3,4)
k_{OA}	3.6×10^9 (l)	3.6×10^9 (nv)	
k_{OH}	1.2×10^9 (l)	1.2×10^9 (nv)	
k_{OP}	2.7×10^7 (l)	2.7×10^7 (nv)	
k_{BX}	2.0×10^9 (e), 1.0×10^8 (l,g)	2.0×10^7	
k_{BP}	1.0×10^4 (e)	9.0×10^4	6×10^4
k_{RB}	1.0×10^9 (e)	5.0×10^8	
k_{RX}	2.0×10^9 (e)	5.0×10^8	
k_{RP}	2.0×10^5 (e)	2.0×10^5	3.0×10^5 (e,s)
k_{YA}	1.0×10^7 (l,g), 3.0×10^3 (l,s)	2.0×10^4	
k_{YH}	1.0×10^5 (e)	1.0×10^4	
k_{YP}	1.0×10^4 (e)	1.0×10^5	
k_{YS}	1.0×10^9 (l)	1.0×10^9	
k_{YY}	1.0×10^9 (e), 5.0×10^7 (l,s)	1.0×10^9	
k_{OF}	1.0×10^9 (l)	1.0×10^9	
k_{SW}	3.0×10^3 (d)	3.0×10^3 (nv)	
k_D	1.48×10^7 (l, pH)	1.48×10^7 (nv,pH)	
k_{OD}	2.4×10^8 (p)		7.3×10^8
k_{RD}	2.5×10^8 (p)		8.0×10^7
k_{SD}	2.5×10^2 (d, upper bound)		10
k_{PA}	0.026 (d)		0.026 (nv)
k_{Mr}	3.5×10^{-4} (d)		3.5×10^{-4} (nv)
k_{OM}	1×10^9 (e)		1×10^9 (nv)
k_{GX}	4.6×10^9 (l)		4.6×10^9 (nv)
k_{GP}	1.5×10^5 (l)		1.5×10^5 (nv)
k_{GD}	2.5×10^8 (p)		2.5×10^8 (nv)
k_{SP}	0.46 (l)		0.46 (nv)
k_{GM}	1×10^5 (e,s)		1×10^5 (nv)
k_{GW}	3×10^6 (e,s)		3×10^6 (nv)
k_{RM}	1×10^5 (e,s)		1×10^5 (nv)
k_{RW}	5×10^6 (e,s)		5×10^6 (nv)

Notes:

1) l=literature value, e=estimate from similar values, s=estimated using semi-quantative structure-activity relationships, g=gas phase value, s=determined in organic solvent, d=experimentally determined, p=value experimentally determined in previous project, pH=pH dependent.

2) After optimization fit for oxygen- and nitrogen-sparged APU experiments. Parameter set BL1a. Model at this point only included the parameters for which there are values shown in column 3.

3) nv=not varied

4) Parameter set BL1h. When no value is shown, it is the same as set BL1a. column 3.

reproducing the final steady-state concentration values, as opposed to the concentration evolution curve describing the approach to steady state. The result of the first round of this parametric variation showed good agreement for most species concentrations except oxygen, for which the predicted value was considerably below the observed concentration. This result suggested that, even though gas was not sparged through the reaction mixture but was gently flowed over the surface in order to sweep gas from the reactor and maintain conditions supporting the initial gas-liquid equilibrium, oxygen consumed by chemical reactions was being replenished by transfer through the gas-liquid interface. The actual rate of oxygen mass transfer under these nonsparging ("gas blanket") conditions was subsequently measured in the laboratory, using the methods described above, and a mass transfer coefficient of 0.0768 min^{-1} was determined for nonsparge conditions. This value is unexpectedly close to the lowest values measured for the sparged system (0.102 min^{-1}), quoted earlier. The use of this measured mass transfer coefficient in the mass transfer term in the existing model gave good agreement between the observed and model-predicted oxygen concentrations.

The data obtained from the nitrogen-sparged system was then fit in the same way, starting with the values determined from the oxygen experiments and varying unknown rate constants that were particularly important in the anoxic system as parameters. Slight changes were made in some of the rate constants determined in the first iteration, and a check was made to verify that these changes did not significantly alter the quality of the fit to the data from the oxic experiment. The final fits resulting from these iterative steps are shown as solid lines in Figures 15 and 16, and the values of the first "baseline" set of rate constants are shown in column 3 of Table 6. The fits to both data sets with one set of rate constants are seen to be reasonably good, with acetaldehyde removal slightly overestimated in the anoxic experiment.

This set of rate constants was then used to simulate the results of an experiment of intermediate oxygen concentration, in which the solutions were first equilibrated with air. Past results had indicated that this system should behave more like the oxygenated system than the anoxic one. It is seen in Figure 17 that acetaldehyde removal was somewhat overestimated, and, as a result, acetic acid production was underestimated. Since considerable effort had gone into arriving at that baseline set of rate constants, it was decided to go on to further calibration with other experimental data from more complicated systems.

DNT Photolysis and H₂O₂/UV Flow Experiments (UD and PUD Systems)

DNT Photolysis

After actinometric experiments (described under **Reactor Characterization**, p 26) were carried out to determine the photon input rate, the model for the DNT photolysis subsystem was calibrated by performing DNT photolysis (UV/DNT or UD) experiments to evaluate the apparent quantum yield of DNT photolysis, since this was expected to be a minor but still significant pathway in the complete system. The apparent quantum yield is based on the ratio of DNT disappearance rate to the photon absorption rate, and thus may describe the final outcome of a series of reactions. This quantum yield is differentiated from the primary quantum yield, which is the quantum yield of the initiating process. All further references to quantum yield in this report refer to apparent quantum yield unless otherwise specified. A series of experiments showed that the DNT quantum yield was different by a factor of approximately two in oxygen-sparged experiments (ϕ_D=5.56$\pm$0.93x10^{-3} [average of three measurements]) compared to nitrogen-sparged experiments (ϕ_D=2.94$\pm$0.44x10^{-3} [average of two measurements]). A similar interesting phenomenon had previously been observed in the 2,4,6-trinitrotoluene (TNT) photolysis system as well.* In addition, it was found that, in the presence of acetaldehyde, values statistically indistinguishable from the higher value of the quantum yield were observed in either nitrogen-sparged (5.50x10^{-3}) or oxygen-sparged (6.47x10^{-3}) experiments (single measurements). A similar effect of hexahydro-1,3,5-trinitro-1,3,5-triazine (RDX) on the measured TNT quantum yield was observed in the previous unpublished work. Results of two DNT flow photolysis experiments, one containing acetaldehyde and one not, are shown in Figure 18, along with modeling results obtained using the above value of the quantum yield. Agreement of the modeling results with the experiments is seen to be good, and the value of ϕ_D=5.6x10^{-3} (molecules/photon) was used in subsequent calculations.

H₂O₂/UV Flow Experiments on DNT

The next step was calibration of the hydrogen peroxide/UV/DNT (PUD) subsystem model, with the primary goal of determination of the rate constant for reaction between DNT and hydroxyl radical. The kinetic model was based on the set

---

* Gary Peyton and Mary LeFaivre, Illinois State Water Survey, unpublished data.

of reactions shown in Figure 19. The upper "square" formed by the cyclic reactions of the $H_2O_2/OH/O_2^-$(POS) system is quite well established in the literature (Buxton et al. 1988), and most of the rate constants are known with confidence, except for that of $S+P \rightarrow OH+HO^-+O_2$ (the "Haber-Weiss" reaction), for which several values ranging from $<10^{-4}$ to 3.7 $M^{-1}s^{-1}$ have been reported (Bielski et al. 1985). Under the experimental conditions used ([DNT]$_o$=3 to 5 μM, P_o=22 to 27 mM), the presence of DNT has little effect on the POS cycle. This fact might be used to obtain a measurement of k_{SP}, since the other rate constants in the upper square are well known.
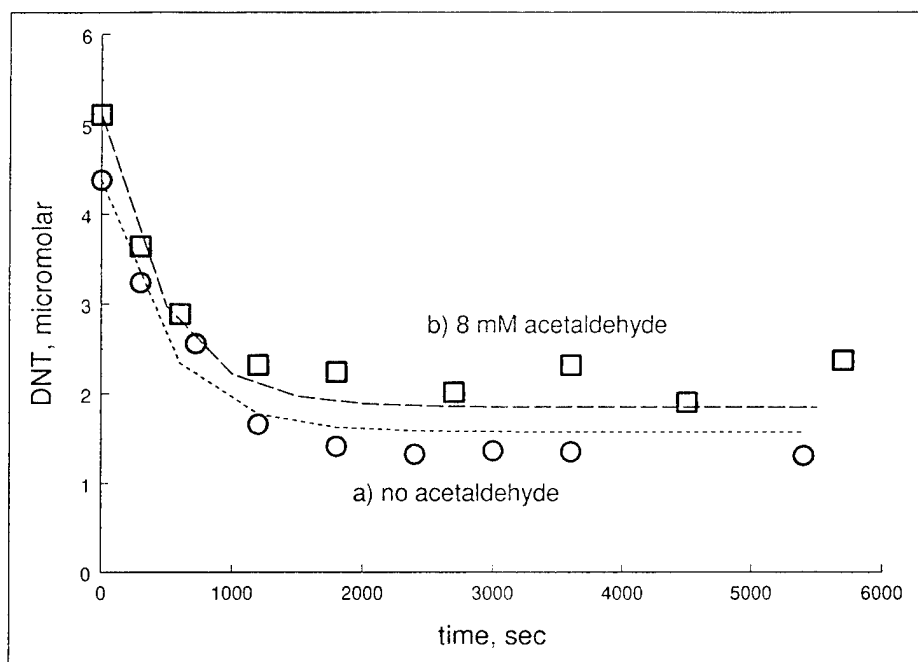
Figure 18. DNT removal in DNT photolysis experiments. a) No acetaldehyde present, oxygen equilibrated, b) 8 mM acetaldehyde present, nitrogen equilibrated. Individual symbols indicate experimental values (averaged) and lines represent predictions from the kinetic model using ϕ_D=5.56x10^{-3}.

The DNT concentration evolution curves for three PUD experiments are shown in Figure 20, where excellent agreement between modeling and experimental results is seen. This modeling resulted in a measured value of k_{OD}=7.3x10^7 $M^{-1}s^1$, compared with 2.4x10^8 $M^{-1}s^{-1}$ measured previously (Maloney, Boddu, and Peyton 1997) using a simpler model on a more complicated system. Thus, the present value is preferred. Agreement for the hydrogen peroxide evolution curves (Figure 21) is good, but all calculated curves for DO (Figure 22) reached steady-state values that were significantly higher than observed values measured with a DO probe mounted in a reactor port. It is not clear what caused this disagreement in the oxygen concentration. The values of k_{OP} and k_d (Table 6) used in these calculations are well established (Buxton et al. 1988; Bielski et al. 1985), including the pH-dependence of k_d. The value used for k_{SP} was 0.46 $M^{-1}s^{-1}$,

a conservative average of several published values. The value of k_{SP}, however, is a moot point in the present case, since the calculated rate of that reaction is three orders of magnitude lower than the flux around the P/OH/S cycle shown in Figure 19, removing the S+P reaction from importance and negating the possibility of measuring k_{SP} in these experiments.

Measurement procedures for experimental quantities of P, I_o, DO, Q, V_R, pH, k_lA, used in this calculation, are all routine and well established with regular quality assurance (QA) procedures, except for k_lA for the so-called "blanket" conditions. The value for k_lA for these conditions was measured only twice. To determine whether this value could cause the agreement problem for DO, k_lA was varied in the model to determine sensitivity of the DO concentration to this value. An increase by a factor of 5 to 0.0065 s^{-1} (0.39 min^{-1}) was required in order to reproduce the experimental oxygen evolution curves (see Figure 22). This value, however, corresponds to more than twice that observed during direct sparging of the reactor contents with an 80 mL/min (0.387V_R/min) gas flow rate, and therefore seems unlikely. The cause of the high calculated oxygen values remains unresolved.
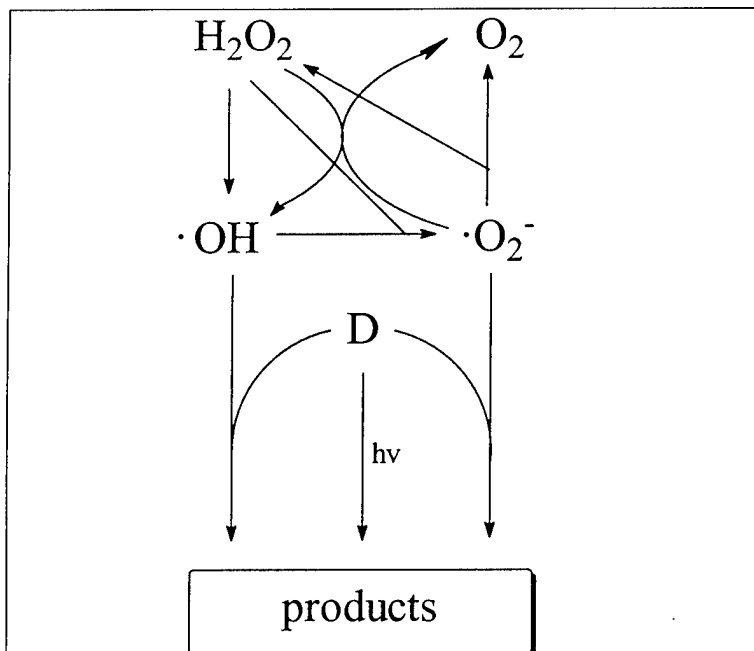
Figure 19. Reaction system during H$_2$O$_2$/UV/DNT experiments.
H_2O_2 is hydrogen peroxide, O_2 is oxygen, •OH is hydroxyl radical,
•O_2^- is superoxide, and D represents DNT.
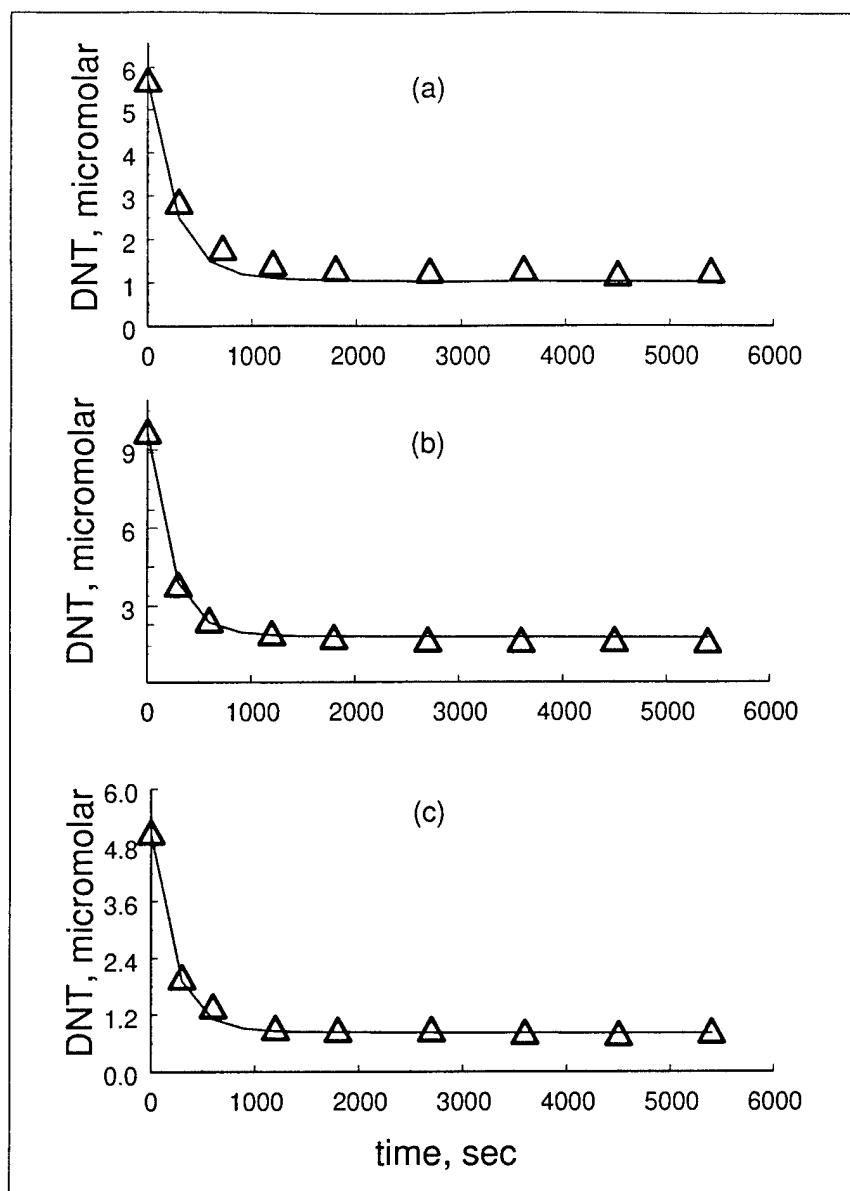
Figure 20. DNT removal in H_2O_2/UV/DNT experiments. (a) $[H_2O_2]_o$=30.5 mM, residence time t_R=19.7 min; (b) $[H_2O_2]_o$ =23.6 mM, residence time t_R=17.5 min; (c) $[H_2O_2]_o$ =22.1 mM, residence time t_R=18.8 min. All experiments run under oxygen blanket. Individual symbols indicate experimental values (averaged) and lines represent predictions from the kinetic model.

The high concentration of superoxide in a system where considerable scavenging of OH radical by hydrogen peroxide occurs, raises the question of participation of a reaction between superoxide and DNT. Superoxide can function as a reducing agent and should be able to reduce DNT at some rate, particularly in view of the electron-poor aromatic ring in DNT. Simulation calculations showed that a rate constant of only k_{SD}=150 L/mole-s would be sufficient for reaction with superoxide to be significant. By comparison, superoxide reduces benzoquinone with a rate constant of about 10^9 (compilation in Bielski et al. 1985, p 1070), so the

above threshold value for DNT, a very electron-poor and easily-reducible compound, is not at all unreasonable. Further calculations performed by setting DNT removal by OH radical to zero (equivalent to assuming that all DNT removal is due to superoxide) in simulating the PUD experiment allowed an upper bound on k_{SD} to be set at 230 L/mole-s.
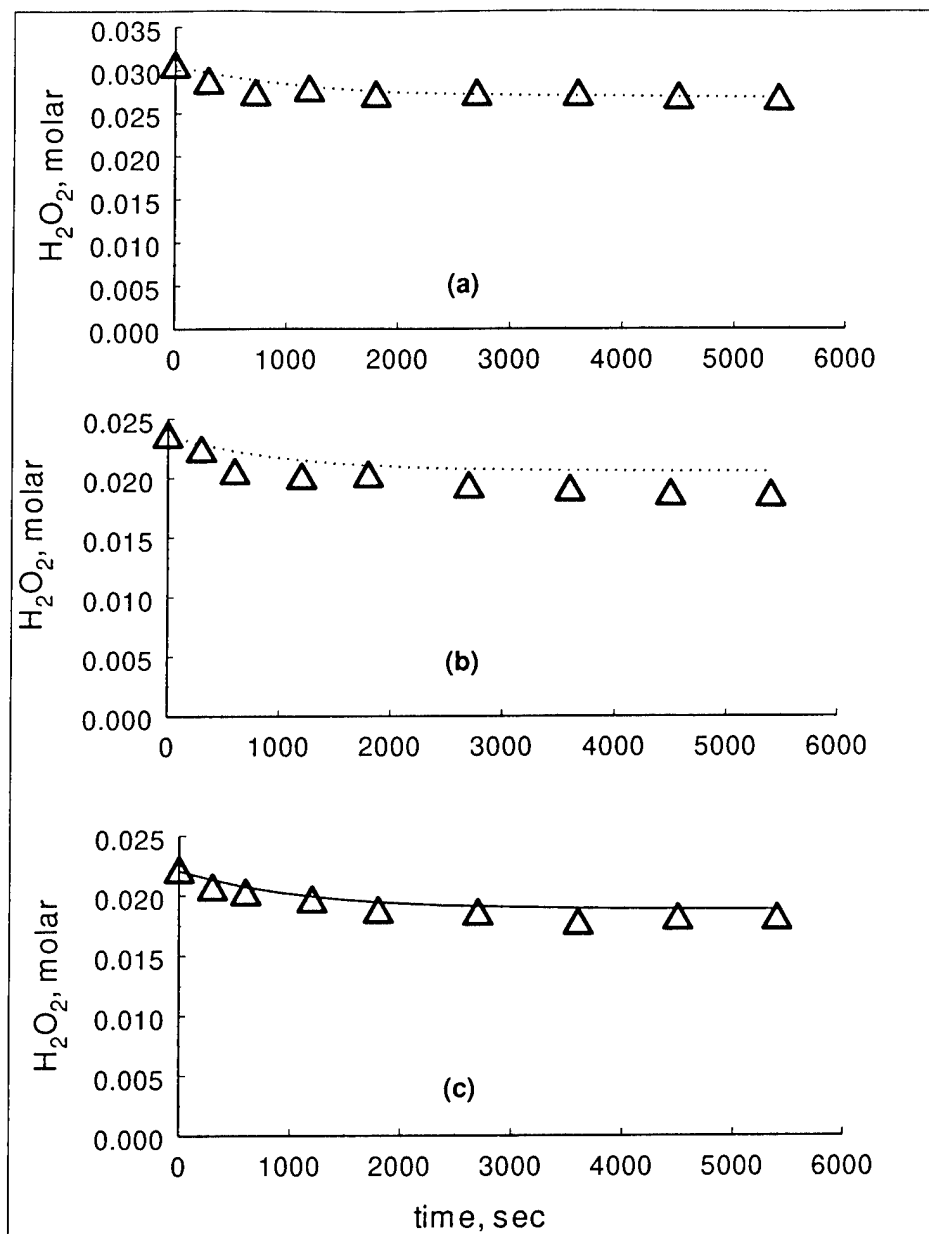
Figure 21. Hydrogen peroxide removal in H_2O_2/UV/DNT experiments. (a) $[H_2O_2]_o$= 30.5 mM, residence time t_R=19.7 min; (b) $[H_2O_2]_o$ =23.6 mM, residence time t_R=17.5 min; (c) $[H_2O_2]_o$ =22.1 mM, residence time t_R=18.8 min. All experiments run under oxygen blanket. Individual symbols indicate experimental values (averaged) and lines represent predictions from the kinetic model.
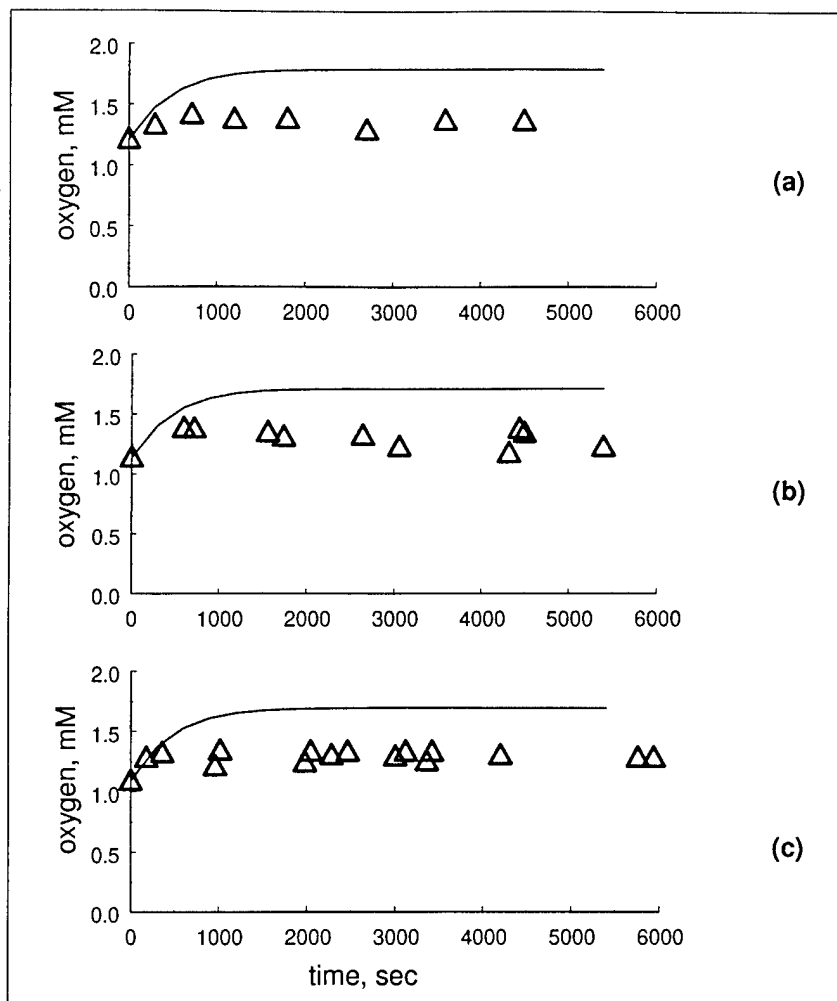
Figure 22. Oxygen evolution in H_2O_2/UV/DNT experiments. (a) $[H_2O_2]_o$ =30.5 mM, residence time t_R=19.7 min; (b) $[H_2O_2]_o$=23.6 mM, residence time t_R=17.5 min; (c) $[H_2O_2]_o$=22.1 mM, residence time t_R=18.8 min. All experiments run under oxygen blanket. Individual symbols indicate experimental values (averaged) and lines represent predictions from the kinetic model.

Since this reaction and rate constant were previously unreported, it was important to investigate them further. Another experiment was designed and carried out at pH 4.8, the pK_a of superoxide (Bielski et al. 1985, p 1044), where the rate of disproportionation of superoxide is greatest. This should lower the superoxide concentration considerably by increasing its rate of disappearance while the production rate remains fairly constant, thereby decreasing the steady-state superoxide concentration and slowing any reaction between superoxide and DNT. The DNT disappearance rate was found in this experiment to be similar to that found in the previous one, supporting the conclusion that reaction between superoxide and DNT was probably not responsible for any significant DNT disappearance. Therefore the reaction was included in the kinetic model, but later optimization steps resulted in a low value (≤ 10 $M^{-1}s^{-1}$) for k_{SD}.

The necessity for modeling in these systems is illustrated by comparison of the
results from a UV photolysis (UD) experiment, an H_2O_2/UV experiment contain-
ing DNT (PUD), and an H_2O_2/UV experiment containing acetaldehyde and DNT
(APUD), shown in Figure 23. DNT removal in the UD experiment is primarily by
direct photolysis, but is very sensitive to formation of a small amount of hydrogen
peroxide (a few μmol/L was semiquantitated in some experiments), which can
photolyze to produce a small dose of hydroxyl radical. Addition of 2 micromolar
H_2O_2 in the UD simulation discussed above increased DNT removal by 15 per-
cent. The DNT disappearance curve obtained from a H_2O_2/UV/DNT (PUD) ex-
periment is also shown in Figure 23 for comparison. Although the curve appears
somewhat similar to that of the UV control experiment, it was found from the re-
sults of simulations using the current model that reaction with OH radical is re-
sponsible for 95 percent of the DNT removal, while DNT photolysis accounts for
only 5 percent of the removal rate. This occurs because the peroxide "masks" the
DNT from UV by absorbing most of the photons. The addition of acetaldehyde to
the reaction mixture at a concentration of 5.5 mM in a subsequent experiment
resulted in a disappearance curve (also shown in Figure 23) very similar to the
previous two, but with a still different distribution of reaction flux between avail-
able pathways. This level of acetaldehyde is sufficient to scavenge 79 percent of
the OH radicals while hydrogen peroxide scavenges another 21 percent with DNT
scavenging only 9×10^{-3} percent Thus, reaction of DNT with OH accounts for only
10 percent of the observed DNT disappearance, photolysis accounts for another 10
percent with the remaining 80 percent accounted for by reaction with reducing
radical. Thus here, as well as throughout this project, widely differing propor-
tioning between suites of reaction channels results in similar-appearing experi-
mental outcomes.
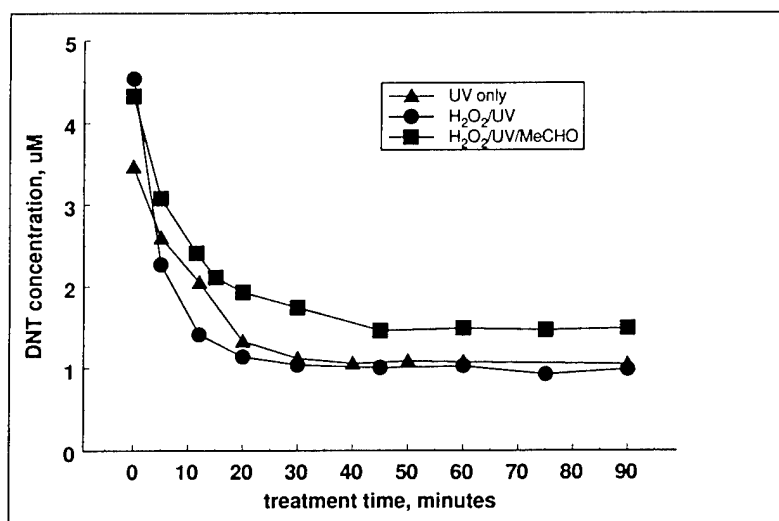
Figure 23. DNT removal in UV, H_2O_2/UV, and H_2O_2/UV/acetaldehyde
flow experiments. Similarity of removal curves and extents of DNT
removal illustrates the need for modeling.

APUD Flow Experiments

Choice of Experimental Conditions

Once the UP, AUP, UD, and PUD systems were characterized and modeled, they were combined to form the APUD system. Several series of flow experiments were designed to identify important questions and rate constants needing evaluation, to provide data for evaluating rate constants and otherwise calibrating the model, and for verification of the model over a range of conditions. Conditions were broken into the ranges in Table 7.

Table 7. Concentrations used in model calibration experiments.

Range	Low		Medium		High	
	conc	symbol	conc	symbol	conc	symbol
DNT (μM)	3-6	D	na	na	90-160	D
H_2O_2 (mM)	2-10	P	10-30	P	30-100	P
Acetaldehyde (mM)	2-6	na	na	na	na	na

na=none in this range   conc = concentration

The important distinction between "high" and "low" concentrations of peroxide is the extent of formation of the adduct hydroperoxide formed by the reaction between acetaldehyde and hydrogen peroxide (see **Formation of a hydrogen peroxide-acetaldehyde adduct** section, p 41). For "low" acetaldehyde concentrations (2-6 mM), typical fractions (F_M below) of remaining A tied up as the adduct M were found (by calculation) to be:

$$P \text{ (mM)} \quad = \quad 2.94 \quad 19.6 \quad 62.6 \quad 101$$
$$F_M \text{ (M/A}_{tot}) \quad = \quad 0.02 \quad 0.08 \quad 0.25 \quad 0.45$$

From these calculations it can be seen that the amount of hydroperoxide present is relatively insignificant at low hydrogen peroxide concentrations, such as those at which the APU calibration experiments were carried out, but represents almost half of the total A (i.e., A+H+M) present at the highest hydrogen peroxide concentrations. It is for this reason that the first set of APU experiments was performed at low hydrogen peroxide concentrations, in order to allow optimization of a smaller set of rate constants. The first set of APUD experiments was performed at "intermediate" P concentrations (20-25 mM) where the fraction F_M was still only about 10 percent set of APUD experiments was run at high P and D to more closely mimic the conditions of the anomolous results in the previous work. No experiments were run at higher A concentrations because the range used already matched that used in previous experiments (Maloney, Boddu, and Peyton 1997). DNT was always (except in the UD series discussed above) used

in a concentration range equal to or smaller than that of P, to avoid conditions under which DNT photolysis was the main DNT removal mechanism.

Parametric Optimization Method

At each stage of model calibration, experimental data were fit with the kinetic model, using unknown reaction rate constants as fitting parameters, constrained where possible by information from the literature such as was discussed earlier for peroxide reduction. Since the optimization was to be carried out manually, it was essential to use good data sets — a fit to incomplete or incorrect data could "mislead" the optimization. Data sets were examined and those with questionable data (improper HPLC performance, scatter in the standard curve, inadequate integrator parameters, etc.) for any of the important parameters (particularly DNT, A, X, and to a lesser extent, AA) were culled, leaving 9 out of 14 experiments for fitting. Parameter optimization for each stage was carried out beginning with the existing "baseline" parameter set (the best resultant fit from the previous optimization stage) and performing simulations using parameter modifications based on educated trial and error. The kinetic modeling program was modified to report instantaneous reaction rates at each time point for which concentrations were reported, so that the fractional contributions of each reaction to the production or consumption of each species could be examined. Thus, if the simulation reported, for example, a steady-state acetaldehyde concentration that was too low, the various sources and sinks of acetaldehyde could be identified, their relative magnitudes examined, and rate constants adjusted to produce a better fit. This process was, of course, iterative since it could not be done simultaneously on all data sets, nor on all reactants. It was done manually, so there was no accurate "steepest descent" or other mechanism to facilitate the fitting process, and no assurance that the fit finally achieved was the best possible fit. Because of the greater number of parameters than measureables, the solution may not be unique. Starting the fitting process with smaller reaction systems, however, helps to minimize this problem by establishing values for important rate constants early in the fitting process.

Results of Parametric Fitting

Figures 24 and 25 show fitting results for nitrogen- and air-sparged experiments, respectively (Experiment No. B-77 and B-78, Table 8). These experiments were among the best fits of the APUD set. The fits for the A→AA→PAA portion of the mechanism are shown in Figures 24 and 25, where the A and AA curves are very similar, despite the fact that the feed solutions were equilibrated with nitrogen in one case and air in the other. The reason for this can be seen from the oxygen concentration curves. Although the steady-state oxygen concentrations are dif-

ferent, they are both above 10^{-4} M, which should be well above the threshold value for reaction with oxygen being the dominant fate of carbon-centered radicals. Both experiments, therefore, lie in the "high oxygen" regime, even though one was presparged with nitrogen. The reason for the high oxygen concentration is the high rate of reaction of oxidizing radicals with H_2O_2, which is present in concentrations sufficiently high enough to be the primary OH radical scavenger. As was seen in Figure 19, OH reaction with H_2O_2 generates superoxide, the predominant fate of which is to disproportionate, yielding H_2O_2 and oxygen. In addition, acetyl radical reacts with H_2O_2 at about 15 percent of the OH reaction rate, adding to oxygen production.

The constant decrease in acetaldehyde concentration in Figures 24 and 25 is due to a continual loss of acetaldehyde from the feed reservoir due to outgassing. As this outgassing rate varied somewhat from day to day, the influent acetaldehyde concentration was measured periodically during an experiment, and a loss rate due to outgassing calculated and used as input to the kinetic modeling program to continually correct the influent concentration to correspond to actual conditions.

Figure 24. Comparison of experimentally observed and calculated values for the species acetaldehyde (A - triangles), acetic acid (AA - diamonds), peroxyacetic acid (PAA — squares and solid line), and oxygen (X — inverted triangle and dot/dash line) in nitrogen-equilibrated system, after calibration of APUD system. Individual symbols indicate experimental values (averaged) and lines represent predictions from kinetic model.
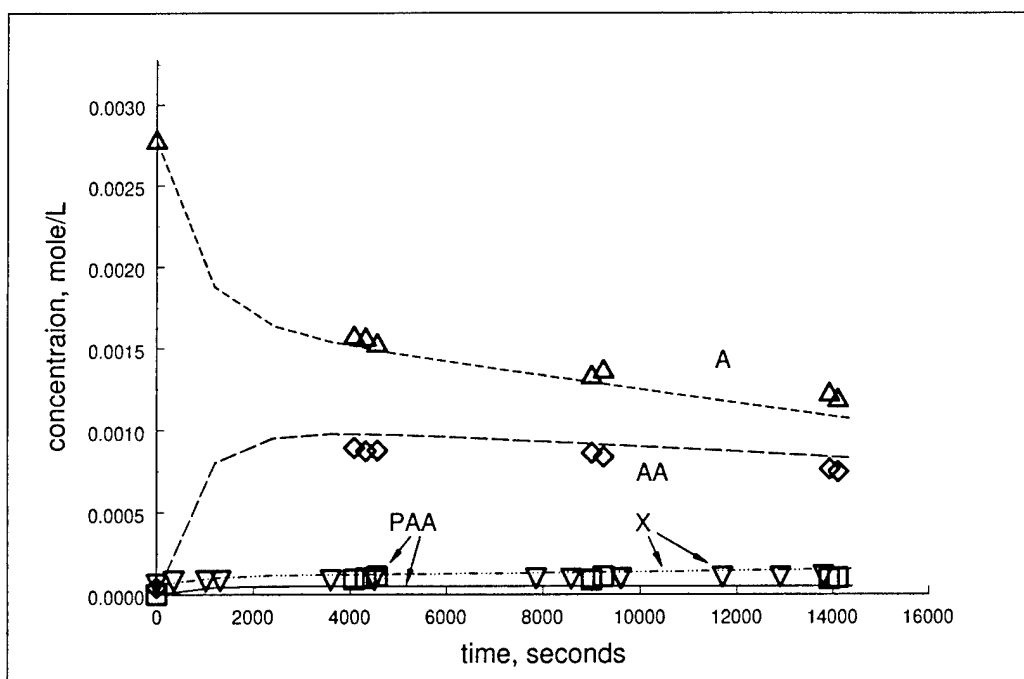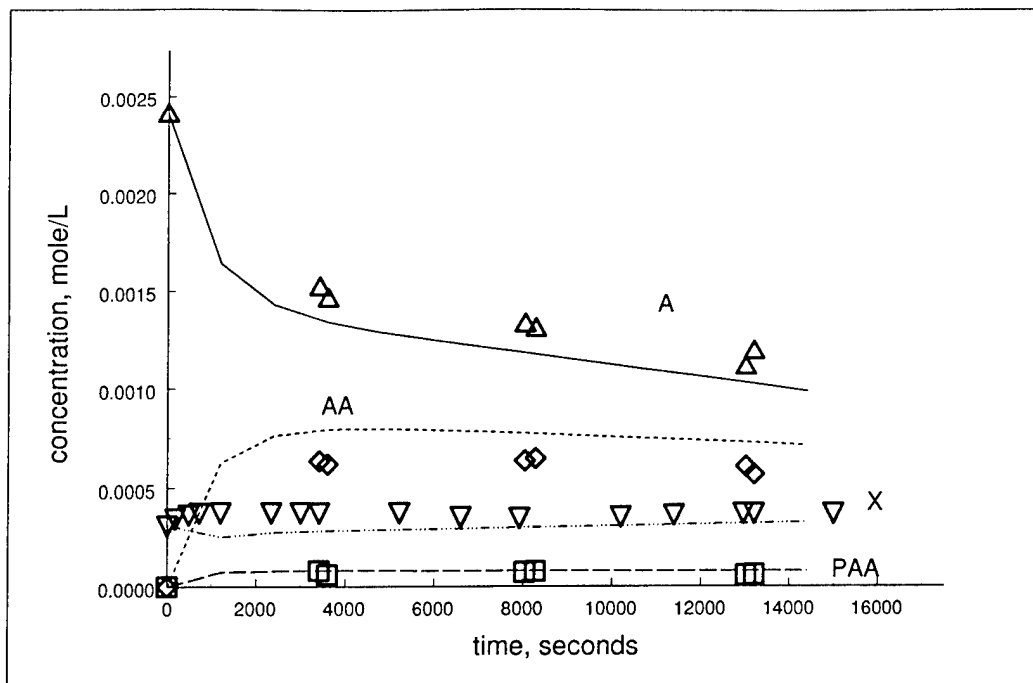
Figure 25. Comparison of experimentally observed and calculated values for the species acetaldehyde (A - triangles), acetic acid (AA - diamonds), peroxyacetic acid (PAA— squares and large dashes), and oxygen (X — inverted triangle and dot/dash line) in air-equilibrated system, after calibration of APUD system. Individual symbols indicate experimental values (averaged) and lines represent predictions from kinetic model.

Table 8. Results of model simulations using BL1g parameter set.

Expt (#, gas)[1]	P_o (mM)[2]	t_R (sec)[3]	DNT[4]			Acetaldehyde[5]		
			D_o (μM)	D/D_o exp	D/D_o calc	A_o (mM)	A/A_o exp	A/A_o calc
B-35, X	2.94	1128	0	n/a	n/a	2.50	0.54	0.55
B-36, N	2.30	1176	0	n/a	n/a	1.87	0.48	0.40
B-38, A	2.42	1182	0	n/a	n/a	1.54	0.31	0.19
B-60a, N	19.6	1242	4.79	0.027	0.054	6.69	0.23	0.33
B-60b, N	19.6	1242	4.79	0.017	0.10	6.69	0.51	0.62
B-74, N	47.4	1018	131	0.56	0.51	3.03	0.68	0.54
B-76, N	57.4	994	113	0.49	0.54	1.87	0.56	0.40
B-77, N	66.3	986	75.3	0.56	0.57	2.78	0.43	0.38
B-78, A	62.6	986	80.0	0.63	0.61	2.41	0.46	0.41

1) X=oxygen, N=nitrogen, A=air.

2) P_o-initial hydrogen peroxide concentration, millimolar.

3) t_R=average liquid residence time in the reactor=V_R(reactor volume)/Q(liquid flow rate).

4) DNT=2,4-dinitrotoluene, D_o=initial DNT concentration (μM).

5) A_o=initial acetaldehyde concentration (mM).

The observed and calculated DNT curves for the same two experiments are shown in Figure 26. Agreement between the calculated and observed values is good. DNT removal is only slightly higher in the nitrogen-sparged water, as expected from the above discussion.
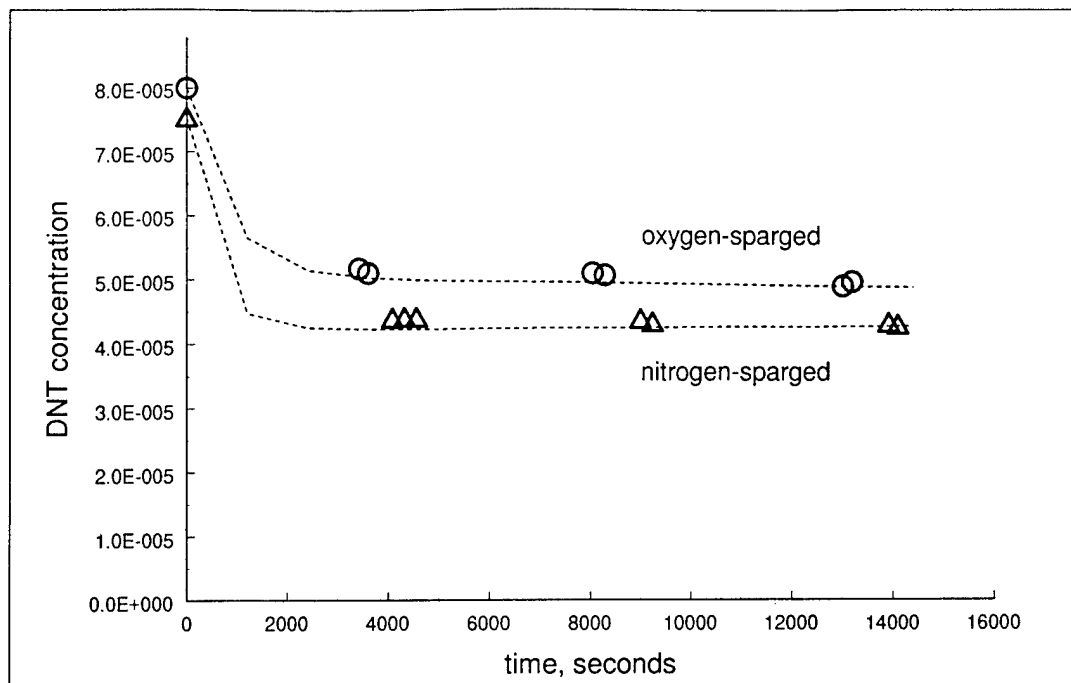
Figure 26. Comparison of experimentally observed and calculated values for DNT in nitrogen- and oxygen-equilibrated system, after calibration of APUD system.

The goodness of fit for the series of nine APU (three experiments) and APUD (six experiments) experiments is shown in Table 8, where the observed (experimental) and calculated values of A/A_o and D/D_o are used as indicators. Acetic acid was not included because of the strong dependence of its calculated concentration on the calculated A concentration. The calculated values of these indicators are plotted versus the observed values in Figures 27 and 28. The correlation line with unit slope corresponds to perfect agreement between calculation and experiment. The distribution in Figure 27 may appear approximately equal above and below the line, but experiment B-60a and B-60b were performed contiguously with the changing of only one setting (liquid flow rate and therefore reactor residence time), so that, from the point of view of varied reaction conditions, the unequal distribution (one set of conditions above and five below the line) probably indicates that significant improvement can be made by further parameter optimization, resulting in less acetaldehyde destruction or more acetaldehyde regeneration (through B+P→A+S). Table 8 shows that acetaldehyde concentrations for experiments 60a and 60b were significantly greater than those for the other experiments.

Figure 27. Comparison of experimentally determined and calculated A/A₀ values for the APU and APUD series of experiments, after model calibration with both series. Symbols are experiment numbers. Line indicates region of perfect agreement.

Figure 28. Comparison of experimentally determined and calculated D/D₀ values for the APU and APUD series of experiments, after model calibration with both series. Symbols are experiment numbers. Line indicates region of perfect agreement.

In the case of the fit to DNT data seen in Figure 28, the next-to-last optimization step (aimed at optimizing A) left all points below the line, so that a decrease in the value of k_{RD} improved the fit considerably for Experiments B-74, -77, and -78, at slight expense to the fit of B-76. At another point in the optimization, when the reactions of reducing radicals with M and PAA had not yet been added into the mechanism, but the other rate constants were at their present values, a fair correlation between indicators for calculation and experiments had been obtained. Adding the R+M and R+PAA reactions to the mechanism (using the initial estimates of their rate constants) without changing anything else, significantly improved the fit for 5 of the 10 indicator values listed in Table 8 for the APUD experiments (A/A_0 and D/D_0 for 5 experiments = 10 indicator values). Three of the values got slightly worse and two values remained the same. This supports the idea that these new reductive reactions are a significant part of the system.

Using the fraction remaining (A/A_0 or D/D_0) as a fitting parameter is probably a more effective strategy for DNT than for acetaldehyde. One reason is that, because of DNT's low concentration and the competition for radicals, DNT removal is expected to be first order, while A removal would have a significant zero-order contribution since acetaldehyde is one of the dominant OH-radical scavengers. Another reason lies in the complexity of the pathways in which A participates. The observation in Figure 27 that the two values lying above the line were for experiments of higher A concentration than those below the line is consistent with zero-order behavior of A. Zero-order behavior means that ΔA (A removal), rather than A/A_0 (fractional removal) would be proportional to the radical dose. This was checked by plotting ΔA_{calc} versus the ΔA_{obs}. The plot, shown in Figure 29, confirms this relationship, indicating that the model predicts too much removal at low A_0 and too little at higher A_0. The agreement between calculation and experiment, however, is still fair to good.

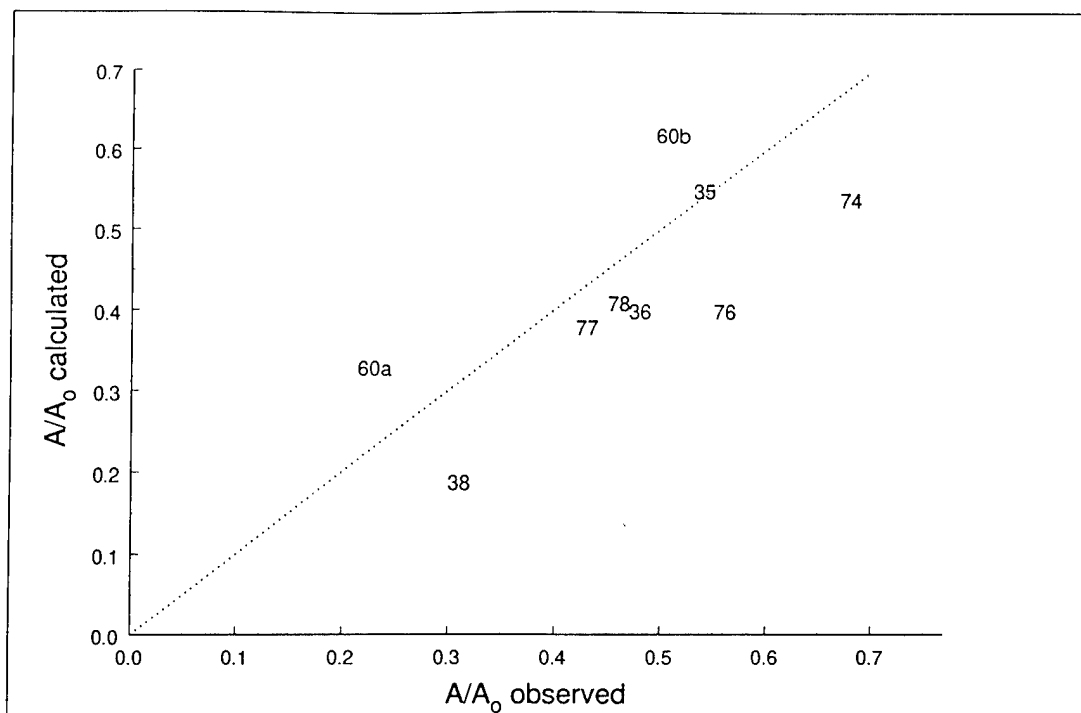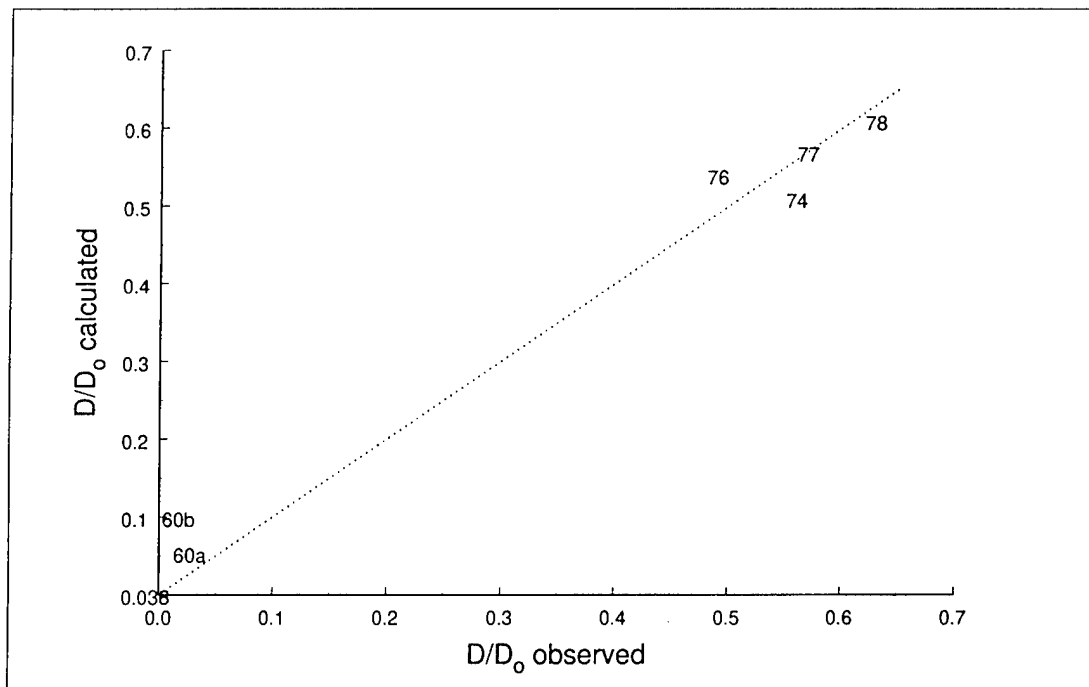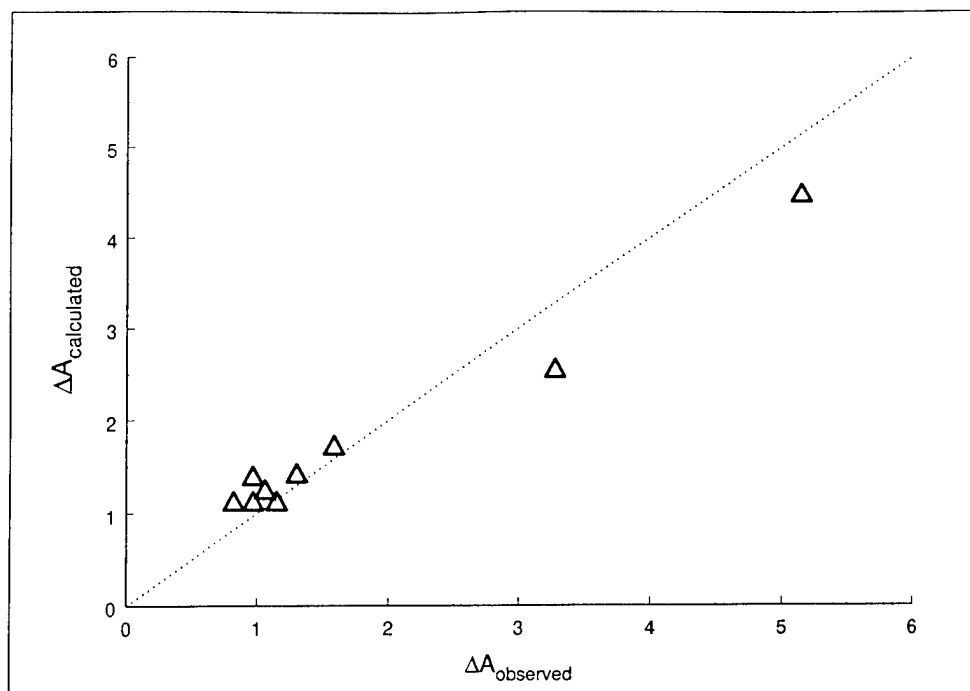**Figure 29. Comparison of experimentally determined and calculated ΔA values for the APU and APUD series of experiments, after model calibration with both series. Line indicates region of perfect agreement.**

Ethanol/Hydrogen Peroxide/UV/DNT Flow Experiments (EPUD System)

Flow Experiments

A series of six flow experiments used a presparge and blanket gas mixture of nitrogen and air, controlled to yield a sparge gas composition of 0, 1, 3, 5, or 20 percent oxygen, in order to span the range of oxygen concentrations in which DNT and organic hydroperoxides become competitive with oxygen for the reducing radical species that are generated in solution. A sparge gas composition of 20 percent oxygen (i.e., air) would give an equilibrium aqueous oxygen concentration of about 2×10^{-4} M O_2, and 1 percent would yield about 1×10^{-5} M O_2, in the absence of chemical reaction. The feedstock contained 8 mM ethanol, 100 mM H_2O_2, and nominally 100 μM DNT, in order to be similar in composition to the feedstock used in ethanol/DNT experiments in earlier projects. Feedstock flow rates were in the range of 12 to 13 mL/min, giving average residence times of about 1,000 seconds (16 min) in the 207 mL reactor. Acetaldehyde was not added directly, but was generated by the oxidation of ethanol. Conditions were otherwise similar to those used in data sets described earlier.

Modeling Parameters

The "baseline" set of rate constants (BL1h, column 4, Table 6), derived by adjusting to fit the UD, PUD, APU, and APUD data sets, was used — along with literature and estimated values for the additional rate constants needed — to fit to the set of data from ethanol/hydrogen peroxide/UV/DNT experiments. The hydroxyethyl radical derived from the reaction of ethanol and OH radical, was given the symbol G in the work presented here. In addition to the rate constants used up to this point, values were also needed for k_{GX}, k_{GD}, k_{GP}, k_{GM}, and k_{GW}, the rate constants for reaction of hydroxyethyl radical G with oxygen, DNT, hydrogen peroxide, 1-hydroxyethylhydroperoxide (M), and peroxyacetic acid (W=PAA), respectively. Literature values were available for $k_{GX}=4.6\times10^9$ $M^{-1}s^{-1}$ (Adams and Wilson 1969) and $k_{GP}=1.5\times10^5$ $M^{-1}s^{-1}$ (Seddon and Allen 1967). Baxendale and Kahn (1969) had reported a value of 3.6×10^8 for k_{GP}, based on kinetic competition between oxygen and p-nitrosodimethylaniline, but Adams and Wilson's value is more in line with later measurements for the reaction of other simple carbon-centered radicals with oxygen (von Sonntag 1987), and was used in all calculations for this study. A value of $k_{GD}=2.5\times10^8$ was determined in an earlier study in this laboratory (Maloney, Boddu, and Peyton 1997), using a simpler model than the present one. The previously measured value of $k_{OD}=2.4\times10^8$ $M^{-1}s^{-1}$ (Maloney, Boddu, and Peyton 1997), also from a simpler model, was replaced with the value $k_{OD}=7.3\times10^8$ $M^{-1}s^{-1}$, measured in the present study (see PUD section in Chapter 4). These values were used to perform simulations of the EPUD data set.

Modeling Results for the EPUD System

Since the UD, PUD, APU, and APUD systems all calibrated with a self-consistent set of rate constants, it was expected that combining the already-calibrated component systems would provide a reasonably good approximation of the EPUD system. This expectation was not found to be the case. Since the new reactions added to the kinetic model involved ethanol, and hydroxyethyl radical (G) was the species primarily responsible for DNT removal, k_{GD} was varied in an attempt to better the fit of the calculated DNT concentration to the data. The best overall fit of the DNT data was given by a value of $k_{GD}=5\times10^7$ $M^{-1}s^{-1}$. This value was considerably lower than the value of 2.5×10^8 reported earlier, but consistent with the lower k_{OD} value found in this study and with the value of $k_{RD}=8\times10^7$ determined in a prior calibration step in the APUD system. This step also improved agreement of calculated acetaldehyde concentrations with observed values somewhat, but the fit was still only fair.

The calculated values and experimental data are compared for the nitrogen- and air-sparged experiments in Figures 30, 31, and 32. The model underpredicts acetaldehyde formation in the nitrogen experiment (Figure 30) by about 20 percent and overpredicts it in the air experiment (Figure 31) by a factor of 2. DNT removal curves (Figure 32) show good agreement for the nitrogen experiment and fair agreement for the air experiment.

Figure 30. Comparison of experimentally observed and calculated values for the species acetaldehyde (A — triangles and dash/dot line), acetic acid (AA — diamonds and large dashes), and oxygen (X - squares) in the nitrogen-equilibrated EPUD system, after calibration of the kinetic model with the APUD system. No PAA was detected.
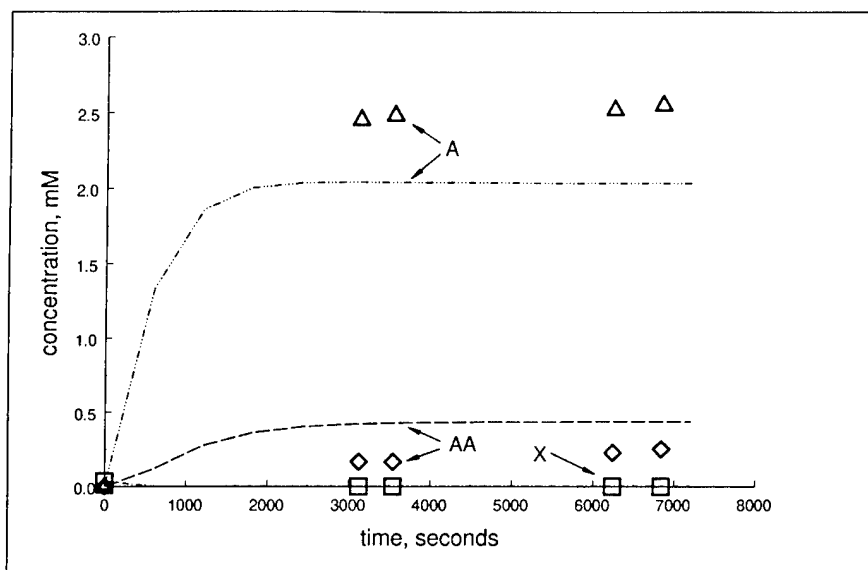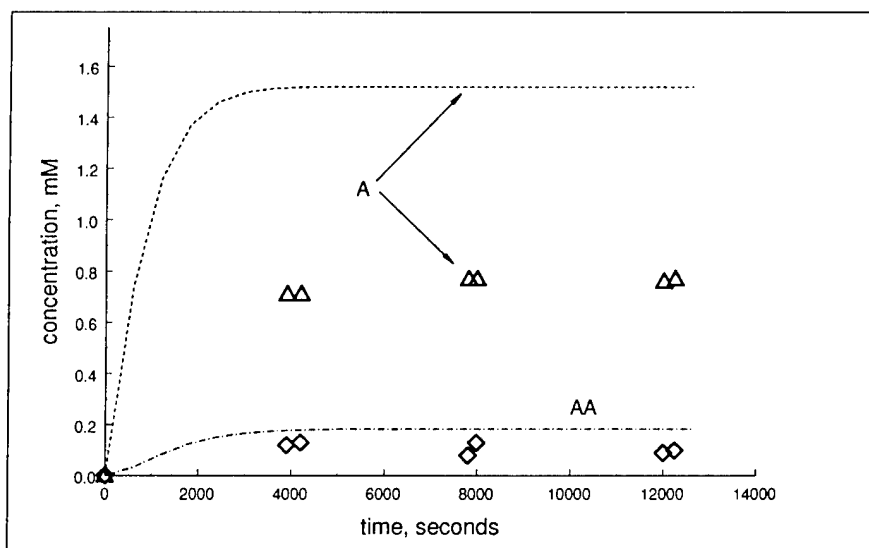

Figure 31. Comparison of experimentally observed and calculated values for the species acetaldehyde (A — triangles and small dashes) and acetic acid (AA — diamonds and dot/dash line) in an air-equilibrated EPUD system, after calibration of the model with an APUD system. No PAA was detected.

DNT concentration, µM
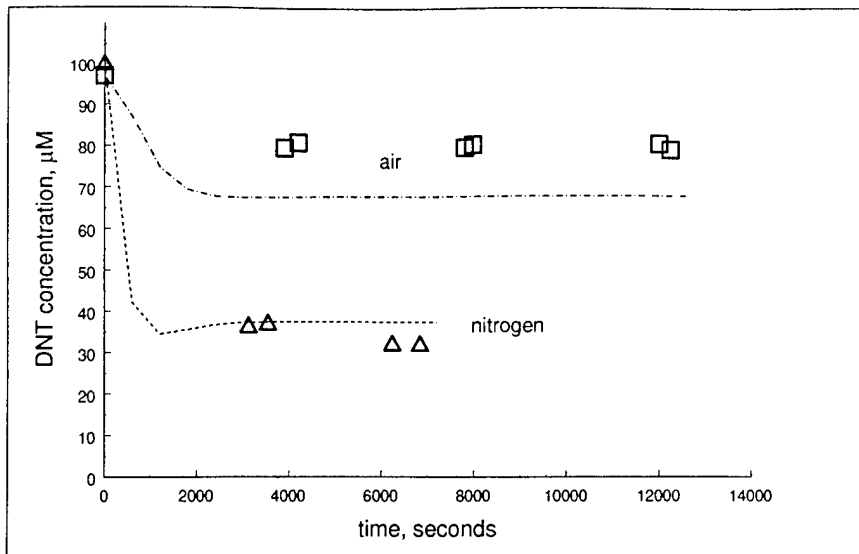
air

nitrogen

time, seconds

Figure 32. Comparison of experimentally observed and calculated values for
the DNT concentrations in an air- and nitrogen-equilibrated EPUD system,
after calibration of the model with an APUD system.

As indicators of the goodness of the fit, the calculated values of D/D_0 and acetal-dehyde concentration (A) were plotted versus the observed values (Figures 33 and 34, respectively). The numbers serving as symbols in Figures 33 and 34 are the oxygen percentage in the sparge/blanket gas. Agreement for both D/D_0 and A was fair to good at low oxygen concentrations (0 to 1 percent in the gas), but poorer at intermediate concentrations, and better again at still higher oxygen concentrations. It is interesting that this same pattern was observed in the APU experiment set, where nitrogen- and oxygen-sparged experiments calibrated to the same parameters, but the air-sparged data were not as well represented by those parameters. In the present data set, it is seen from Figures 33 and 34 that the predicted DNT and A concentrations were relatively unaffected by the com-position of the equilibration gas, except for the experiment using air (20 percent oxygen in the equilibration gas). Similar calculations were performed using higher values of the mass transfer coefficient to determine whether higher gas transfer rates would have affected the outcome, and to confirm that no rotameter calibration error could account for the effect. It was found that mass transfer coefficients (and therefore, to a first approximation, gas flow rates) would have to be 10 to 100 times higher than those used to have an appreciable positive effect on the calculated results for DNT, and 100-1000 times higher to affect the acet-aldehyde values significantly. The lower change needed to affect DNT is due to the direct sensitivity to oxygen of the reductive DNT removal. Even so, the lower value would correspond to direct sparging with 200 mL/min of gas, and the higher value, to 2 L/min, compared with the 10 mL/min of gentle blanket gas flow used in the experiment. Thus, the difference between calculated and ex-perimentally observed values for acetaldehyde and DNT cannot be explained by

a mass transfer effect, and it was concluded that the reason that the use of a higher gas transfer rate helped the simulation of A is that a higher oxygen utilization rate is required by some reaction(s) in order to simulate the system; therefore, the rate constant for that reaction is too low. Increasing the rate of that reaction would also consume more oxygen, thereby lowering the lower oxygen concentration and increasing the calculated DNT removal.

Figure 33. Comparison of experimentally determined and calculated D/D_o values for the EPUD series of experiments, after model calibration with the APUD series. Number symbols indicate the percentage of oxygen in the equilibration gas. Line indicates region of perfect agreement.

Figure 34. Comparison of experimentally determined and calculated A concentration values for the EPUD series of experiments, after model calibration with the APUD series. Number symbols indicate the percentage of oxygen in the equilibration gas. Line indicates region of perfect agreement.

The data were visualized in another manner to gain further insight. Figure 35 shows a comparison of the observed and calculated fraction of DNT remaining as a function of % oxygen in the equilibration gas concentration. It is clear from the observed fractions that the concentration of oxygen in the gas does indeed have an effect on DNT removal. A plot of log[DO] (DO is dissolved oxygen in μmole/L) in the liquid phase versus gas phase oxygen concentration (Figure 36) corroborates that effect, but whereas the measured DO concentration appears to drop steeply below 5 percent in the gas, calculated oxygen concentration fails to drop appreciably in that region. The sharp drop in measured acetaldehyde concentration with an increase in oxygen concentration (Figure 37), where there is no drop in the calculated values, seems particularly significant. It probably indicates an underestimation in the kinetic model of an important oxygen-dependent reaction that removes acetaldehyde. The most obvious choice for this reaction is B+X→Y, i.e.,

$$CH_3C(O) \bullet + O_2 \rightarrow CH_3C(O)O_2 \bullet$$
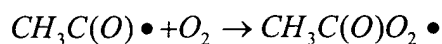
for which the rate constant that emerged from the first optimization stage seems low, compared to that of most carbon-centered radicals with oxygen; however, the only literature value available for this rate constant in a liquid-phase system, is also uncharacteristically low. This reaction aids the "removal" of acetaldehyde not only by Y+A→B, but also because the reaction competes with hydrogen abstraction and electron transfer reactions of B [$CH_3C(O)$], which regenerate acetaldehyde.
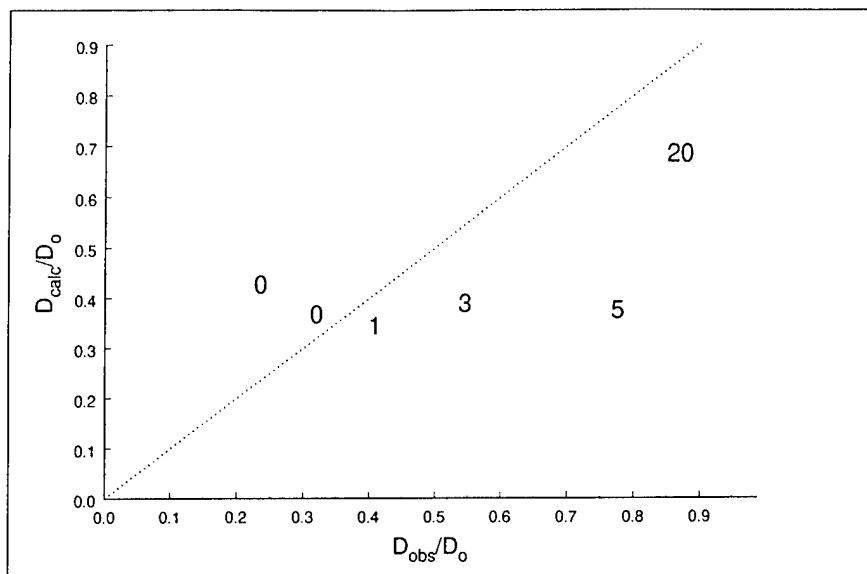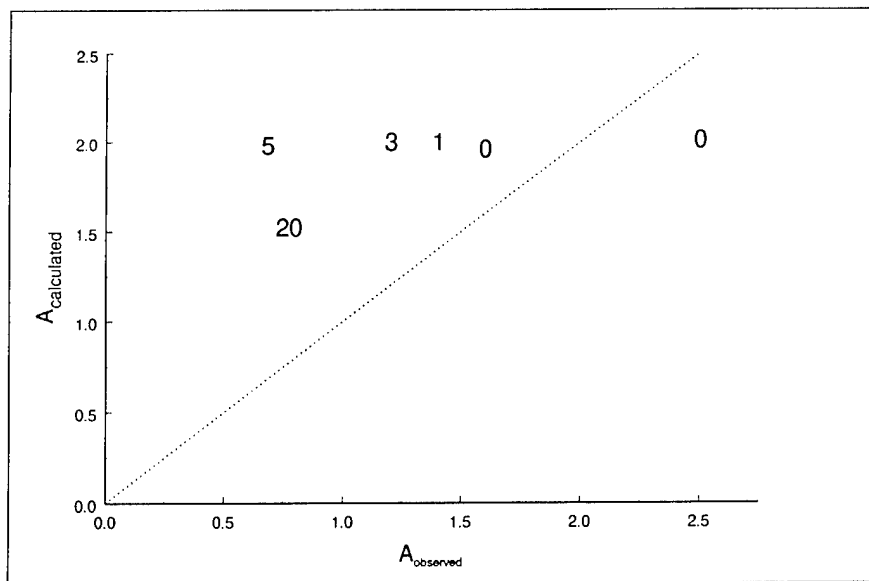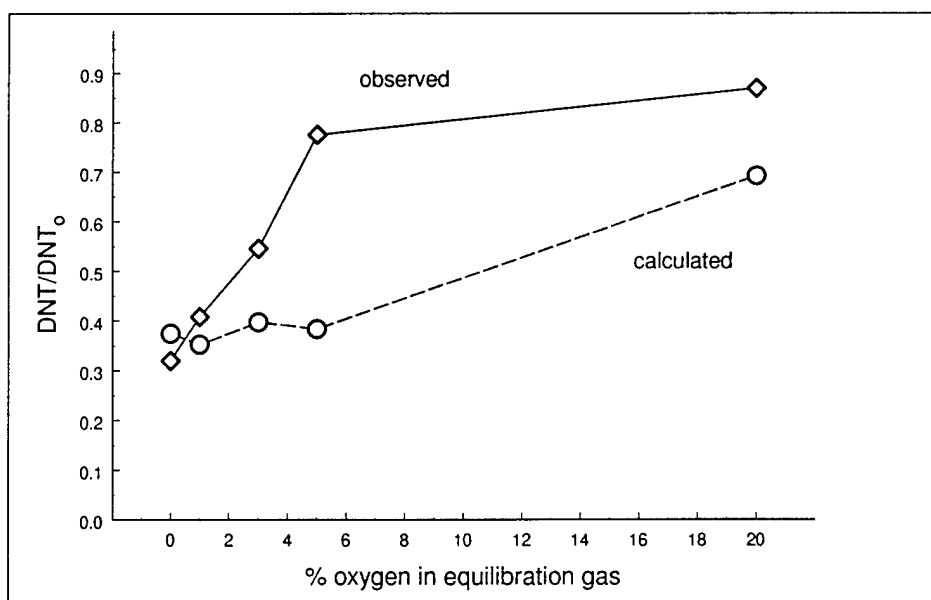

Figure 35. Comparison of experimentally determined and calculated D/D₀ values for the EPUD series of experiments, as a function of the percentage of oxygen in the equilibration gas.
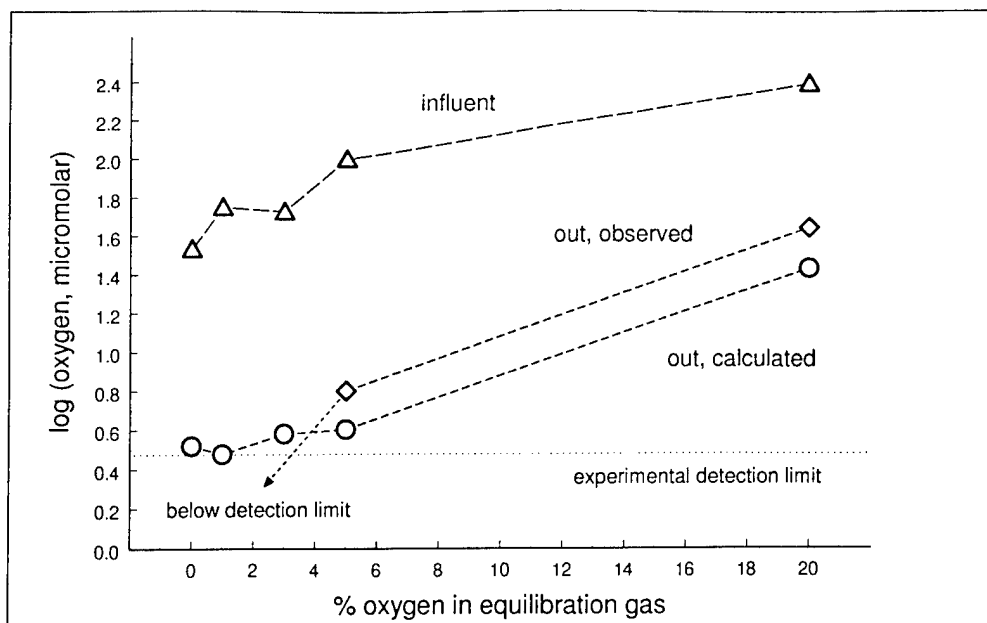
Figure 36. Comparison of experimentally determined and calculated log DO concentrations (μM)] for the EPUD series of experiments, as a function of the percentage of oxygen in the equilibration gas. Also shown is the DO concentration in the feed solution.
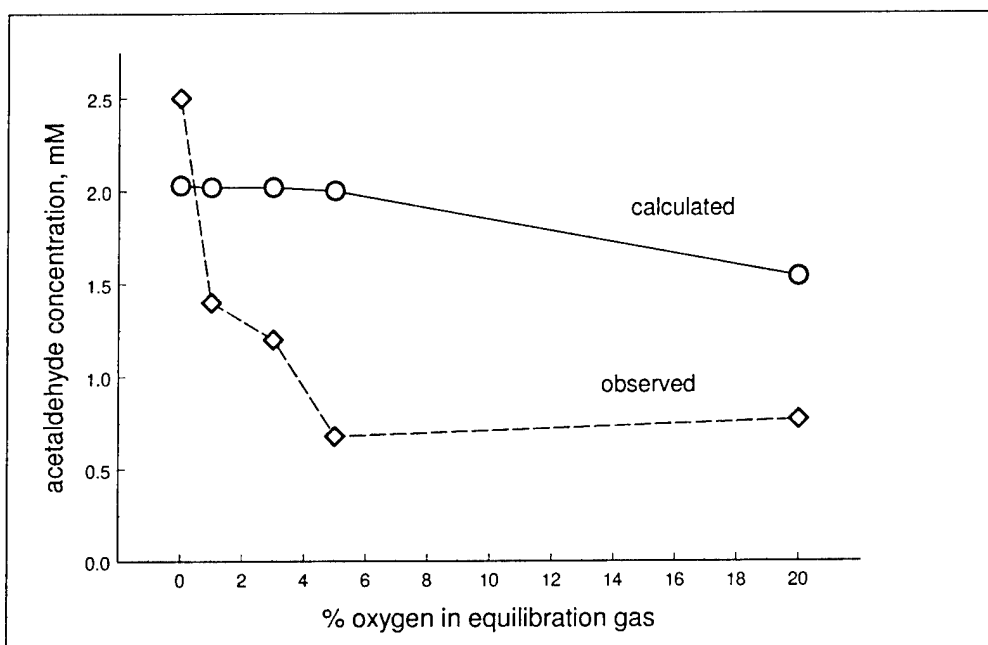

Figure 37. Comparison of experimentally determined and calculated acetaldehyde concentrations for the EPUD series of experiments, as a function of the percentage of oxygen in the equilibration gas.

Finally, the plot of hydrogen peroxide consumption P_o-P versus oxygen gas fraction (Figure 38) offers an explanation of the previously observed high peroxide consumption. Consumption is high at very low oxygen concentration, then falls rapidly as oxygen concentration increases, in the same region that acetaldehyde consumption increased. Steady-state P photolysis rates in experiments B-79 (N_2) and B-84 (air) were 1.4 μM/s, generating OH at twice that rate. However, P scavenged about 17 percent of the OH produced, leaving a rate of OH generation R_g of about 2.3 μM/s in these experiments (these numbers can be calculated independently of the kinetic model). Thus the total dose of photogenerated OH• that escapes scavenging by P is $R_g t_R$ =(2.3μM/s)(950s)=2.2mM OH radical. However, P consumption as high as 14 mM was observed in Experiment B-79, even after P regeneration from superoxide. By comparison, the model predicts only 4 mM consumption for that experiment. If the measured concentrations are indeed correct, a chain reaction that consumes hydrogen peroxide is implied. Although some scatter is obvious in Figure 38, the apparent chain length decreases with increasing oxygen concentration, with a minimum in the 3 to 5 percent gas region, which is the same region in which the acetaldehyde curve flattened out and the DO dropped below the detection limit of 3 μM. Above 5 percent (3 μM DO), the chain length may again increase, although it may not be the same chain that is responsible for the high P consumption at low oxygen concentrations.

Figure 38. Comparison of experimentally determined and calculated hydrogen peroxide removal during the EPUD series of experiments, as a function of the percentage of oxygen in the equilibration gas.
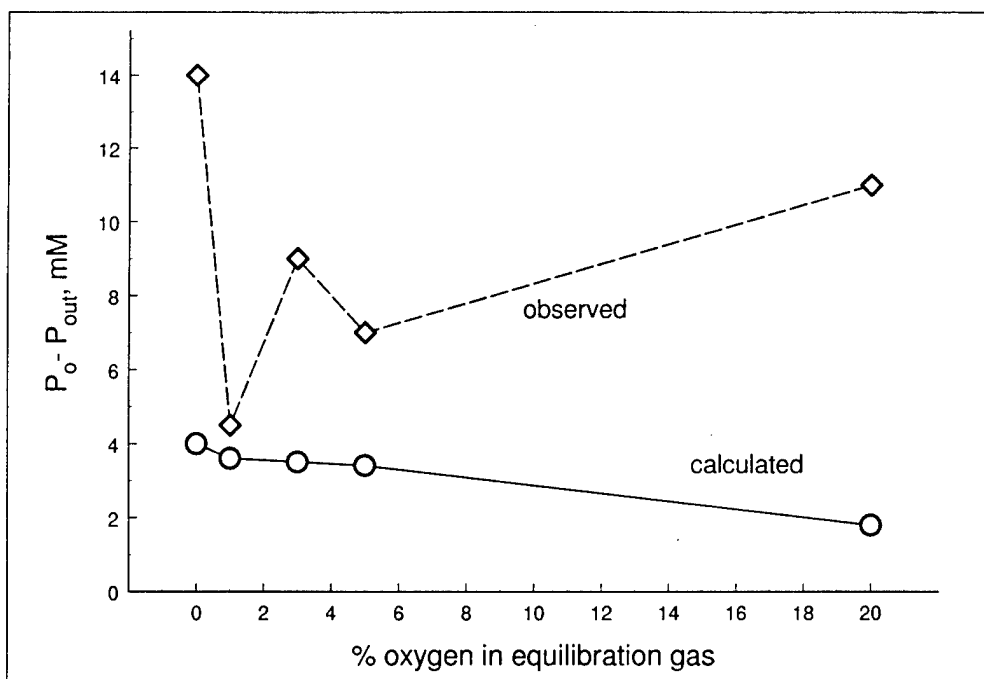
The observed data are consistent with the proposed mechanism in the following ways: At low oxygen concentration, reducing radicals R and G are not well-scavenged by oxygen, and can react with hydrogen peroxide to form additional OH radicals, which contribute to further peroxide destruction. At the same time, acetyl radicals are also not as well-scavenged by oxygen and also react with hydrogen peroxide consuming it further. The reaction of acetyl radical with hydrogen peroxide also regenerates acetaldehyde, so that the apparent acetaldehyde removal rate is less, and a higher A concentration results. As more oxygen is present, these reactions decrease in importance and, consequently, less peroxide is destroyed and less acetaldehyde is regenerated.

In the 0 to 5 percent region, increasing oxygen results in decreased reducing radical concentrations and, therefore, higher DNT survival. At still higher oxygen concentrations, more acetylperoxyl radical is formed, and reaction of acetyperoxyl radical (Y) with hydrogen peroxide increases in importance, again increasing peroxide consumption. Since the reaction Y+P→W+S does not regenerate acetaldehyde, the acetaldehyde concentration observed at 20 percent gas concentration is about the same as that observed at 5 percent.

The fact that reaction of OH with ethanol generates only a reducing radical, while OH with acetaldehyde generates oxidizing and reducing radicals in equilibrium, creates an important difference between systems initially containing ethanol and those initially containing acetaldehyde. When the ethanol radical (G) or the hydrated acetyl radical (B) react with peroxide (P), no oxygen is formed, whereas reaction of the acetyl radical with P generates superoxide (S), the major fate of which is disproportionation to produce oxygen and hydrogen peroxide: 2S→X+P. Since all carbon-centered radicals react with and consume oxygen as well, the ethanol system, producing only reducing radicals, tends to depress the oxygen concentration, while the oxidizing radicals in the acetaldehyde system tends to increase oxygen concentration. This effect is more pronounced at higher hydrogen peroxide concentration, which encourages reaction of the radicals with P.

This effect has been demonstrated with the model, but can also be seen in the observed data. Table 9 compares steady-state DO concentrations (μM) for the experimental data analyzed in this report.

Table 9. Comparison of steady-state DO concentrations.

Organic reducing-radical precursor	P concentration	Equilibration gas		
		Nitrogen	Air	Oxygen
ethanol	>15 mM	<3 (3)	44	n/a
acetaldehyde	>15mM	<3, 5, 55, 113	350	830
	<15 mM	<3 (1)	100	790

For "high" peroxide concentrations (>15 mM), acetaldehyde experiments consistently produced higher DO concentrations than did ethanol experiments (number of experiments given in parentheses). For acetaldehyde experiments, high peroxide concentrations consistently produced higher DO values than low peroxide concentrations. Two of the three experiments listed under ethanol/nitrogen actually had 1 and 3 percent oxygen in the equilibration gas, but still reached steady state oxygen concentrations of <3 μM.

Summary of the Kinetic Model Status

When the previous results (Maloney, Boddu, and Peyton 1997) were published, the essence of the mechanistic model was the six reactions shown in Figure 1, plus OH scavenging by hydrogen peroxide and acetaldehyde. At the beginning of the present study, the proposed mechanism consisted of about 15 reactions, with rate constants known for 6 of those. During the course of this investigation, the number of reactions included in the final kinetic model grew to more than 30, with several other reactions being considered and proven insignificant. Of these 30 reactions, rate constants were known for 9 and were determined for another 4. Of the 16 species listed as dependent variables in the kinetic model, only 8 can be experimentally measured. Under these conditions, unknown rate constants cannot be uniquely determined mathematically, and other constraints such as comparison with literature values for similar reactions must be used. Experiments on limited subsystems helped to reduce the ambiguity. During manual optimization, however, the possibility always exists that a pseudo-optimum set of rate constants will be obtained, which would correspond conceptually to a local minimum in the surface of the optimization criterion function (e.g., sum of the squares of the errors, etc.) in parameter space, which is not the deepest minimum.

The formation of a hydroxyhydroperoxide from acetaldehyde and hydrogen peroxide in the experiments performed using concentrated solutions (such as were used in the previous flow experiments) has become as a major complication. This introduced several new reactions with unknown rate constants, requiring more extensive experimentation and calibration of the model at high concentrations, to better characterize the reactions of the hydroperoxides. This was not possible within the present resources of the project, and therefore, semiquantitative SARs were used to estimate unknown rate constants. A more complete description of that subsystem would undoubtedly lead to a better description of the reaction system by the kinetic model.

The results of modeling the EPUD system support the assumed mechanism, with respect to qualitative behavior. Good quantitative agreement between

model and experiment has been obtained for each of the subsystems of UD, PUD, and APU, and fair to good agreement found for the combined APUD system. These systems contain all of the required reactions to describe the EPUD system, except for reactions involving ethanol and its radical, the 1-hydroxyethyl radical, but several of these reaction rate constants were already known. Good quantitative agreement between observation and calculation, however, was not obtained in the EPUD system, with respect to prediction of the flux through the ethanol→acetaldehyde→peroxyacetic acid pathways, or for hydrogen peroxide consumption. This leads to the conclusion that the mechanism is fundamentally correct but that further optimization of the rate constants by calibration with additional experimental data sets is necessary.

In particular, a more detailed study of the reactions of the hydroxyhydroperoxides and hydroperoxides with OH and reducing radicals is needed, not only to elucidate products but also to measure rate constants that could only be estimated in the present study. Following this, the rate constant set should be recalibrated by performing APU experiments using mixtures with sufficiently high acetaldehyde and H_2O_2 concentrations that appreciable adduct $[CH_3CH(OH)O_2H]$ is present. This should improve the predictive ability of the model. It is possible that omission of these reactions in earlier calibration steps resulted in rate constants that compensated somewhat for the omission. Nonetheless, the ethanol experiments were performed at high concentrations because of the desire to compare with previous results from Maloney, Boddu, and Peyton (1997), as described in the next section.

Inclusion of Acetaldehyde Chemistry in Calculations for Previous DNT Flow Experiments

One objective of this work was to include the acetaldehyde system in the mechanism used to describe the results of earlier treatability studies (Maloney, Boddu, and Peyton 1997) on DNT in the presence of ethanol, for the purpose of recalculating rate constants determined in that work. In those studies, acetaldehyde was considered as a hydroxyl radical scavenger, but not in the capacity of active species precursor; therefore, analysis of that data using a more complete model could be expected to lead to different values for the rate constants that were determined. Unfortunately, this comparison cannot be done directly. The simpler mechanism assumed in the earlier work means that the system of rate equations was solved analytically in the steady-state approximation to eliminate radical concentrations, yielding a rate equation for DNT in terms of rate constants and observables. Just the acetaldehyde subsystem, as we currently understand it, by itself produces a set of equations that is sufficiently unwieldy to prevent such a

simplification. Inclusion of this system as a subsystem in the DNT/ethanol system would, therefore, yield a more complicated system for which an analytical solution could not be obtained.

In view of these difficulties, it was necessary to take a different approach in the present studies, in order to evaluate the effect of the additional reactions on the previously determined rate constant. The previous flow results were simulated using the present model, including the ethanol reactions and the reaction of 1-hydroxyethyl radical with DNT. The value for the escape fraction in the previous mechanism was set to 0.3, as found in Peyton et al. (1995). In the previous model, the resulting DNT concentration was expressed as a function of the liquid-phase DO concentration, while the present numerical model simulates DO behavior by *ab initio* calculations, as for any other reactant. Thus, DO was the independent variable in the previous work and a dependent variable in the present work. The present model was therefore modified to accept oxygen as an independent variable, in order to generate a diagram of D/D_o versus oxygen, as was shown in Figure 4-21 of Maloney, Boddu, and Peyton (1997). Conditions used in the previous experimental work were used as input to the complete kinetic model, along with the values of the rate constants given in Table 5 for the BL1h parameter set. The reactor conditions were:

Photon input rate	$I_o = 1.41 \times 10^{-6}$ E/L-s
Average liquid residence time in reactor	$t_R = V_R/Q = 65.4$ min $= 3924$ sec
Average pH = 4.3 →	$k_d = 2 \times 10^7$ M^{-1}s^{-1}
Average ethanol concentration in feed	$E_o = 7.0$ mM
Average DNT concentration in feed	$D_0 = 160$ μM

The results of the simulation are shown in Figure 39, superimposed on the data from Maloney, Boddu, and Peyton (1997). The shape of the calculated curve is essentially the same as was obtained with the simpler model, but shifted to lower oxygen concentration by about ½ log unit. Although the newer, more complicated model was calibrated entirely by fitting to data collected during this project, the newer curve appears to fit the data as well or somewhat better than the old calculation. The sigmoid curve is shifted about 0.66 log units to the left of the previous value, or a factor of 4.6. The magnitude of this shift is close to the factor of 5 by which the value of k_{GD} was lower in this project than that used to obtain the previous results. The value was lowered from the previous value of 2.4×10^8 to improve the fit with DNT data in the EPUD series of experiments. The behavior of acetaldehyde was not predicted very well in these experiments, so the changes in rate constants that would improve the A fit in further optimization steps could result in a value of k_{GD} that was closer still to the previous value. The two values are in reasonably good agreement, considering the differences in reactor conditions, concentrations, etc., in the two projects.
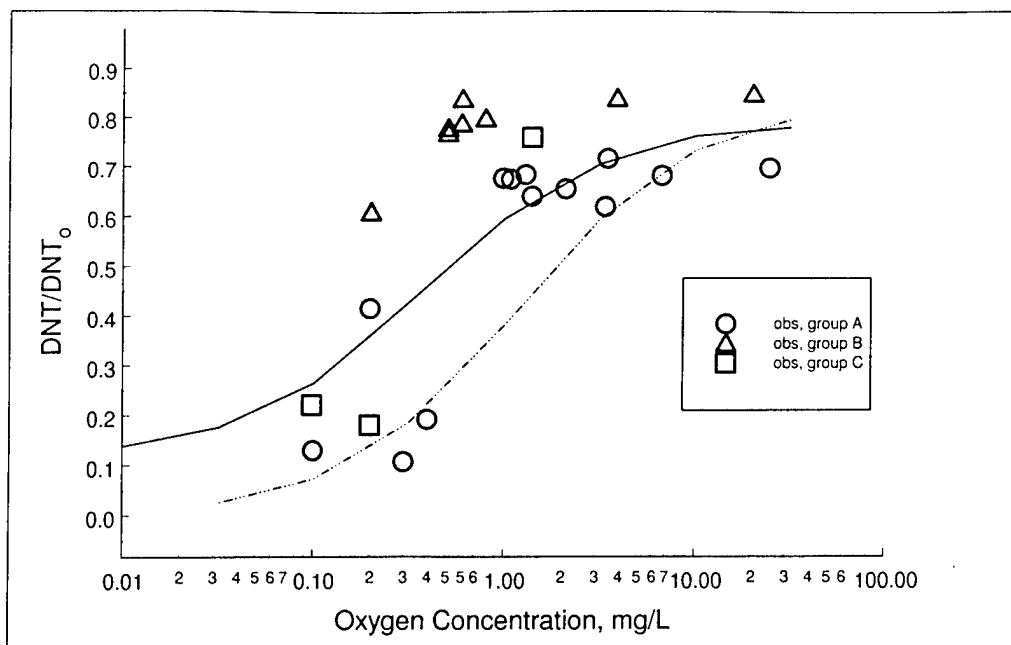
Figure 39. Comparison of simulation results for the flow data of Maloney, Boddu, and Peyton (1997) using the present kinetic model (solid line) and the simpler model reported earlier. Results are similar to those of previous calculations using the earlier model, but are displaced by 0.46 log units toward lower oxygen concentrations. The present model gives a better overall prediction of the DNT concentrations.

No multistable behavior was predicted from the kinetic model, because the values of k_{BX} and k_{YA} resulting from the fit are too low to support a chain reaction that is fast enough to run away. As stated before, these results do not prove that no multistable behavior can occur, but simply that none have been found.

Multistability in Closely Related Chemical Systems

New Information

Late in the study, a publication was found in the chemical engineering literature in which Zeyer and coworkers reported multistable behavior during the treatment of ethanol using Fenton's reagent (iron II or III and H_2O_2) at elevated temperatures (40-80 °C). This system was shown to be a thermokinetic oscillator (i.e., it appeared to be driven by temperature changes in the system, rather than by availability of species [concentration]). The authors wrote the chemical reaction set in general terms such as:

$$H_2O_2 + CH_3CH_2OH \xrightarrow{\quad catalyst \quad} CH_3CHO + 2H_2O$$
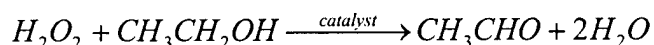
where the catalyst was not specified but was implied to be an iron species. Five different such reactions were written, including:

$$catalyst + CH_3COOH \rightarrow catalyst* \qquad \text{and}$$

$$catalyst* \rightarrow catalyst + CH_3COOH$$
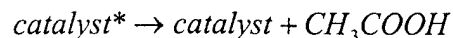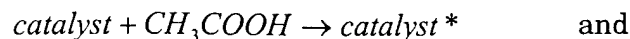
Arrhenius expressions were written for the five reactions, and activation energies are presumed to have been determined by fitting, since no reference is given other than the dissertation (Hafke 1972, as cited in Zeyer et al. 2000) in which the model was developed. At the time of the dissertation, detailed knowledge of free radical reactions was being explored, and many reactions were unknown. Since the reaction mixture has to be heated to start the reaction, the initiation step is probably the thermal decomposition of hydrogen peroxide to produce hydroxyl radical, which attacks ethanol, producing 1-hydroxyethyl radical. This radical reduces Fe(III) to produce Fe(II), which reduces H_2O_2 to regenerate hydroxyl radical in a chain reaction. Thus the system bears many similarities to the system presently under study, but differs in the initiation mechanism and initial concentrations, which were H_2O_2 9 percent, ethanol 10 percent, iron 2 percent in the feedstock, and H_2O_2 0 percent, ethanol 23 percent, iron 0.2 percent initially in the reactor for initiation.

The authors heated the initial reactor charge (containing no hydrogen peroxide) to 54 °C, than began dosing with feedstock, whereupon the temperature rose to 80 °C. When cooling by water coils internal to the reactor was started, the temperature dropped to 55 °C and small oscillations appeared. Further cooling caused the oscillations to grow in amplitude until a 40-degree excursion was observed between peaks and troughs of the oscillations. The authors noted that if the experiment was begun by starting feedstock flow and then warming from room temperature, the reaction would run away at the inset of oscillations, with danger of material expulsion or explosion. Addition of acetaldehyde to the feedstock was an additional complication, which resulted in frequency doubling and quadrupling of the oscillation frequency.

Additional Experimentation

As a result of this new information, two additional experiments were performed. In one, an experiment similar to those of Zeyer et al. (1999) was performed, but at somewhat lower concentrations of ethanol and peroxide, since the small reactor used did not have cooling coils. The reactor was immersed in a water bath at 60 °C and flow begun. The flask was cooled to 54 °C and very small but regular

oscillations (a few tenths of a degree by digital thermometer) were noted. Flow was stopped, bath temperature raised to 64 °C, and flow resumed. Temperature in the flask increased quickly to 65-67 °C with periodic oscillations slightly larger than before. The solution was cooled slightly by lowering the bath, then warmed again, and the temperature increased quickly to 70 °C, confirming the exothermicity of the reaction. Problems with the peroxide feed pump prevented maintaining the oscillations for very long, but allowed confirmation that the oscillations reported by Zeyer et al. (1999) for the Fenton/ethanol system could be reproduced in this laboratory.

The other experiment series was an attempt to detect thermal oscillations in an ethanol/H_2O_2/UV experiment. For safety, low concentrations were used in the first experiment, but were gradually raised to 10 percent ethanol and 13 percent hydrogen peroxide in the feedstock. In a typical experiment, the reactor contents were warmed to 50-60 °C, then flow was started while monitoring the temperature in the reactor was monitored with a digital thermometer. When no initiation was observed, the UV lamp was switched on. When no evidence of initiation was observed, the heating bath was lowered, in case the reaction had initiated without appreciable heat release. No temperature oscillations were observed in any of the ethanol/H_2O_2/UV experiments.

Conclusions From Additional Experiments

Apparently iron is an essential ingredient for the thermal oscillations observed by Zeyer et al. (1999) and for this work. An examination of the probable mechanism indicates that mediation by iron reroutes some of the chain reaction pathways compared with the photochemical system, so that no important reaction is completely terminal (i.e., some chain carriers always result). The important termination reaction in the photochemical system

$$2O_2^- \rightarrow H_2O_2 + O_2$$
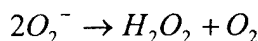
is not important in the Fenton system as carried out by Zeyer et al., because at such high iron concentrations, the reaction

$$Fe(III) + O_2^- \rightarrow Fe(II) + O_2$$
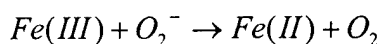
is orders of magnitude faster. This implies that inclusion of even a small amount of Fe(III) in the H_2O_2/UV system could greatly improve the efficiency in some cases. This system is known as the Photo-Fenton.

Thermal oscillations would be expected to be less important in a photon-driven rather than a photochemical system because, in the photochemical system (1) the activation energy is supplied by the photons and (2) after initiation, all important reactions are free-radical reactions, which depend much less on activation energy, than are "thermal" reactions. The need for thermal initiation in the Fenton system indicates that the crucial reactions in that system are thermal, which was supported by the lack of an observed photochemical initiation in the Fenton system experiment. It is concluded that, if the photochemical system is indeed multistable, it results from a different mechanistic feature than do the thermal oscillations in the Fenton system.
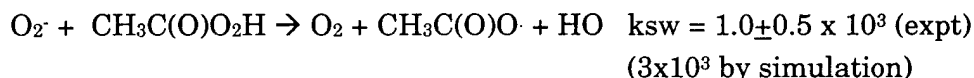
5 Conclusions and Recommendations

Conclusions

1. A mechanism has been developed to describe the complex chemistry of acet-aldehyde in the presence of hydroxyl radical, and the action of the resulting reducing radicals on DNT. This reaction system requires the inclusion of more than 30 reactions for its complete description, many of which were pre-viously unknown, but were hypothesized based on known similar reactions.

2. The central unique feature of this mechanism is the reaction of hydroxyl radical with both acetaldehyde and its hydrate, 1,1-dihydroxyethane, to form oxidizing and reducing radicals respectively, which are in rapid equilibrium with each other. The reducing radical (1,1-dihydroxyethyl radical) is capable of reducing DNT, while the oxidizing radical (acetyl radical) is involved in a chain reaction propagated by reaction with oxygen to form a peroxyl radical, which can react with acetaldehyde to produce more acetyl radical. Reduction of DNT occurs in competition with reaction of the reducing radical with oxy-gen.

3. The kinetic model derived from this mechanism provides a good to fair repre-sentation of the data obtained from experiments performed in a flow configu-ration for the APU, UD, PUD, and APUD subsystems. Prediction of the EPUD system was fair to poor. However, even calculated results that are not in particularly good quantitative agreement with the experimental EPUD re-sults are in qualitative support of the mechanism. All of the rate constants resulting from the fit of the data have reasonable values, compared with known literature values for similar reactions.

4. The kinetic model, in its present form, calibrated entirely from the data ob-tained during the course of this project, gave a good prediction of the experi-mental results from a previous project (Maloney, Boddu, and Peyton 1997). The resulting plot of DNT/DNT_0 versus log [oxygen] was offset from that of previous results for the same system (Maloney, Boddu, and Peyton 1997) by 0.66 log units, which is the factor by which the presently determined value of the rate constant for the reaction of ethanol radical (1-hydroxyethyl radical)
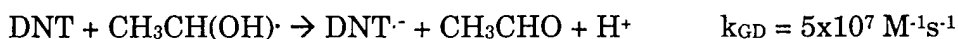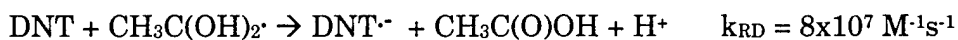
with DNT differs from the previously determined value. This result is despite the fact that the previous mechanism was relatively simple and somewhat incomplete, while the present mechanism is complex and exhaustive.

5. Modeling of the system was complicated by the formation of 1-hydroxyethylhydroperoxide with the addition of hydrogen peroxide across the carbon-oxygen double bond of acetaldehyde. This hydroperoxide was insignificant when hydrogen peroxide and acetaldehyde concentrations were both in the mM range, but could account for half of the speciation of acetaldehyde when 100 mM hydrogen peroxide concentrations were used. Photolysis of the hydroperoxide was shown to be unimportant in our system, but it was necessary to include its reaction with OH radical and with electron donors in the mechanism.

6. During the course of attempting to model this reaction system, some new reactions have been hypothesized, evidence gathered for their validity, and rate constant values tentatively measured:

$$O_2^- + DNT \rightarrow O_2 + DNT^{-\cdot}$$
$$k_{SD} < 250\ M^{-1}s^{-1}$$
(10 by simulation)

$$O_2^- + CH_3C(O)O_2H \rightarrow O_2 + CH_3C(O)O^\cdot + HO^-$$
$$k_{SW} = 1.0\pm0.5 \times 10^3\ (\text{expt})$$
$$(3\times10^3\ \text{by simulation})$$

$$CH_3CHO + CH_3C(O)O_2H \rightarrow 2\ CH_3CO_2H$$
$$k_{AW} = 0.018\pm0.014\ M^{-1}s^{-1}$$

$$DNT \xrightarrow{h\vartheta} products$$
$$\phi_D = 2.94\pm0.44\times10^{-3}$$
$$(\text{under nitrogen})$$
$$5.56\pm0.93\times10^{-3}$$
$$(\text{under oxygen})$$

$$DNT + \cdot OH \rightarrow products$$
$$k_{OD} = 7.3\times10^7\ M^{-1}s^{-1}$$

In addition, the following reactions were postulated and rate constant values were obtained as a result of fitting the kinetic model to experimental data:

$$DNT + CH_3C(OH)_2^\cdot \rightarrow DNT^{-\cdot} + CH_3C(O)OH + H^+$$
$$k_{RD} = 8\times10^7\ M^{-1}s^{-1}$$

$$DNT + CH_3CH(OH)^\cdot \rightarrow DNT^{-\cdot} + CH_3CHO + H^+$$
$$k_{GD} = 5\times10^7\ M^{-1}s^{-1}$$

Finally, by analogy with known reactions, the reactions

$$HR\cdot + R'OOH \rightarrow H^+ + R + R'O\cdot + HO^-$$
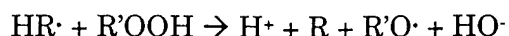
were postulated, in which R=CH$_3$C(O)H and CH$_3$C(O)OH, and R'=H-, CH$_3$C(O)-, and CH$_3$CH(OH)-.

Recommendations

Further refinement of the model should be carried out, addressing issues such as determining rate constants for reactions of 1-hydroxyethylhydroperoxide with hydroxyl radical and reducing radicals, and further calibration of the acetaldehyde/H$_2$O$_2$/UV system at high hydrogen peroxide concentrations. It is anticipated that considerable improvement in the model could be accomplished.

Now that the complete reaction system appears to have been identified, the search for bistable behavior should be carried further, since it is likely that the reactions of the hydroperoxide are important from this standpoint. Although this research is higher-risk from the viewpoint of probability of success in finding such behavior, compared to more typical projects such as treatability studies, the importance of such a discovery would be great and could significantly impact the use of advanced oxidation processes (AOPs) for ordnance and halogenated contaminant treatment.

References

Adams, G.E. and R.L. Wilson, "Pulse Radiolysis Studies on the Oxidation of Organic Radicals in Aqueous Solution," *Trans. Farad. Soc.*, vol 65 (1969), pp 2981-2987.

Allan, J.T., "The Action of Ionizing Radiations on Aqueous Oxygenated Solutions of Acetaldehyde," *J. Phys. Chem.*, vol 68 (1964), pp 2714-2716.

Baxendale, J.H. and A.A. Kahn, "The Pulse Radiolysis of p-Nitrosodimethylaniline in Aqueous Solution," *Intl. J. Radiat. Phys. Chem.*, vol 1 (1969), pp 11-24.

Bielski, B.H.J., D.E. Cabelli, R.L. Arudi, and A.B. Ross, "Reactivity of HO_2/O_2^- Radicals in Aqueous Solution," *J. Phys. Chem. Ref. Data*, vol 14 (1985), pp 1041-1100.

Boissonade, J., and P. De Kepper, "Transitions from Bistability to Limit Cycle Oscillations," *J. Phys. Chem.*, vol 84 (1980), pp 501-506.

Buxton, G.V., C.L. Greenstock, W.P. Helman and A.B. Ross, "Critical Review of Rate Constants for Reactions of Hydrated Electrons, Hydrogen Atoms, and Hydroxyl Radicals in Aqueous Solution," *J. Phys. Chem. Ref. Data*, vol 17 (1988), pp 513-886.

Davies, M. and M.E. Deary, "Determination of Peracids in the Presence of a Large Excess of Hydrogen Peroxide Using a Rapid and Convenient Spectrophotometric Method," *Analyst*, vol 113 (1988), pp 1477-1479.

Gray, P. and S.K. Scott, *Chemical Oscillations and Instabilities* (Clarendon Press, Oxford, 1990).

Hafke, C., *Theoretische und experimentelle Analyse des dynamischen Verhaltens eines kontinuierlich betriebenen Rührkesselreaktors*, PhD thesis, Universität Stuttgart, Germany (1972).

Kooijman, K.L. and W.L. Ghijsen, "Properties and Constitution of the Peroxides Prepared by Oxidizing Propane and Their Analysis," *Rec. Trav. Chim.* vol 66 (1947), pp 205-216.

Maloney, S.W., V.M. Boddu, and G.R. Peyton, "Advanced Oxidation Treatment of Army Industrial Wastewaters: Propellant Wastewater," USACERL Technical Report 97/137/ADA339159, September 1997.

Parker, G.A., in *Colorimetric Determination of Nonmetals*, edited by D.R. Boltz and J.A. Howell (Wiley, New York, 1928), p 301.

Peyton, G.R., O.J. Bell, E. Girin, and M.H. LeFaivre, "Reductive Destruction of Water Contaminants during Treatment with Hydroxyl Radical Processes," *Environ. Sci. Technol.*, vol 29 (1995), pp 1710-1712.

Peyton, G.R., M.A. Smith, and B.M. Peyton, "Photolytic Ozonation for Protection and
        Rehabilitation of Ground Water Resources: A Mechanistic Study," *Water Resources Center
        Research Report No 206, UILU-WRC-87-206* (University of Illinois, 1987), pp 19-20.

Ross, A.B. and P. Neta, "Rate Constants for Reactions of Aliphatic Carbon-Centered Radicals in
        Aqueous Solution," National Bureau of Standards monograph NSRDS-NBS 70, 1982.

Schuchmann, M.N. and C. von Sonntag, "The Rapid Hydration of the Acetyl Radical. A Pulse
        Radiolysis Study of Acetaldehyde in Aqueous Solution," *J. Am. Chem. Soc.,* vol 110 (1988),
        pp 5698-5701.

Seddon, W.A. and A.O. Allen, "Radiation Chemistry of Aqueous Solutions of Ethanol," *J. Phys.
        Chem.,* vol 71 (1967), pp 1914-1918.

Swern, D., *Organic Peroxides* (Wiley-Interscience, New York, 1970).

von Sonntag, C., *The Chemistry of Radiation Biology* (Taylor-Francis, New York, 1987), p 65.

Zeyer, K.-P., M. Mangold, T. Obertopp, and E.D. Gilles, "The Iron (III)-Catalysed Oxidation of
        Ethanol by Hydrogen Peroxide: A Thermokinetic Oscillator," *J. Phys. Chem.,* vol 103
        (1999), pp 5515-5522.

Zeyer, K.-P., S. Pushpavanam, M. Mangold, and E.D. Gilles, "The behavior of the iron(III)-
        catalyzed oxidation of ethanol by hydrogen peroxide in a fed-batch reactor," *Phys. Chem.,*   .
        vol 2 (2000), pp 3605-3612.

Acronyms, Abbreviations, and Symbols

A	acetaldehyde
AA	acetic acid
AOP	advanced oxidation process
APU	acetaldehyde/hydrogen peroxide/ultraviolet (reaction system)
APUD	acetaldehyde/hydrogen peroxide/ultraviolet/DNT (reaction system)
B	acetyl radical
CSTR	continuous(ly) stirred tank reactor
DNPH	dinitrophenylhydrazine
DNT	2,4-dinitrotoluene
DO	dissolved oxygen
ξ	decadic extinction coefficient
EPUD	ethanol/hydrogen peroxide/ultraviolet/DNT reaction system
F	formaldehyde
f_{ij}	fraction of species I that reacts with species j
G	1-hydroxyethyl radical
HE	1-hydroxyethyl
HPLC	high-performance liquid chromatography
I_o	photon dose rate, einsteins/L-time
k_{ij}	second-order reaction rate constant for reaction between species i and j
k_lA	mass transfer coefficient
L	liter
M	as a concentration: molar (moles/L)
M	as a species identifier: 1-hydroxyethyl hydroperoxide

P	hydrogen peroxide
PAA	peracetic acid or peroxyacetic acid
PCBs	polychlorinated biphenyls
PTFE	polytetrafluoroethylene
PUD	hydrogen peroxide/UV/DNT (reaction system)
Q	liquid flow rate
QA	quality assurance
Q_g	gas flow rate
R	1,1-dihydroxyethyl radical
R_p	rate of photolysis
S	superoxide
SAR	structure-activity relationship
t_R	average liquid residence time in a well-stirred reactor
UD	UV/DNT reaction system (i.e., DNT photolysis)
UV	ultraviolet (radiation)
V_R	reactor liquid volume
W	peroxyacetic acid
X	oxygen
Y	acetylperoxyl radical
ϕ_e	quantum yield

CERL Distribution

Chief of Engineers
    ATTN: CEHEC-IM-LH (2)

Operations Support Command
    ATTN: SOSMA-ISE-P (2)

Engineer Research and Development Center (Libraries)
    ATTN: ERDC, Vicksburg, MS
    ATTN: Cold Regions Research, Hanover, NH
    ATTN: Topographic Engineering Center, Alexandria, VA

Defense Tech Info Center 22304
    ATTN: DTIC-O

        8
       9/01

REPORT DOCUMENTATION PAGE

1. REPORT DATE (DD-MM-YYYY) 12-2001	2. REPORT TYPE Final	3. DATES COVERED (From - To)

4. TITLE AND SUBTITLE
Chemical Reductive Transformations of Synthetic Organic Compounds:
Probe Compound Studies and Mechanistic Modeling

5a. CONTRACT NUMBER

5b. GRANT NUMBER

5c. PROGRAM ELEMENT NUMBER

6. AUTHOR(S)
Gary R. Peyton, Mary H. LeFaivre, and Stephen W. Maloney

5d. PROJECT NUMBER
611102BT25

5e. TASK NUMBER

5f. WORK UNIT NUMBER
J20

7. PERFORMING ORGANIZATION NAME(S) AND ADDRESS(ES)
U.S. Army Engineer Research and Development Center (ERDC)
Construction Engineering Research Laboratory (CERL)
P.O. Box 9005
Champaign, IL 61826-9005

8. PERFORMING ORGANIZATION REPORT NUMBER
ERDC/CERL TR-01-70

9. SPONSORING / MONITORING AGENCY NAME(S) AND ADDRESS(ES)
Headquarters. U.S. Army Corps of Engineers
441 G Street, NW.
Washington, DC 20314-1000

10. SPONSOR/MONITOR'S ACRONYM(S)

11. SPONSOR/MONITOR'S REPORT NUMBER(S)

12. DISTRIBUTION / AVAILABILITY STATEMENT
Approved for public release; distribution is unlimited.

13. SUPPLEMENTARY NOTES
Copies are available from the National Technical Information Service, 5285 Port Royal Road, Springfield, VA 22161.

14. ABSTRACT
Advanced Oxidation Processes (AOPs) can be used to selectively remove DNT (2,4-dinitrotoluene) from a complex waste stream by adding a precursor compound such as ethanol, which forms a reducing radical upon reaction with hydroxyl radical. A kinetic model that was previously developed to describe the results of batch AOP treatment by H_2O_2/UV did not give satisfactory predictive results obtained when extended to describe flow experiments. The present study further investigated the chemistry of this system, including the oxidation by-product acetaldehyde, which was known to have multiple degradation pathways involving the formation of both oxidizing and reducing radicals.

During the course of the investigation, the mechanism required to describe the system grew from 8 to over 30 reactions, with several new reactions found and several rate constants measured. The mechanism successfully described subsystems during calibration and upon combination of some subsystems, but the combined model for the entire reaction system did not give satisfactory prediction for some by-products when ethanol was added to the system. This is thought to be partly due to participation of unknown by-products from some of the new reactions, which require further study. The combined model gave better prediction of experimental results from the previous flow experiments than did the simpler model developed earlier. No multistability was found.

15. SUBJECT TERMS

chemical reduction	industrial wastewater treatment	dinitrotoluene (DNT)
munitions wastes disposal	propellants	hydroxyethyl (HE)

16. SECURITY CLASSIFICATION OF:

a. REPORT	b. ABSTRACT	c. THIS PAGE	17. LIMITATION OF ABSTRACT	18. NUMBER OF PAGES	19a. NAME OF RESPONSIBLE PERSON Dr. Stephen W. Maloney
Unclassified	Unclassified	Unclassified	SAR	96	19b. TELEPHONE NUMBER (include area code) (217) 352-6511 x3482